



Dominik Gilg, BSc.

Crashworthiness Study of a Battery Case for Advanced Automotive Application

Masterarbeit

Angestrebter akademischer Grad: Diplom-Ingenieur

Masterstudium: Production Science and Management

Technische Universität Graz

Fakultät für Maschinenbau und Wirtschaftswissenschaften

Institut für Fahrzeugtechnik

Institutsvorstand: Univ.-Prof. Dipl.-Ing. Dr.techn. Peter Fischer

Betreuer:

Federico Coren, MSc.

Graz, 02. Februar 2021

Thanks

I want to thank my tutor Federico Coren MSc for the great support received and Dipl.-Ing. Severin Huemer-Kals that helped me with some questions and constructive advice.

Furthermore, I would like to thank Univ.-Prof. Dipl.-Ing. Dr.techn. Peter Fischer for the opportunity to carry out this work as well as for the pleasant working environment at the institute.

A special thank to my family for the love, support, and constant encouragement I have gotten over the years and throughout my whole studies.

STATUTORY DECLARATION

Ich erkläre an Eides statt, dass ich die vorliegende Arbeit selbstständig verfasst, andere als die angegebenen Quellen/Hilfsmittel nicht benutzt, und die den benutzten Quellen wörtlich und inhaltlich entnommenen Stellen als solche kenntlich gemacht habe.

Graz, am 02.02.2021

(Unterschrift)

I declare that I have authored this thesis independently, that I have not used other than the declared sources/resources, and that I have explicitly marked all material which has been quoted either literally or by content from used sources.

Graz, am 02.02.2021

(Date)

(Signature)

Abstract

Carbon Fiber Sheet Molding compounds (CF-SMC) are a promising class of materials with the potential to replace aluminum and steel in many structural automotive applications. This thesis investigates the use of a CF-SMC material model for a lightweight battery case concept for electrically powered vehicles.

A limiting factor for the use of such a material is the difficulty in modeling its mechanical behavior and failure prediction with a computational effective methodology.

This thesis deals with the development of a simulation method to simulate the structural behavior of a large CF-SMC battery case. The used modeling methodology was developed at the TU Graz. It gives the ability to simulate large structures designed out of CF-SMC material by using shell elements with relatively low computational effort, while maintaining the ability to predict complex failure mechanisms.

The focus of this work is double: validate the modelling method and verify the mechanical soundness of the battery case. Specifically a destructive crush test involving the battery case was simulated. The whole methodology was then evaluated against simulation data from a simulation with three different material models for the Battery Case. For the comparison a aluminum, steel and quasi isotropic CF-SMC model were used. The comparison of the simulation results showed good prediction of the force displacement curves for the CF-SMC modeling methodology. Furthermore, the performances of the CF-SMC as a structural material for the battery case have been evaluated.

Kurzfassung

Carbon Fiber Sheet Molding Compounds (CF-SMC) sind eine vielversprechende Materialklasse mit dem Potenzial, Aluminium und Stahl in vielen strukturellen Automobilanwendungen zu ersetzen. Diese Arbeit untersucht die Verwendung eines CF-SMC-Materialmodells für ein Leichtbau Batteriegehäusekonzept für elektrisch angetriebene Fahrzeuge.

Ein begrenzender Faktor für die Verwendung von CF-SMC ist die Schwierigkeit, sein mechanisches Verhalten und seine Fehlervorhersage mit einer möglichst recheneffizienten Methodik zu modellieren.

Diese Arbeit befasst sich mit der Entwicklung einer Simulationsmethode zur Simulation des strukturellen Verhaltens eines CF-SMC-Batteriegehäuses. Die verwendete Modellierungsmethode wurde an der TU Graz entwickelt. Sie bietet die Möglichkeit, große Strukturen aus CF-SMC-Material zu simulieren und komplexe Fehlermechanismen vorher zu sagen. Durch die Verwendung von Schalenelementen wird der Rechenaufwand stark reduziert.

Der Schwerpunkt dieser Arbeit liegt auf der Vorhersage, ob das CF-SMC-Materialmodell für eine große Komponente gute Ergebnisse liefert. Im Rahmen dieser Arbeit wurde ein Crashtest für ein Leichtbau Batteriekonzept simuliert. Die neuartige Modellierungsmethode wurde für das CF-SMC-Gehäuse des Batteriekonzepts verwendet. Die gesamte Methodik wurde dann anhand von Simulationsdaten aus einer Simulation mit drei verschiedenen Materialmodellen für das Batteriegehäuse bewertet. Für den Vergleich wurden ein Aluminium-, Stahl- und ein quasi-isotropes CF-SMC-Modell verwendet. Die Simulationsergebnisse zeigten eine gute Vorhersage der Kraft-Verformungsverläufe für die CF-SMC-Modellierungsmethode. (ähnlich als die englische Version)

Content

Thanks	iv
STATUTORY DECLARATION	vi
Abstract.....	viii
Kurzfassung	x
Content	xii
Abbreviations.....	xv
Symbols.....	xvii
1. Introduction	1
2. CF-SMC Battery Pack and Material Modeling.....	2
2.1 Battery Case	2
2.1.1 Function of a battery pack	3
2.2 Material of the Battery Case	4
2.2.1 Sheet Molding Compound	4
2.2.2 HexMC®	7
2.3 Derivation of the linear law of elasticity for SMC materials	8
2.3.1 Tricline anisotropy	9
2.3.2 Orthotropy	9
2.3.3 Transverse isotropy.....	10
2.4 Strengths and failure modes of a Unidirectional (UD)-Element	11
2.4.1 Fracture behavior.....	12
2.5 Failure criteria	15
2.6 Material Modeling	16
2.6.1 Linear vs Non-linear material response	16
2.6.2 Hashin Criterion	17
2.6.3 Damage evolution	20
3. Methodology.....	25
3.1 Finite Element Model description.....	25
3.1.1 General overview of used Elements	28
3.1.2 Lower- and upper-case model	29
3.1.3 Cross brace.....	30

3.1.4	Heat conduction plate	31
3.1.5	Mounting blocks	31
3.1.6	Battery modules	32
3.1.7	Crush Plate.....	34
3.1.8	Contacts.....	35
3.1.9	Distributing coupling constraint	37
3.1.10	Adhesive connection	37
3.1.11	Bolt connection	38
3.1.12	Boundary Conditions and Loads.....	39
3.1.13	Meshing of the FEM-Model.....	41
3.2	Material Definition	43
3.2.1	Orthotropic material behavior	43
3.2.2	Quasi-isotropic material behavior	46
3.2.3	Aluminium	46
3.2.4	Steel.....	48
3.2.5	Cohesive Material.....	48
3.3	Simulation Technique.....	52
3.3.1	Static vs. Dynamic.....	52
3.3.2	Implicit vs. Explicit	52
4.	Results and conclusion	55
4.1	Loading Rate	55
4.2	Energy Balance	57
4.3	Analysis of the influence of the fiber orientations.....	58
4.3.1	Total displacement of the Crush plate	58
4.3.2	3-point bending test	60
4.3.3	Deformation of the simulation model for the fiber orientations.....	61
4.4	Comparison of the results of the different materials.....	66
4.4.1	Total displacement of the Crush Plate	66
4.4.2	Comparison of the total deformation of the simulation model.....	71
4.5	Damage Distribution in the CF-SMC Orthotropic FEM model.....	76
4.5.1	Weight of the Battery case.....	77
5.	Discussion	78

5.1	Modelling of the Battery Case	78
5.2	Computational effort	78
5.3	Stability of the Simulation.....	79
5.4	Simulation Modell.....	79
5.5	CF-SMC Material model	79
6.	Conclusion.....	80
	Figures.....	I
	Tables.....	V
A	Appendix	VI
8.	Literatur	VII

Abbreviations

SMC	Sheet-Molding-Compound
CF-SMC	Carbon Fiber Sheet Molding Compounds
BEV	Battery Electric Vehicle
BMS	Battery Management System
ALLIE	Total Strain Energy
ALLKE	Kinetic Energy
UD	Uni Directional
CNC	Computerized Numerical Control
E-Modulus	Elastic Modulus

Symbols

σ_f^+	tensile failure stress in fiber mode
σ_f^-	compressive failure stress in fiber mode
σ_m^-	tensile failure stress in matrix mode
σ_m^+	compressive failure stress in matrix mode
τ_f	shear failure stress in fiber mode
τ_m	shear failure stress in matrix mode
L_c	characteristic length of element
α	weighting factor for the shear stress, Hashin criteria
η_i	coefficient of viscosity in respective direction
$\delta_{i,eq}^z$	equivalent displacement in respective direction
σ_{ij}	normal stress in respective direction
τ_{ij}	shear stress in respective direction
ν_{ij}	Poisson's ratio in respective direction
d_i^z	damage variable
D_{ijkl}	compliance matrix
E_{ij}	Young's Modulus in respective direction
G	Shear Modulus
G_i^z	Fracture energy in respective direction
R_i^z	Strength in respective direction
δ	density
t_i	traction stress in respective direction
$(..)_i^z$	
	$(..)_f^+$ physical variable fiber direction tension
	$(..)_f^-$ physical variable fiber direction compression
	$(..)_m^+$ physical variable matrix direction tension
	$(..)_m^-$ physical variable matrix direction compression
$(..)_{ij}$	physical variable in respective coordinate direction

1. Introduction

The transport sector in Europe is one of the biggest CO₂ emitters, contributing up to 27% of the Eu's total Emissions. Of this, passenger cars alone account for up to 41 %. [2]

In order to reduce CO₂ emissions, a possible way would be increasing the number of electrically powered vehicle on our road and cities. The generation of electricity in power plants, is way more efficient than burning fossil fuels inside combustion engines. The Fraunhofer institute made a study on the electrification of vehicles in Germany and calculated that the impact on the CO₂ reduction might be between 28% and 42%, depending on the used fuel and car type. [3]

Electric vehicles draw their current usually from battery systems. Nowadays lithium ion batteries represent the most adopted solution to electrical energy in chemical form. Due to the relatively low energy density of the battery compared to gasoline or diesel fuel, vehicles with long ranges present a high weight penalty, mostly deriving from battery mass. As a rough estimate 100 kg battery mass allow for ca 100 km range . [4]

Due to the high mass of the battery packs, the total mass of an electric vehicle is higher compared to a traditional internal combustion vehicle. To compensate it, it is possible to reduce the weight of electric cars by using advanced materials. Big components like battery trays, can provide some of the greatest absolute weight savings. Materials based on carbon fiber, are among the natural candidates to replace traditional heavier metals.[5]

The use of fiber composite materials in structural components requires reliable modelling methods. Heavy overloads might occur in vehicles in case of accidents. Therefore, to develop a performing component, it is important to be able to take failure mechanisms into consideration.[6, 4]

Within the framework of this work a crash test FEM simulation model for a lightweight battery case was developed. For the battery case a novel simulation methodology has been used, which is able to predict the failure mechanism of the material. To make predictions of the accuracy of the CF-SMC material model for large components the model was verified by comparing the CF-SMC battery case with one made of metals. Aluminum and steel were used given the great availability of literature data.

2. CF-SMC Battery Pack and Material Modeling

This chapter gives an overview over the battery pack, the used CF-SMC material and the modeling methodology of the material.

2.1 Battery Case

Figure 1 shows the Concept of a Battery Case developed at the FTG/TU Graz. This particular battery is designed for a medium sized electric vehicle with an approximate range of 400km (50 kWh) and has a weight of about 500 kg. The commonly used materials for such cases are aluminum or steel [7]. Metals have a lower stiffness to weight ratio compared to unidirectional carbon fiber but have the advantage of being price competitive and easier to manufacture. [8, 9]

The concept in Figure 1 uses a Carbon fiber Sheet Molding Compound for the battery external case. This material has a unique combination of properties: being lightweight, having a high mechanical strength values, being crack tolerant and under certain circumstances can be price-competitive. [9, 7]

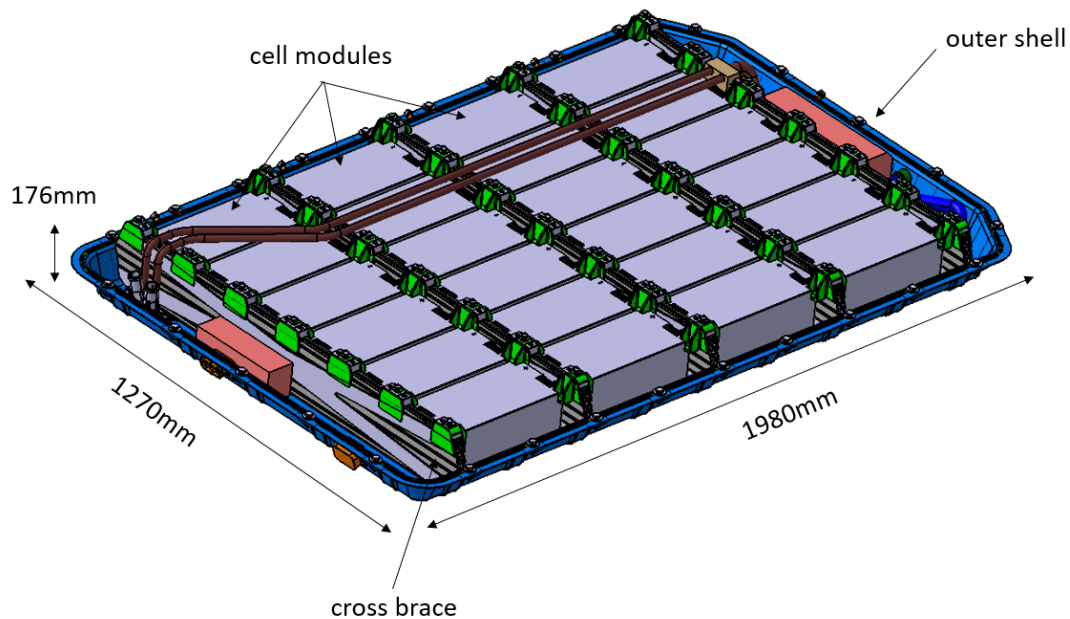


Figure 1 Battery Case Concept developed at the FTG/TU Graz: Showing the outer shell made of CF-SMC and the inner components such as the battery cells and auxiliaries [7]

2.1.1 Function of a battery pack

The Lithium-Ion battery is a commonly used technology to store electrical energy in BEV (Battery Electric Vehicle). This technology is used given its high energy density (6,7 kg/kWh [7]) and good lifetime. [6]

The Lithium Ion battery cells are combined in a first assembly to form a so called cell modules, shown in Figure 2. [10]

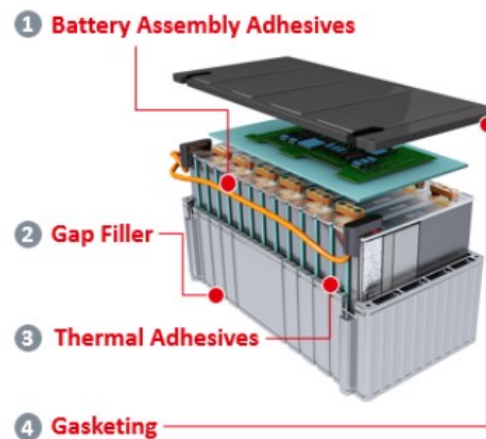


Figure 2 Inner components of a Battery Module for s BEV [11]

Several modules are connected and form a battery system. The modules are monitored and controlled by the battery management system (BMS).

The cooling system in lithium-ion cells, plays an important role. As a matter of fact, the working-temperature window is limited. During charging and discharging the batteries are going to produce heat, that has to be discharged into the environment. Cold temperatures are a problem as well, since they reduce the current output of the cell and might in extreme case damage the internal components.

A good battery case has to provide secure positioning of all components inside. In addition it has to protect the electrical components in the event of an accident and a battery malfunction or thermal run-off. [12, 7] Damage of the battery modules can have serious consequences in the worst case it can lead to fire. The exact test requirements for this can be found in International Standards [12, 13]. In addition to these central tasks, battery cases have other requirements as well, some of which are heavily dependent on the vehicle structure. The detailed structure is therefore often different. [10, 6]

2.2 Material of the Battery Case

The Battery Case in this thesis uses a Carbon Fiber Sheet Molding Compounds material. Using this material to replace aluminum can lead to a weight reduction of about 30 % while maintaining the mechanical properties. [7]

2.2.1 Sheet Molding Compound

In this process, fiber matrix mats (semi-finished products) are pressed into components using a press under defined pressure and temperature. The SMC-Process is an industrial widely used process and follows a highly automated process flow. [1]



Figure 3 Semi-finished CF-SMC material before the SMC-Process

The areas of application for SMC components are broad. These include, electrical engineering (e.g. control cabinets) or vehicle construction (e.g. driver's cab, engine hoods). Other well-known products made of SMC materials are bathtubs, telephone boxes or Mailboxes. [1]

For illustration, a component from the vehicle industry is shown in Figure 4. shows a transmission cross member of a car made from a CF-SMC material. Due to the lack of paint, the characteristic fiber bundles near the surface can be seen.[9]



Figure 4 Transmission cross member of a car out of a SMC material [9]

2.2.1.1 Semi-finished product

The matrix of a SMC material has a significant contribution to properties such as density, strength and rigidity. The main task of the matrix is to keep the fibers in the desired position and to introduce the forces into the fibers or to transfer them between the fibers. Loads are also transferred directly by the matrix; this is the case for load cases in the transverse direction of the fiber and compressive stress in the longitudinal direction of the fiber. The matrix of the SMC semi-finished product consist out of unsaturated polyester resins. [1]

To achieve great strength and stiffness properties the fibers in the SMC-material must have strong atomic bonds. The first two rows of the periodic table have these properties. This means that the fiber materials often contain carbon or boron. In addition, a low density characterizes these materials. [1]

The fibers in the SMC semi-finished product have a length of about 1-50mm. They are distributed stochastically, which is why macroscopically, isotropic material properties occur in the plane (quasi-isotropic stress state) of the resin mats. During the hot pressing process the fibers can align, which can result in locally anisotropic properties. The fiber content measured on the total weight is usually 25-30%, but in some cases, it can be increased up to 60%. [1]

In addition to the matrix material and the fibers, an SMC semi-finished product contains other components. Mineral fillers are added to reduce material costs and to increase the modulus of elasticity and flow ability. There are also thermoplastic additives that help to reduce the shrinkage of the pressed part completely. In order to facilitate the subsequent extrusion process, internal release agents are added to the semi-finished product. Inhibitors are used to increase the storage stability. [14]

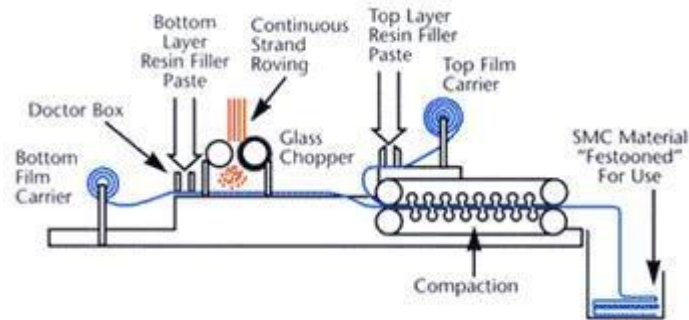


Figure 5 SMC Manufacturing Process [15]

In a first step, the various components, such as resin, thickener or fillers, are mixed in the doctor blade boxes. The fiber-resin-filler mixture is then evenly applied to the bottom carrier film. The fibers, wound endlessly on roving spools, reach the fiber-resin-filler mixture via the cutting unit in the required size. After that, a top layer with resin and filler paste is applied to the bottom layer fiber resin filler mixture. An upper carrier film then covers this layer. The "fiber and paste sandwich" is then compacted into a continuous sheet of molding compound by a series of rollers. The process ends when the finished mats are rolled up. [1, 15]

2.2.1.2 Processing of the semi-finished SMC material

Pre-impregnated resin mats are used as semi-finished products in the SMC process, shown in Figure 3. [1]

The processing of the SMC semi-finished products into components is primarily carried out by means of extrusion processes. Before the pressing process, the SMC mats are cut into blanks, which make up around 30% to 70% of the projected component surface. These blanks are then placed in layers in the press tool. The number of layers depends on the component dimensions. The positioning of the semi-finished product in the press tool is important for the component properties. Depending on the flow path of the SMC package, different flow paths of the individual fibers arise, which leads to undesirable fiber orientations or anisotropic material properties. For this reason, the exact insertion is done by machine, computerized numerical control (CNC) or manually by means of laser beam positioning. This is followed by pressing with a heated tool (approx. 130 ° C-165 ° C) and a brief hardening under pressure for approx. 5-10 seconds. [6]

2.2.2 HexMC®

This material is used for the model of the battery case in this thesis. It is a CF-SMC-Material with the trademark name HexMC-i/C/2000/M77 manufactured by Hexcel®.

Table 1 Specification of HexMC® [16]

Fiber	HS Carbon
Matrix	M77 Hexel Epoxy
Nominal fiber volume	57%
Cure time	3 minutes
Curing temperature	150 °C
Material density	1.55 g/cm ³

HexMC®-i is a high performance-molding compound, designed for compression molding. It is an alternative to lightweight metal alloys such as (Al, Mg,Ti). The semi-finished material consist of an epoxy resin matrix, with a high content of carbon fiber chips, the fiber chips have a length of 50mm and a width of 8mm. [7].

HexMC®-I has the following mechanical properties:

Table 2 mechanical properties HexMC® material. These are typical values obtained with samples cut from 4mm thick moulded plate, cured 3 min at 150°C [16]

Stress condition	Strength (MPa)	Modulus (GPa)	Standard
Flexural	500	30	ASTM D3039
Tensile	300	38	ASTM D790
Compression	290	38	EN 6036

2.3 Derivation of the linear law of elasticity for SMC materials

With the law of elasticity, the relationship between stresses and strains is described for materials in the linear elastic range. The simplest load case, is the single-axis normal load, this relationship is described by a constant, the modulus of elasticity.

$$\sigma = E * \varepsilon$$

2-1

In the case of a multi-axis loading state, there are a total of nine stresses in a volume element with the three main directions 1, 2 and 3. Of these, σ_1 , σ_2 and σ_3 are the normal stresses and τ_{23} , τ_{32} , τ_{13} , τ_{31} , τ_{12} and τ_{21} are the shear stresses, as shown in Figure 6. In this case, the relationship between the nine stresses and the distortions is described by an elasticity tensor with 81 constants. The constants are reduced by various properties and symmetries, which are briefly described in this chapter. [1, 17]

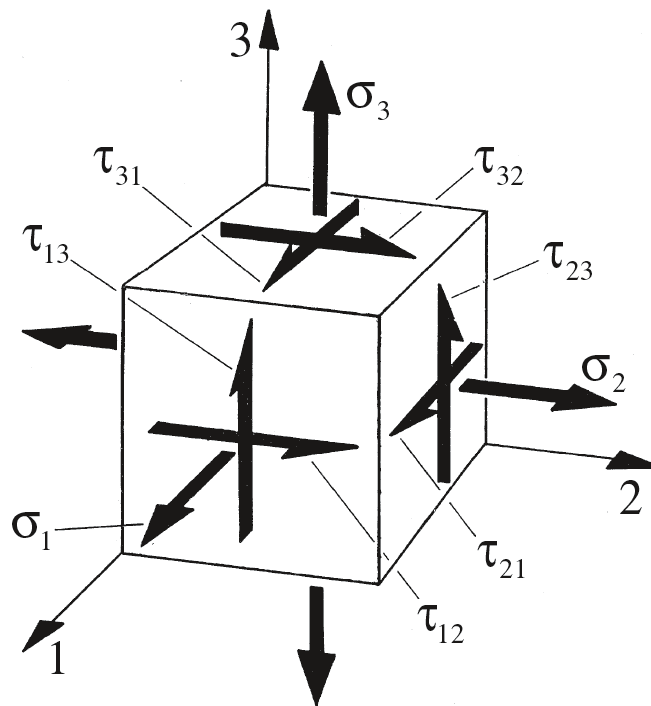


Figure 6 Stresses on an incremental volume element dV [1]

2.3.1 Tricline anisotropy

Due to the equilibrium of moments in a sectional plane, the shear stresses are always assigned in pairs, which is why the shear stresses are reduced from six to three. This results in the 6x6 compliance matrix shown in equations 2-2 and 2-3 with 36 unknown quantities. Due to energy considerations, there is a symmetry around the main diagonal in the compliance matrix. This reduces the number of unknown constants to 21. This is the general anisotropic case when there are no symmetries in the material. [1, 18]

$$\varepsilon_{ij} = D_{ijkl} * \sigma_{kl} \quad 2-2$$

$$\begin{pmatrix} \varepsilon_1 \\ \varepsilon_2 \\ \varepsilon_3 \\ \gamma_{23} \\ \gamma_{31} \\ \gamma_{21} \end{pmatrix} = \begin{pmatrix} S_{11} & S_{12} & S_{13} & S_{14} & S_{15} & S_{16} \\ S_{21} & S_{22} & S_{23} & S_{24} & S_{25} & S_{26} \\ S_{31} & S_{32} & S_{33} & S_{34} & S_{35} & S_{36} \\ S_{41} & S_{42} & S_{43} & S_{44} & S_{45} & S_{46} \\ S_{51} & S_{52} & S_{53} & S_{54} & S_{55} & S_{56} \\ S_{61} & S_{62} & S_{63} & S_{64} & S_{65} & S_{66} \end{pmatrix} * \begin{pmatrix} \sigma_1 \\ \sigma_2 \\ \sigma_3 \\ \tau_{23} \\ \tau_{31} \\ \tau_{21} \end{pmatrix} \quad 2-3$$

2.3.2 Orthotropy

Orthotropic material behavior exists when three planes of symmetry, which are orthogonal to each other, and three preferred directions normal to the respective planes of symmetry exist. In this case the independent constants are reduced to nine. [18, 1]

$$\begin{pmatrix} \varepsilon_1 \\ \varepsilon_2 \\ \varepsilon_3 \\ \gamma_{23} \\ \gamma_{31} \\ \gamma_{21} \end{pmatrix} = \begin{pmatrix} S_{11} & S_{12} & S_{13} & 0 & 0 & 0 \\ S_{21} & S_{22} & S_{23} & 0 & 0 & 0 \\ S_{31} & S_{32} & S_{33} & 0 & 0 & 0 \\ 0 & 0 & 0 & S_{44} & 0 & 0 \\ 0 & 0 & 0 & 0 & S_{55} & 0 \\ 0 & 0 & 0 & 0 & 0 & S_{66} \end{pmatrix} * \begin{pmatrix} \sigma_1 \\ \sigma_2 \\ \sigma_3 \\ \tau_{23} \\ \tau_{31} \\ \tau_{21} \end{pmatrix} \quad 2-4$$

2.3.3 Transverse isotropy

The transverse isotropy is a special case of orthotropy. There is an isotropic plane, perpendicular to that an infinite number of planes of symmetry exist. This means that the same properties prevail on all cutting planes perpendicular to the isotropic plane. Equation 2-5 shows the law of elasticity. In this case the isotropic plane is the plane orthogonal to axis 3. The representation takes place in the engineering constants modulus of elasticity E, shear modulus G and Poisson's ratio v.

$$\begin{pmatrix} \varepsilon_1 \\ \varepsilon_2 \\ \varepsilon_3 \\ \gamma_{23} \\ \gamma_{13} \\ \gamma_{12} \end{pmatrix} = \begin{pmatrix} \frac{1}{E_1} & -\frac{\nu_{12}}{E_1} & -\frac{\nu_{31}}{E_3} & 0 & 0 & 0 \\ -\frac{\nu_{12}}{E_1} & \frac{1}{E_1} & -\frac{\nu_{31}}{E_3} & 0 & 0 & 0 \\ -\frac{\nu_{13}}{E_1} & -\frac{\nu_{13}}{E_1} & \frac{1}{E_3} & 0 & 0 & 0 \\ 0 & 0 & 0 & \frac{1}{G_{31}} & 0 & 0 \\ 0 & 0 & 0 & 0 & \frac{1}{G_{31}} & 0 \\ 0 & 0 & 0 & 0 & 0 & \frac{2(1+\nu_{12})}{E_1} \end{pmatrix} * \begin{pmatrix} \sigma_1 \\ \sigma_2 \\ \sigma_3 \\ \tau_{23} \\ \tau_{13} \\ \tau_{12} \end{pmatrix} \quad 2-5$$

Due to the isotropic plane, the following simplifications are made for the flexibility matrix D_{ijkl} in equation 2-5:

- $E_1=E_2$
- $G_{23}=G_{31}$
- $\nu_{23}=\nu_{31}$
- The energy analysis of the stiffness matrix gives the following relationship:

$$\frac{\nu_{12}}{E_1} = \frac{\nu_{21}}{E_2}; \frac{\nu_{13}}{E_1} = \frac{\nu_{23}}{E_2} \quad 2-6$$

- The shear modulus of the isotropic plane is calculated with the young's modulus and the Poisson's ratio of the plane:

$$G_{12} = \frac{E_1}{2(1+\nu_{12})} \quad 2-7$$

From these relationships it follows that in the case of transverse isotropy only five material parameters are needed: two moduli of elasticity, one shear modulus and two transverse contraction numbers. [1, 6, 18]

2.4 Strengths and failure modes of a Unidirectional (UD)-Element

Compared to isotropic materials, like steel, fiber composite materials consist out of different components. For this reason, the failure analysis of fiber composite materials is much more complex. Failure is understood here as the failure of the material as a result of mechanical stresses and thus the exceeding of the breaking resistance. There are other types of failure as well, such as heat or chemical decomposition. [1]

The following strength analysis relates to a volume element, the so-called Unidirectional (UD)-Element. The stresses shown in Figure 7 Stresses at the UD-Element [1]Figure 7 are derived from the loads on the UD layer respectively the overall model. [1]

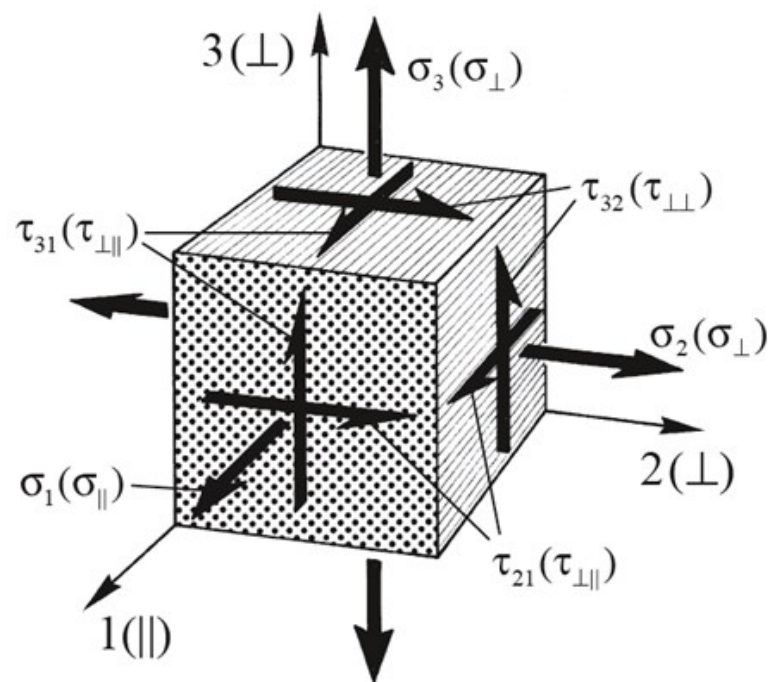


Figure 7 Stresses at the UD-Element [1]

Due to the symmetries of the transverse isotropy there are four different load cases that have to be considered, which increase to six due to the distinction between tension and compression for the normal stresses:

- Longitudinal loading σ_{\parallel} ; tension σ_{\parallel}^+ and compression σ_{\parallel}^-
- Transverse loading σ_{\perp} ; tension σ_{\perp}^+ and compression σ_{\perp}^-
- Transverse-longitudinal shear stress $\tau_{\perp\parallel}$
- Transverse-transverse shear stress $\tau_{\perp\perp}$

These six loadings counterpart by six strength values for the stress analyses, see Table 3. [1]

Table 3 Loading vs Strength

Loading	Strength
$\sigma_{ }^+$	$R_{ }^+$
$\sigma_{ }^-$	$R_{ }^-$
σ_{\perp}^+	R_{\perp}^+
σ_{\perp}^-	R_{\perp}^-
$\tau_{ }$	$R_{\perp }$
τ_{\perp}	$R_{\perp\perp}$

2.4.1 Fracture behavior

There are various modes of fracture with fiber composite materials, due to the different mechanical properties of fiber and matrix. In general there is distinction made between fiber failure and inter fiber failure. [1]

2.4.1.1 Fiber failure

The fiber failure is characterized by crack propagation across the longitudinal direction of the fiber and is usually triggered by stress along the main fiber direction, either through tensile or compressive stress. This type of failure only occurs with high loads, since the fibers of composite materials have high strength values. The breaking of the fiber bundle ultimately leads to the total failure of the component. Fiber Failure occurs as a result of $\sigma_{||}$ tension or pressure in fiber direction. [1]

In the event of fiber failure due to tension, the fibers will tear as shown in Figure 8. This form is recognized by a loss of longitudinal stiffness and slow crack growth. [1]

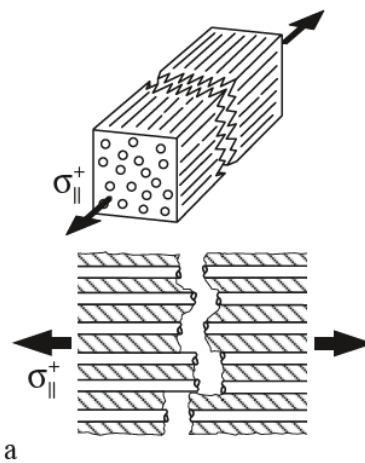


Figure 8 Fiber Failure under tension [1]

Under longitudinal compression $\sigma_{||}^-$, shown in Figure 9, buckling occurs in the fibers due to the compressive stress. The breaking plane is not created perpendicularly by the normal compressive stress, but rather an inclined breaking plane is created due to shear stresses. The reason for this is that the breaking resistance against the normal compressive stresses is significantly higher than that of the shear stresses. The triggering of this shear buckling is described with the compressive strength in the longitudinal direction of the fibers $R_{||}^-$. [1, 6]

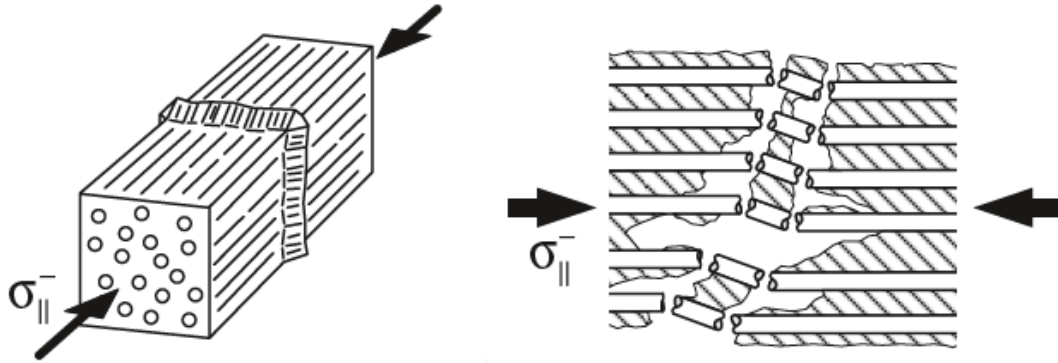


Figure 9 Fiber Failure under pressure [1]

2.4.1.2 Matrix failure

Matrix failure or Inter fiber breakage is a crack propagation parallel to the longitudinal direction of the fiber and occurs in the matrix or on the boundary layer between the fiber and the matrix. Because of the lower strength values of the matrix, the crack formation occurs at much lower load compared to fiber failure. The inter-fiber break is caused by various stress and tension states: [1]

- Transverse tensile stress σ_{\perp}^+
- Transverse pressure loading σ_{\perp}^-
- Transverse-longitudinal shear stress $\tau_{\perp||}$
- Transverse-transverse shear stress $\tau_{\perp\perp}$

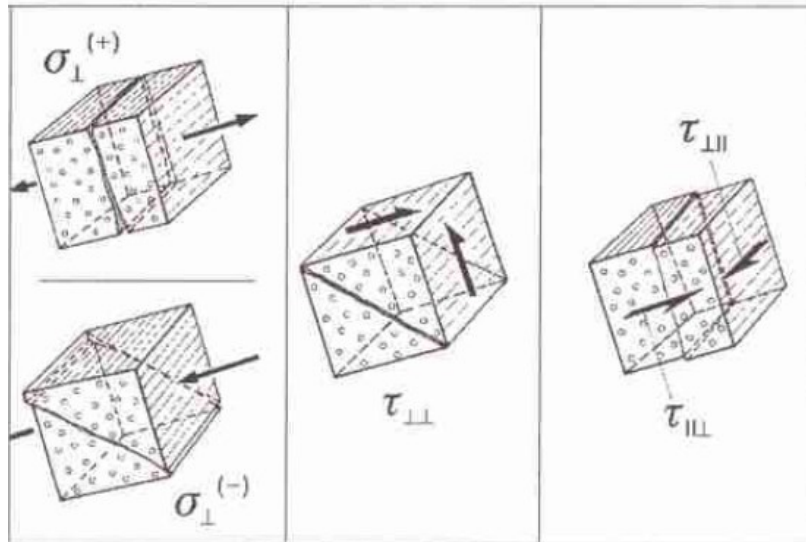


Figure 10 Possible Matrix failure Modes for a UD-Element [17]

The most common cause of matrix failure is the failure under transverse tensile stress σ_{\perp}^{+} . The entire load is absorbed by the matrix and cannot be distributed over the fibers. [1, 6]

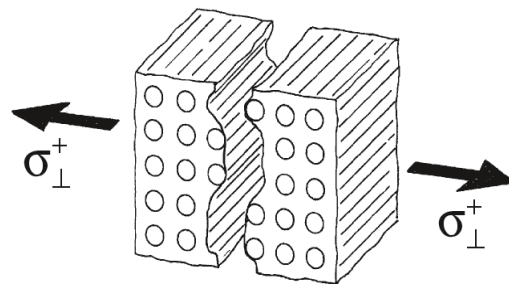


Figure 11 Matrix failure under transverse tensile stress σ_{\perp}^{+} [1]

2.4.1.3 Delamination

A third mode of composite failure after matrix and fiber failure is the delamination between the plies of the carbon fiber material. This type of damage can only occur with laminates with multiple layers and is triggered by so-called inter laminar stresses [1]. This work will not go into further detail here, because the material model used only consists of a single-layer shell model. Therefore, delamination cannot be included in damage modelling in this thesis.

2.5 Failure criteria

In order to be able to dimension a component with a sufficiently high level of security against failure, the occurring loads determined from the stress analysis must be compared with the strength values of the material. Usually there is a multiaxial stress state with interacting normal and shear stresses, thus dependencies must be taken into account in the strength analysis. [1]

Numerous different failure criteria for carbon fiber reinforced composite have been developed for this purpose ([19], [20], [21], [22], [23]). The task of these criteria is to provide a statement with the help of a calculation rule whether failure occurs under a certain load.

Hashin is a simple fatigue failure criterion used for unidirectional fiber reinforced materials. A series of tests demonstrated good conformance of the criterion with experimental data. [20]

The Hashin criterion differentiates between the stress interaction and between four failure modes [19]. Furthermore, a single shell layer model is used to for the battery case, therefore it makes no sense to use a failure model, which can predict the location of the fracture plane.

For these reasons the Hashin Criterion is used in this thesis for the CF-SMC material of the battery case.

2.6 Material Modeling

2.6.1 Linear vs Non-linear material response

One factor of a simulation is how the material response is being calculated within the simulation. If the stresses only stay in the linear-elastic region, it is possible to use a linear material model. The advantage of such a model is that the material definition is simple, easy to measure and computationally efficient. Figure 12 shows the linear (red line) and the non-linear response. If the linear material stress passes its yield point ϵ_{yp} it is treated as, it was in its liner-elastic region. [24]

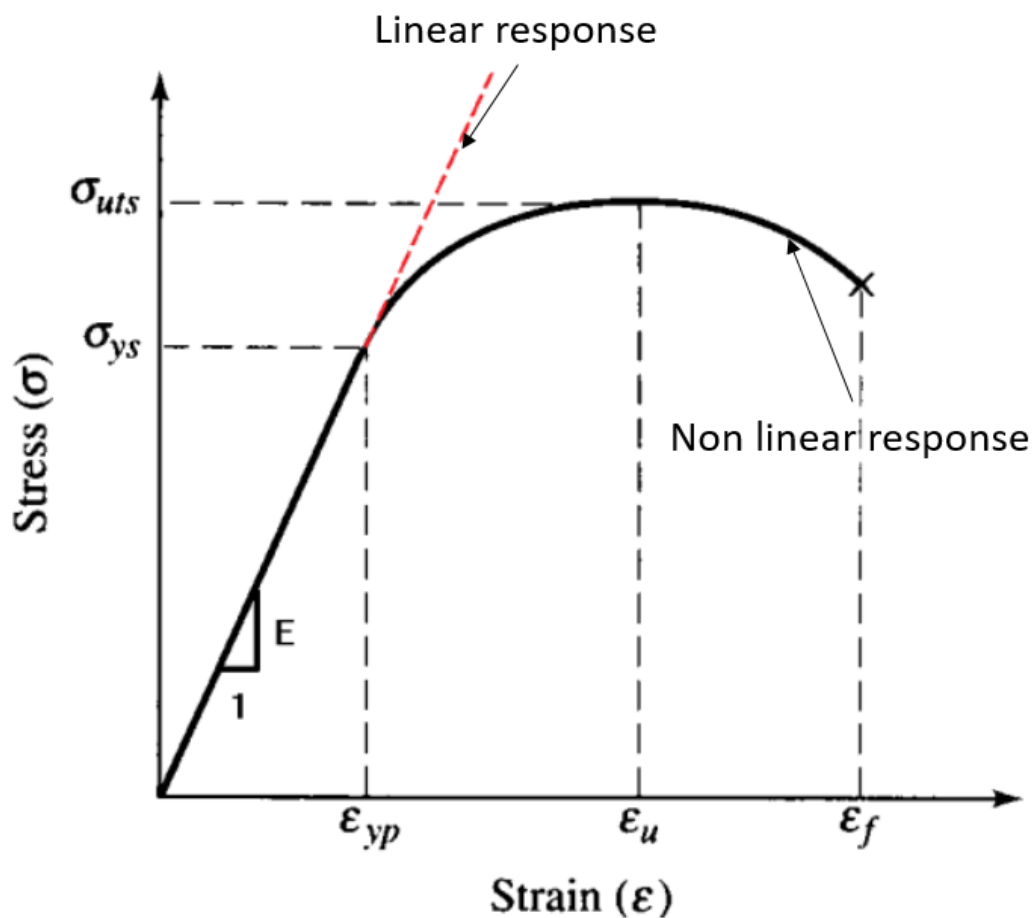


Figure 12 Linear vs. Non-linear martial response [24]

In this thesis, uses non-linear-material model, because the stresses in the material are exceeding the yielding point. In addition, a linear model does offer the capabilities to use a failure model to predict the damage of the parts.

2.6.2 Hashin Criterion

In order to simulate the behavior of composite material two aspects must be considered damage evolution and damage initiation. The Hashin criterion was adopted as a criterion for the damage Initiation.[7]

The Hashin criterion uses both the failure mode and the stress interaction for the prediction of the damage. Several modes can occur:

- Breaking of the fiber in tension
- Breaking of the matrix in tension
- Breaking of the fiber in compression
- Breaking of the matrix in compression

In most cases, these modes occur simultaneously, for the description of this criterion uses four equations for describing the occurrence of damage, see equations: 2-14, 2-15, 2-16, 2-17. [25, 6]

2.6.2.1 Hashin Damage Initiation Criterion

Damage Initiation simply describes the point where the material is affected first. Four damage initiation variables were considered:

- Fiber Tension F_{FT}
- Matrix Tension F_{MT}
- Fiber Compression F_{FC}
- Matrix Compression F_{MC}

The failure criterion is separated into two primary failure modes: fiber failure and matrix failure. Fiber failure can be rupture caused by tension or buckling due to compression, while matrix failure leads to cracks parallel to the fiber. The actual location of the fracture plane is not considered. Since the battery case model uses a single shell layer model, this does not make a huge difference. [24, 6]

Figure 13 shows a generic laminar shell element. The element is referred to a fixed coordinate system x_1, x_2 and a by an angle Φ turned material coordinate system. Fibers are oriented along the x'_1 direction and the transverse direction is x'_2 . [7]

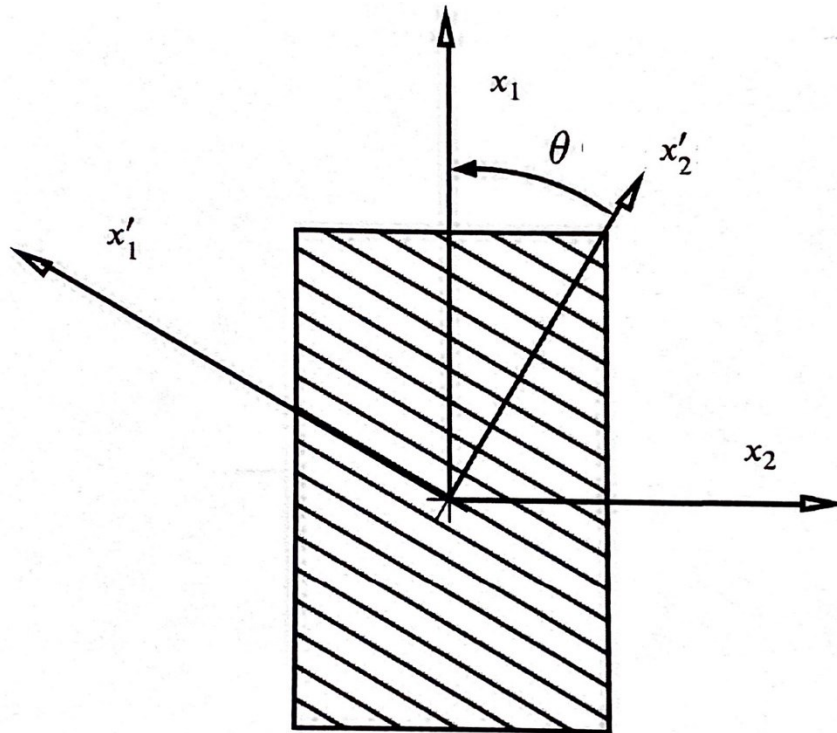


Figure 13 Generic element x_1, x_2 are the reference system. x'_1, x'_2 are the material reference system. [7]

A plane stress state $\sigma_{11}, \sigma_{22}, \sigma_{12}$ is transformed into $\sigma'_{11}, \sigma'_{22}, \sigma'_{12}$ with respect to the material system. The notations are adopted where f stands for fiber and m for matrix. [7]

$$\sigma'_{11} = \sigma_f \tag{2-8}$$

$$\sigma'_{22} = \sigma_m \tag{2-9}$$

$$\sigma'_{12} = \tau_f \tag{2-10}$$

The simplest scenario is a uniform uniaxial stress applied in the x_1 direction. The calculation for the stress state in the material system results in: [7]

$$\sigma_f = \sigma_{11} \cos^2 \theta \tag{2-11}$$

$$\sigma_m = \sigma_{11} \sin^2 \theta \tag{2-12}$$

$$\tau_f = \sigma_{11} \sin \theta \cos \theta \tag{2-13}$$

For each mode, two scenarios are possible: compressive or tensile. The choice of the particular failure mode for the plane stress state depends on the sign of the diagonal components of the stress tensor.

The four modes for the two dimensional failure state are: [7]

- Tensile Fiber Mode ($\sigma_{11} \geq 0$)

$$F_f^+ = \left(\frac{\sigma_{11}}{\sigma_f^+}\right)^2 + \alpha \left(\frac{\sigma_{12}}{\tau_f}\right)^2 \quad 2-14$$

- Fiber Compressive Mode ($\sigma_{11} < 0$)

$$F_f^- = \left(\frac{\sigma_{11}}{\sigma_f^-}\right)^2 \quad 2-15$$

- Tensile Matrix Mode ($\sigma_{22} \geq 0$)

$$F_m^+ = \left(\frac{\sigma_{22}}{\sigma_m^+}\right)^2 + \left(\frac{\sigma_{12}}{\tau_m}\right)^2 \quad 2-16$$

- Compressive Matrix Mode ($\sigma_{22} < 0$)

$$F_m^- = \left(\frac{\sigma_{22}}{2\tau_m}\right)^2 + \left[\left(\frac{\sigma_m^-}{2\tau_m}\right)^2 - 1\right] \left(\frac{\sigma_{22}}{\sigma_m^-}\right) + \left(\frac{\sigma_{12}}{\tau_f}\right)^2 \quad 2-17$$

α in Equation 2-14 determines the contribution of the shear stress to the fiber tensile initiation criterion. This Thesis uses the model by Hashin and Rotem [20] by setting $\alpha=0$ and $\tau_m = 0.5\sigma_m$ [21],

σ_{11} , σ_{22} and σ_{12} are components of the effective stress tensor $\hat{\sigma}$, that is used to evaluate the initiation criteria which is calculated from:

$$\hat{\sigma} = \mathbf{M}\sigma \quad 2-18$$

where σ is the nominal stress and \mathbf{M} is the damage matrix:

$$\mathbf{M} = \begin{bmatrix} \frac{1}{(1-d_f)} & 0 & 0 \\ 0 & \frac{1}{(1-d_m)} & 0 \\ 0 & 0 & \frac{1}{(1-d_s)} \end{bmatrix} \quad 2-19$$

Before any damage initiation takes place the damage variables d_f , d_m and d_s are zero and the matrix \mathbf{M} is simply a 3x3 identity matrix, so the effective stress equals the nominal stress:

$$\hat{\sigma} = \sigma \quad 2-20$$

If damage initiation and evolution occur for at least one mode, the damage matrix becomes important in the criteria for damage of the other modes. One simple example for this is if the matrix gets damaged due to tension, it can no longer carry as much shear load, even if there was no shear stress to degrade it. [24, 26]

2.6.3 Damage evolution

If the damage initiation criterion is satisfied for an element, the local stiffness of the material decreases. To model this behavior a progressive failure model is used. This model describes the connection between the damage and the elastic behavior of the material in order to model the material behavior after the damage initiation. Fiber-reinforced plastics have an elastic-brittle fracture behavior; therefore it makes no sense to use plastic deformation in the progressive damage model. [22, 21]

Equivalent stresses and strains are used to calculate the damage in an element. Therefore, a characteristic length L_c is introduced in the formulation. This length is derived from the element geometry.

This allows the constitutive equation to be expressed as equivalent stress σ_{eq} and equivalent displacement δ_{eq} instead of stress σ and strain δ .

In Figure 14 there are two areas. The first part consists of the linearly rising line, which corresponds to the linear elastic material behavior before the failure criterion is met and the second part consists of the progressive damage model. [7, 6]

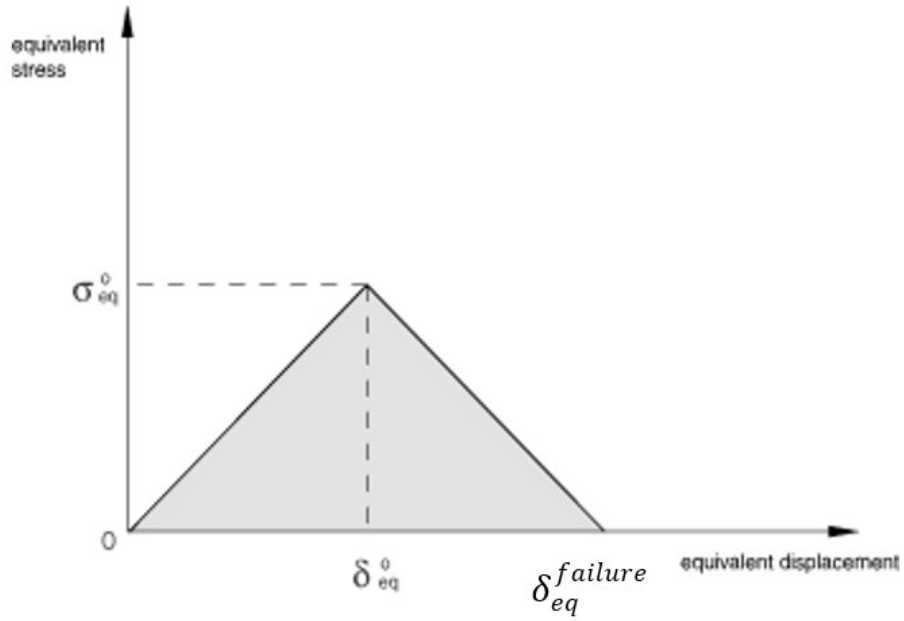


Figure 14 Equivalent Stress vs. equivalent Displacement δ_{eq}^0 corresponds to the damage initiation, $F=1$. At $\delta_{eq}^{failure}$ the element has failed and there is no mechanical resistance for that failure mode. [7, 26]

The equivalent stress and equivalent displacement values for each of the four modes are defined as a function of the characteristic length L_c :

- Fiber Tension ($\sigma_{11} \geq 0$)

$$\delta_{f_eq}^+ = L_c \sqrt{\langle \epsilon_{11} \rangle^2 + \alpha \epsilon_{12}^2} \quad 2-21$$

$$\sigma_{f_eq}^+ = \frac{\langle \sigma_{11} \rangle \langle \epsilon_{11} \rangle + \alpha \tau_{12} \epsilon_{12}}{\delta_{f_eq}^+ / L_c} \quad 2-22$$

- Fiber Compression ($\sigma_{11} < 0$)

$$\delta_{f_eq}^- = L_c \langle -\epsilon_{11} \rangle \quad 2-23$$

$$\sigma_{f_eq}^- = \frac{\langle \sigma_{11} \rangle \langle \epsilon_{11} \rangle}{\delta_{f_eq}^- / L_c} \quad 2-24$$

- Matrix tension ($\sigma_{22} \geq 0$)

$$\delta_{m_eq}^+ = L_c \sqrt{\langle \epsilon_{22} \rangle^2 + \epsilon_{12}^2} \quad 2-25$$

$$\sigma_{m_eq}^+ = \frac{\langle \sigma_{22} \rangle \langle \epsilon_{22} \rangle + \alpha \tau_{12} \epsilon_{12}}{\delta_{m_eq}^+ / L_c} \quad 2-26$$

- Matrix compression ($\sigma_{22} < 0$)

$$\delta_{m_eq}^- = L_c \sqrt{\langle -\epsilon_{22} \rangle^2 + \epsilon_{12}^2} \quad 2-27$$

$$\sigma_{m_{eq}}^- = \frac{\langle -\sigma_{22} \rangle \langle -\epsilon_{22} \rangle + \alpha \tau_{12} \epsilon_{12}}{\delta_{m_{eq}}^- / L_c} \quad 2-28$$

The $\langle \ \rangle$ represents the Macaulay bracket operator, which is defined as:

$$\langle x \rangle = \frac{(x + |x|)}{2} \quad 2-29$$

[26]

By the use of this operator, Abaqus ensures that the solver calculates the equivalent stress and displacement for each mode individually. [24]

Once the damage initiation criterion occurs, the four damage variables are assigned to the material. The damage variables: d_f^+ , d_f^- , d_m^+ , d_m^- get calculated directly from the equivalent displacements with Equation 2-30. Each mode has its own unique displacements, so that the damage variables are independent from each other. [21]

$$d = \frac{\delta_{eq}^{failure} (\delta_{eq} - \delta_{eq}^0)}{\delta_{eq} (\delta_{eq}^{failure} - \delta_{eq}^0)} \quad 2-30$$

In Equation 2-30 δ_{eq}^0 is the equivalent displacement at which the damage initiation criterion for the material is met and $\delta_{eq}^{failure}$ the equivalent displacement at which it is completely failed. [7]. The fifth damage variable shear damage d_s is dependent from the fiber and matrix damages.

$$d_s = 1 - (1 - d_f^+)(1 - d_f^-)(1 - d_m^+)(1 - d_m^-) \quad 2-31$$

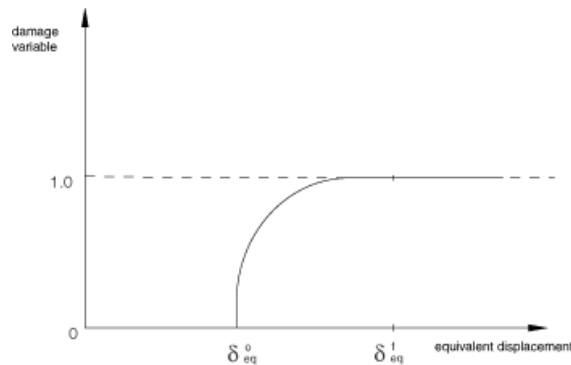


Figure 15 Damage variable as a function of equivalent displacement [26]

Figure 15 shows the damage evolution till δ_{eq}^0 the damage variable remains zero, no damage has occurred. After reaching δ_{eq}^0 , d starts to increase to one. At $d=1$ the critical equivalent displacement $\delta_{eq}^{failure}$ is reached and the element doesn't offer a resistance against deformation. The upper limit of the damage variable can be set to values below one in Abaqus. This can help with stability issues were elements are removed from the model to late and cause an error. [7, 24]

After the point of damage initiation is reached, the material response is calculated with the following equation:

$$\sigma = \mathbf{C}_d \varepsilon \quad 2-32$$

where ε is the strain tensor and \mathbf{C}_d is the damaged stiffness matrix which is defined:

$$\mathbf{C}_d = \frac{1}{D} \begin{bmatrix} (1 - d_f)E_1 & (1 - d_f)(1 - d_m)v_{21}E_1 & 0 \\ (1 - d_f)(1 - d_m)v_{12}E_2 & (1 - d_m)E_2 & 0 \\ 0 & 0 & (1 - d_s)GD \end{bmatrix} \quad 2-33$$

$$\text{with } D = 1 - (1 - d_f)(1 - d_m)v_{12}v_{21}$$

E_1 , E_2 and GD are the undamaged material moduli and v_{12} , v_{21} are the undamaged Poisson's ratios. The damage variables d_f , d_m have different values for compression and tension, therefore a proper damage index is specified for every load case. The variables can have values between zero and one, as described previously. At complete damage the damage variable reaches a value of one, the consequence is the E-Moduli of the stiffness matrix at the location gets zero and there is no stiffness in this direction. [21]

$$d_f = \begin{cases} d_f^+ & \text{if } \sigma_{11} \geq 0 \\ d_f^- & \text{if } \sigma_{11} < 0 \end{cases} \quad 2-34$$

$$d_m = \begin{cases} d_m^+ & \text{if } \sigma_{11} \geq 0 \\ d_m^- & \text{if } \sigma_{11} < 0 \end{cases} \quad 2-35$$

2.6.3.1 Dissipated energy for the failure mode

For the calculation of the five damage conditions, for each of the four modes: fiber tension, fiber compression, matrix tension and matrix compression a specific dissipated energy G needs to be defined.[24]

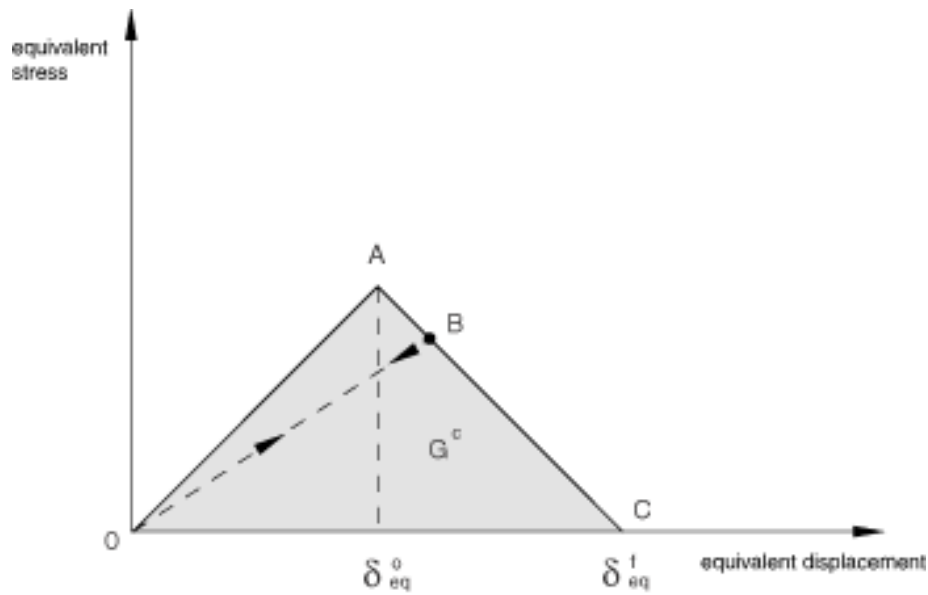


Figure 16 Linear Damage Evolution: Loading-unloading path [26]

Figure 16 shows the general response of the material in Abaqus. From 0-A the material gets loaded the response is linear-elastic. At A the damage ignition criterion is satisfied and the material gets damaged. In case of unloading at a damage state (point B), the new elastic modulus will be represented by the gradient of the straight 0-B. If the element gets loaded again the line 0-B will be used instead of 0-A. The total energy dissipated during the damage, G^c , is the area of the square 0-A-C. [7, 24]

2.6.3.2 Damage stabilization

In Abaqus Explicit simulations, viscous regulations can be used to model the strain rate dependency of a material. The regulations slow down the rate of the damage growth in the material, by increasing the fracture energy as the deformation rate increases. [24]

The results of the 3 point bending test showed that from a simulation time of 1,2s the influence of the viscosity coefficient can hardly be seen any more. [6]

3. Methodology

3.1 Finite Element Model description

The basis of the simulation model in this thesis is the 3D-CAD model of the battery case shown in Figure 17. The upper case, wiring and battery management system are not shown in this figure, for a better overview.

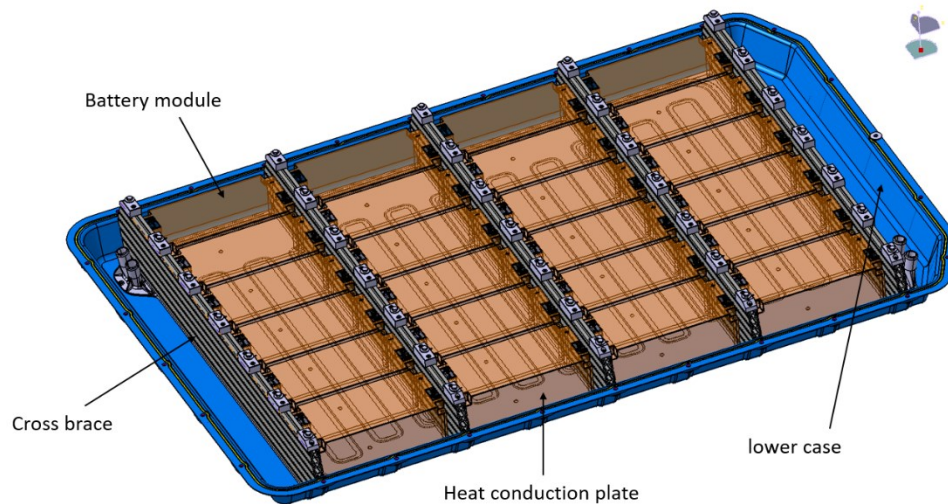


Figure 17 CAD-Concept developed by the TuGraz/FTG. Only lower half of the case is shown without wiring and battery management system

For the crash simulation of the 3D-CAD model the whole battery pack needed to be simplified. Components that have no significant influence on the overall stiffness of the case have been neglected. Such parts are: the wiring, the battery management system and seals, the Heat conducting pads under the battery modules and the mounting of the battery modules is simplified. The simplified model is shown in Figure 18. Figure 19 is showing the whole simulation model developed in this thesis. Nevertheless the model comprises of 480000 elements.

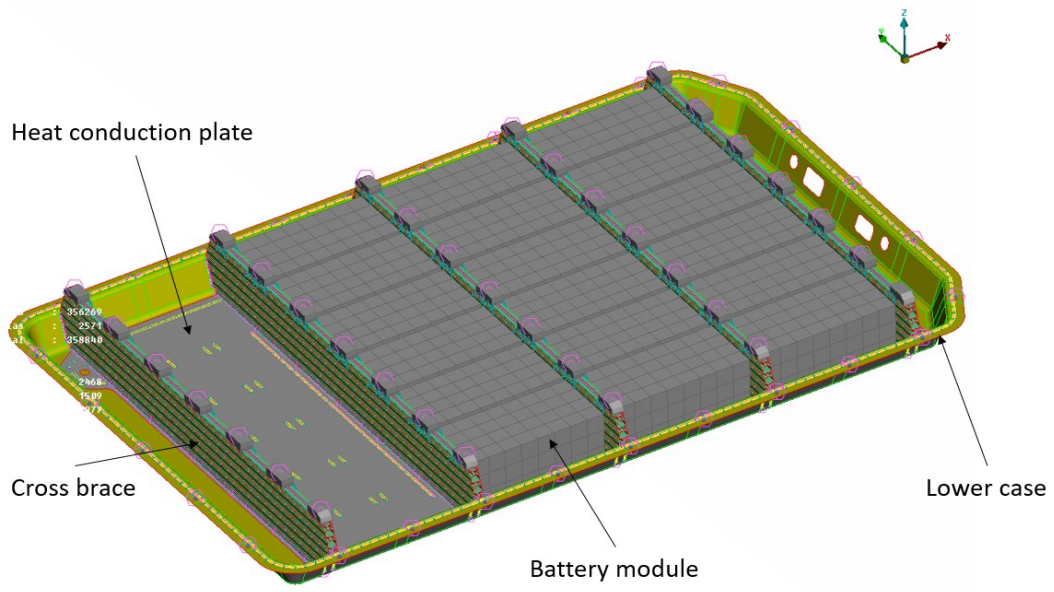


Figure 18 Simplified model of the Battery case that is used for the Crash Simulation in Abaqus

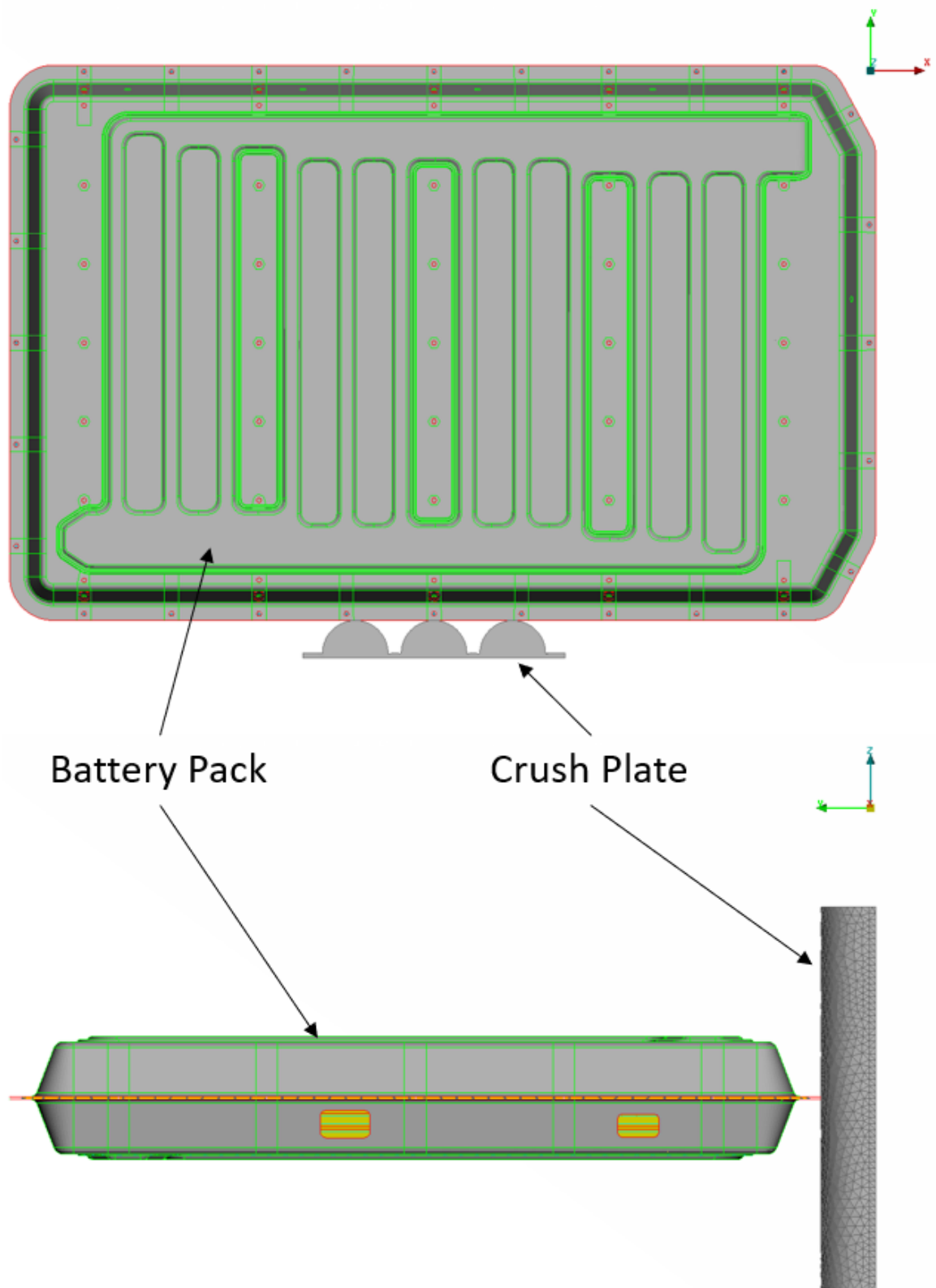


Figure 19 Top view and side view of the FEM Simulation model undeformed state. With the modeled crush Plate, see 3.1.7, that's used for the Crash Test simulation.

3.1.1 General overview of used Elements

This Table should give an rough overview about the components of the battery pack and the amount of elements.

Table 4 General overview over the elements used for the Battery Case Model

Component	Element Type and quantity	Element Type and quantity	Material
Lower Case	115313 S4 Shells	693 S3 Shells	C-SMC
Upper Case	116440 S4 Shells	1178 S3 Shells	C-SMC
Cross brace	187100 S4 Shells	1820 S3 Shells	C- SMC
Heat conduction plate	53856 S4 Shells	58 S3 Shells	Aluminum
Battery Modules	2304 C3D8 Solids		-
mounting Blocks and slot nuts	740 C3D8 Solids		Steel
\sum Elements	476392 Shell Elements	3044 Solid Elements	

3.1.1.1 Description of the used Elements

3.1.1.1.1 Shell Elements

Two types of shell elements are used in the simulation model, shown in Figure 20.

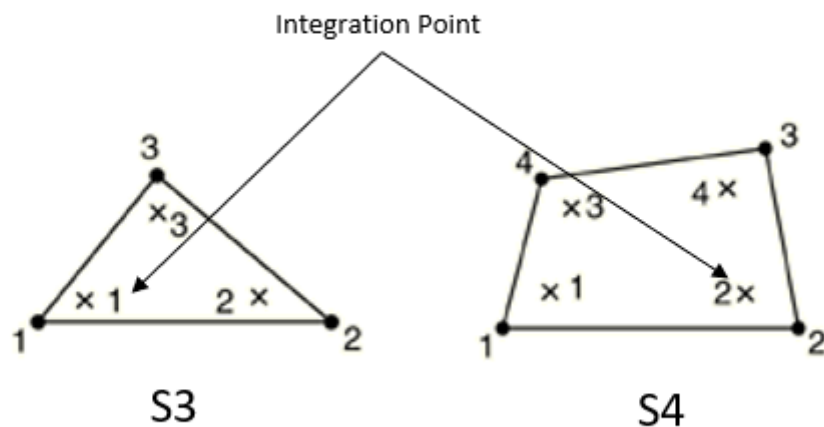


Figure 20 S4 and S3 element with their integration points [26]

These elements are used for the parts in the model where the thickness dimension is significantly smaller than the other dimension and the stresses in the thickness direction are negligible. This is the case for the Head conduction plate, the cross brace and the battery case.

It should be mentioned that S3 elements can cause stiffness problems. The S3 elements make up less than one percent of all shell elements (S3 + S4). That is why their influence on the stiffness of the overall model could be neglected.

Figure 20 shows the integration points of the shell elements. The S3 elements have 3 integration points and the S4 elements four. In FEM the constitutive response of an individual finite element is usually obtained by numerical integration through one or more integration points within an element. [27]

3.1.2 Lower- and upper-case model

The Battery Case consist out of two half's: a upper case and a lower case. The element Type S4 and S3 are used for the case. To increase the stiffness of the model there are 56 ribs evenly distributed around the circumference. At each rib, the case is bolted together, in total there are 28 bolts. The shells have a thickness of 2mm, only at the reinforcing ribs the elements are 6mm thick. At the flange area there is also an adhesive line to improve the stiffness of the connection of the two halves.

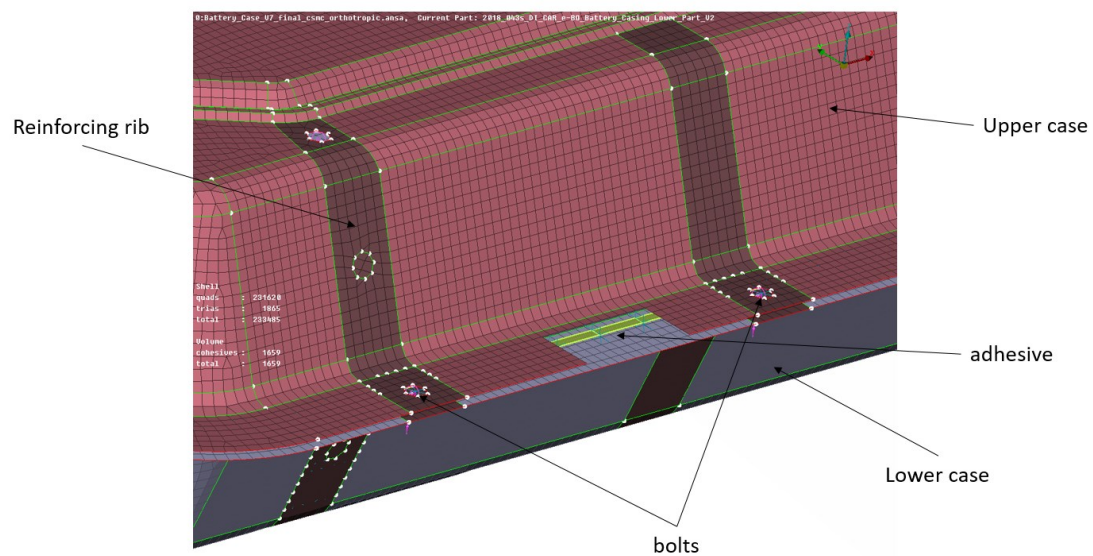


Figure 21 Upper and lower case with adhesive line and bolt connection

3.1.3 Cross brace

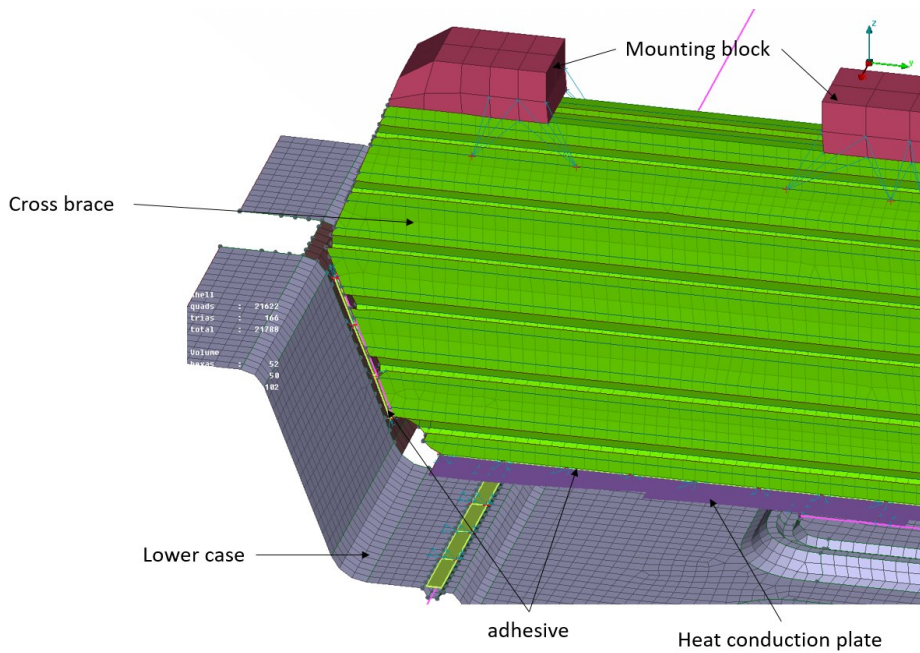


Figure 22 Connection of the cross brace with the other components of the case

Five cross braces are used to improve the overall stiffness of the battery case and to ensure a secure fit of the battery modules in the case. The braces are made out of a machined aluminum Item™ 2025.04 Profile, with a 2mm wall thickness. There are adhesive lines between the side wall of the lower case and the head conduction plate, located at the bottom of the case. A bolting connection

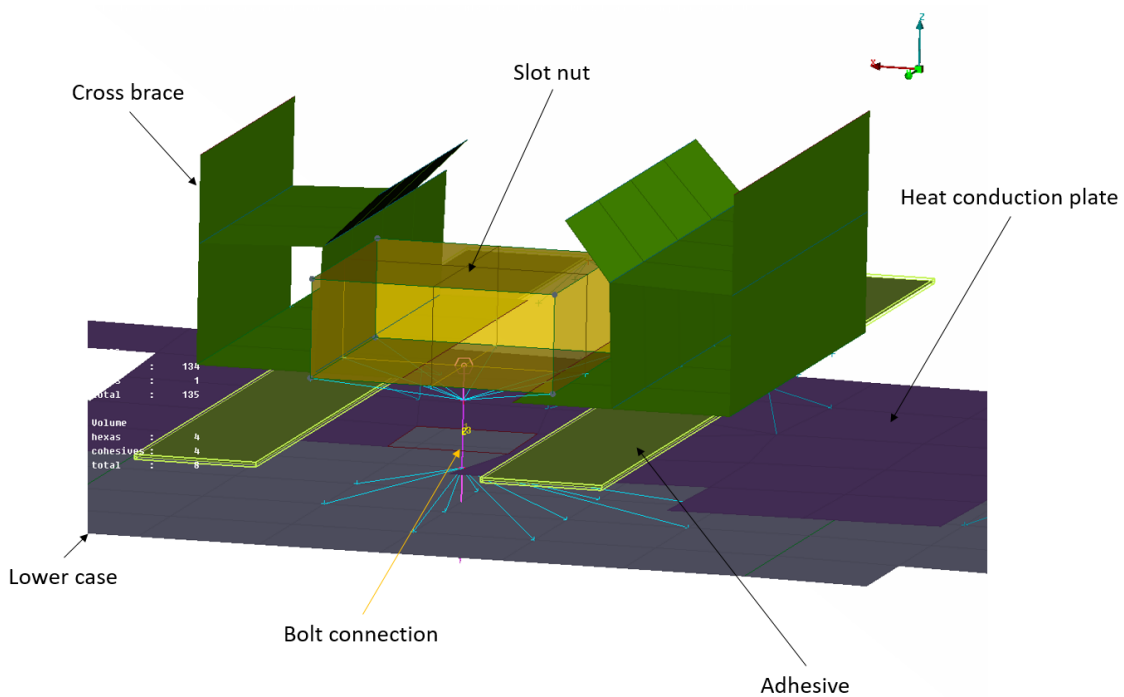


Figure 23 Detail view connection of the cross brace with the lower case

between the slot nut, which has a tied contact with the cross brace, and the lower case, shown in Figure 23 , ensures a solid connection. On the upper side of the cross brace the Mounting blocks have a tied contact with the brace and the upper case half.

3.1.4 Heat conduction plate

The Heat conduction plate is a 1mm thick aluminum plate, its task is to conduct the heat from the battery modules to the coolant and to separate it from the rest of the battery components. To ensure the separation and secure fit there is a gasket and an adhesive between the lower case and the head conduction plate. Figure 24 shows the modeled adhesive connection between the case and the heat conduction plate, the gasket are neglected because they have no impact on the overall stiffness of the model

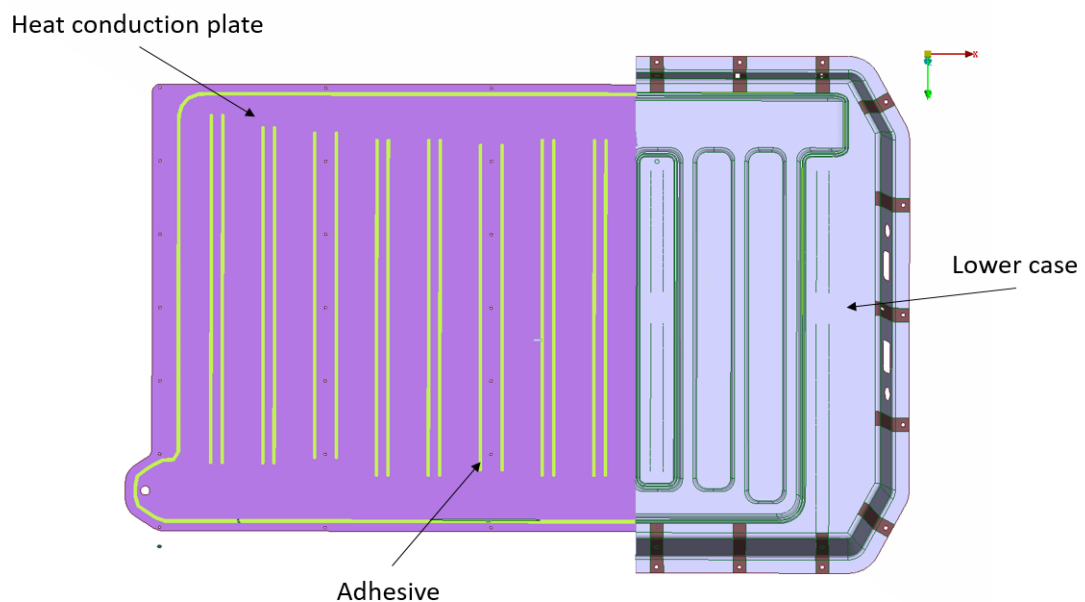


Figure 24 Model of the Heat conduction plate with the adhesive connection to the lower case

3.1.5 Mounting blocks

The mounting blocks are attached to the cross brace and the upper case by means of a tied contact, shown in Figure 25. To keep the model as simple as possible the mounting block is designed as a rectangular box with 16 C3D8 solid elements.

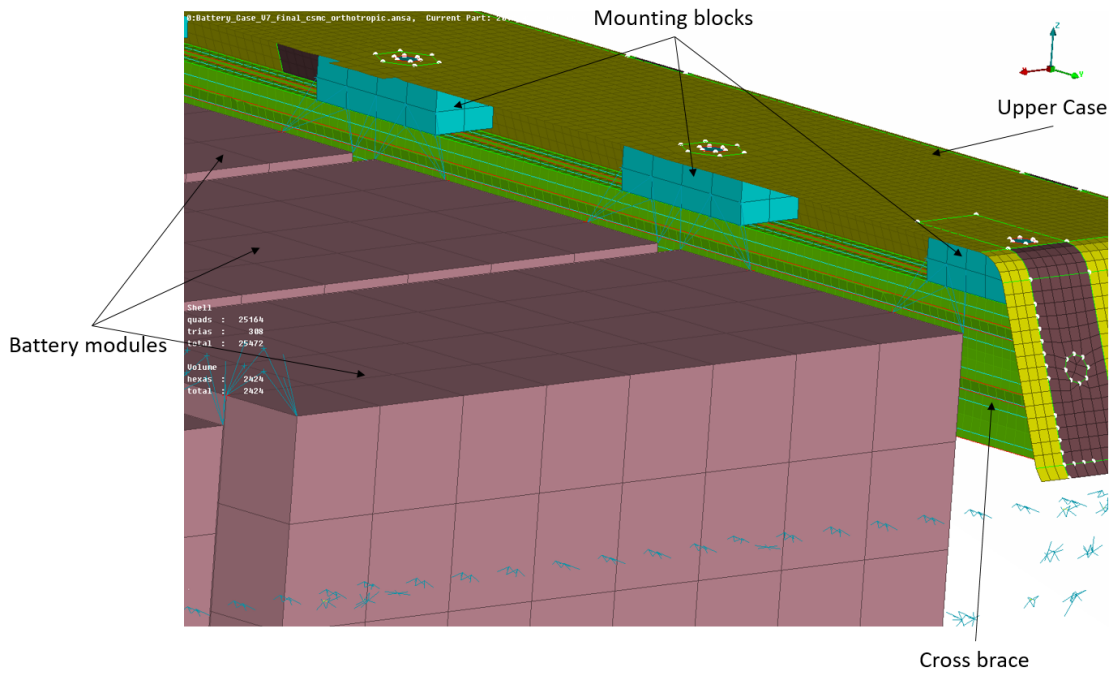


Figure 25 Mounting blocks with their connections to the other components of the battery

3.1.6 Battery modules

In the battery case there are 24 battery modules. The modules are designed as a rectangular box out of 72 C3D8 solid elements for each. This simplification was made because there is no interest in the behavior of the components in the module. A more precise modeling would lead to a larger number of elements and increase the calculation effort.

The Battery module is connected with the heat conduction plate with an adhesive connection Figure 26. Figure 27 shows the upper side of the module, a Distributing coupling between the mounting block ensures a fixed connection with the upper battery half.

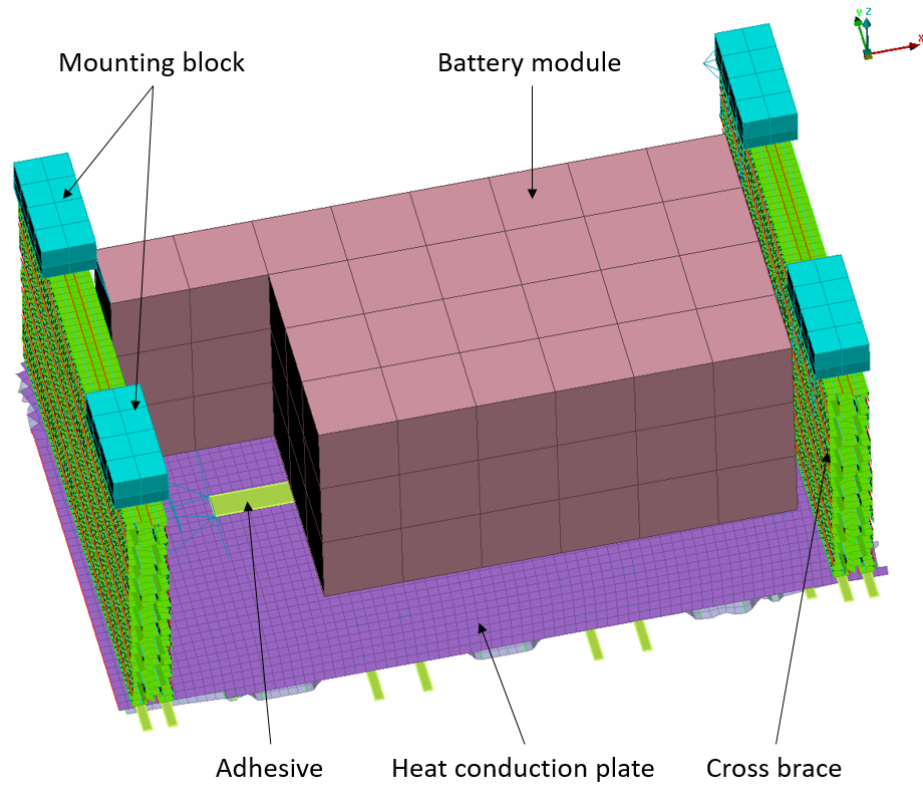


Figure 26 Battery module with the adhesive connection to the Heat conduction Plate

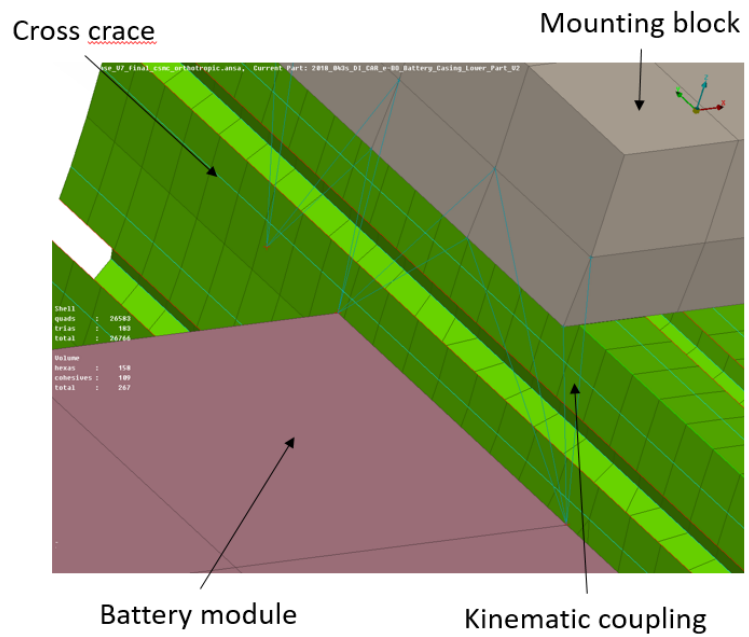


Figure 27 Detailed view distributing coupling between the mounting block and the battery module

3.1.7 Crush Plate

The crush plate is modeled according to ISO 12405-3:2014(E) [28]. It has a dimension of 600 mm x 600 mm, with three half cylinders with a radius of 75 mm. The geometry of the plate is described in the simulation using 35478 RC3D4 elements. The "RC3D4" in Abaqus denotes a three-dimensional rigid element with four nodes. The element size was chosen to be small, so that the circular contour of the crush plate is approximated as closely as possible. Furthermore, the edge length of the rigid element does not influence the time increment in the explicit time integration scheme. That means a small element size can be used and does not affect the calculation cost. The 'rigid body' couples the movement of the individual nodes of the rigid elements and brings them together on a reference node of the 'rigid body'. Thus the relative position of the nodes of the rigid elements to the reference node always remains the same. For this reason, the boundary conditions and loads are always applied to the reference node of the rigid body. By using this definition for the crush plate elements, they are no longer deformable and the element stiffness calculations are not performed for these elements. [26]

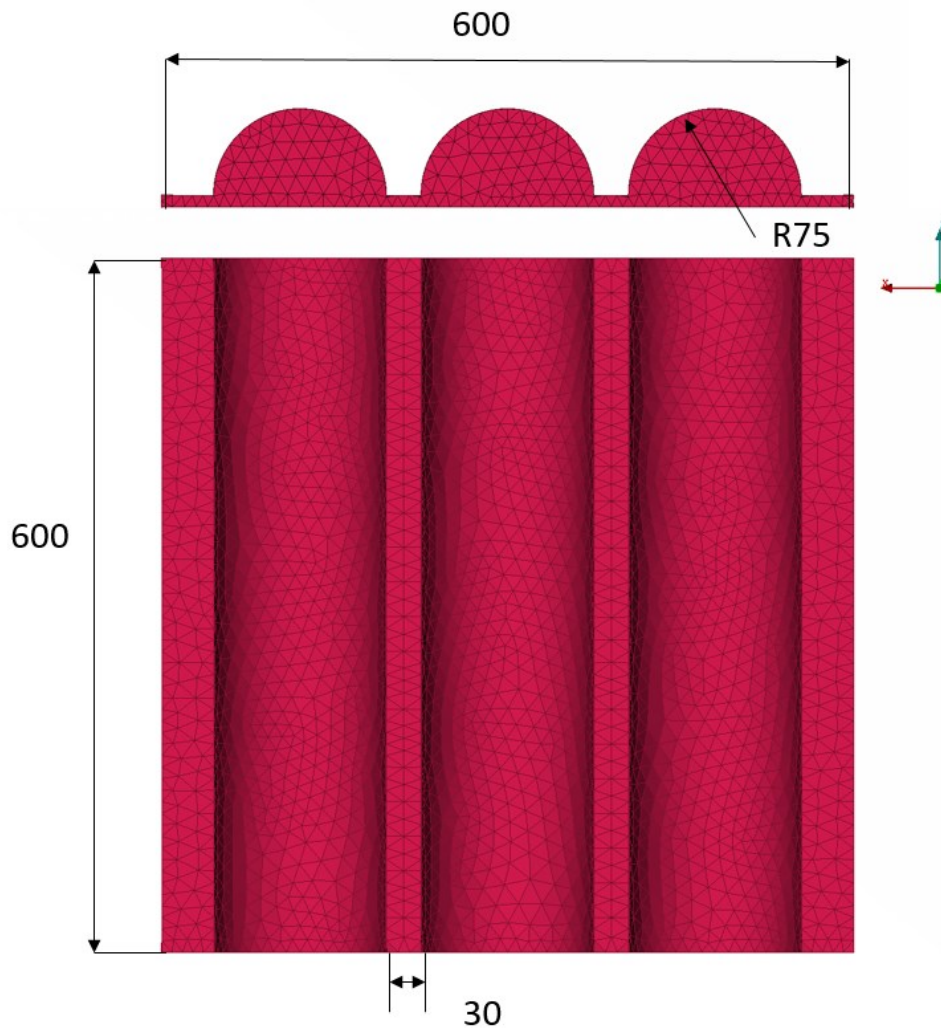


Figure 28 Crush Plate used for the crash simulation of the battery case. Dimensions after ISO 12405-3:2014(E)

3.1.8 Contacts

For the simulation, contact conditions must be defined between the individual components that have a contact to each other. The contacts in this model are explained here.

3.1.8.1 Tied Contact

A tied contact in Abaqus can be understood as two surfaces that are glued together for the time of the simulation. That means that each node of the slave surface has the same value of displacement, temperature, pore pressure or electrical potential as the point of the master surface that it contacts. In general, the mesh size of the slave surface needs to be smaller as the mesh of the master surface. The master surface is able to penetrate the slave but not vice versa [26]

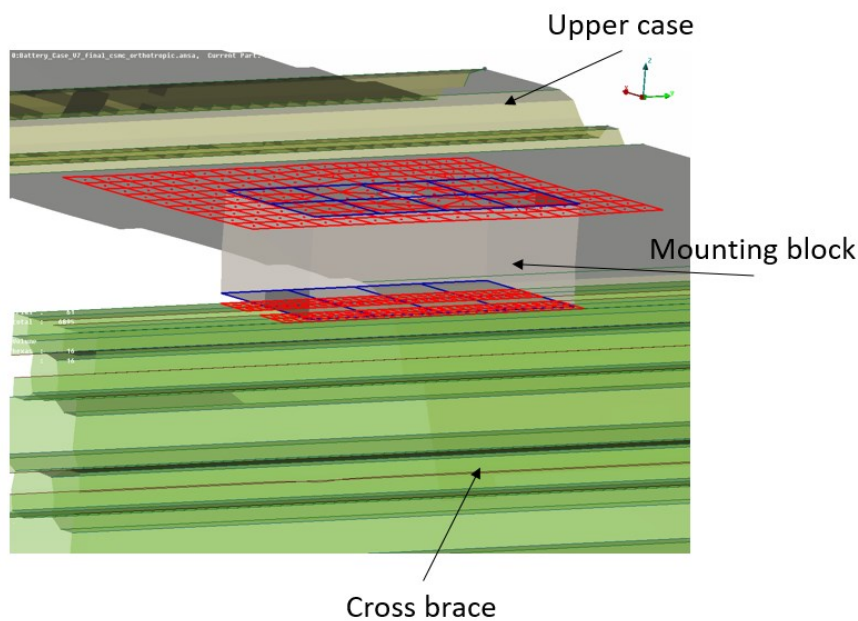


Figure 29 Tied contact between the mounting block, the cross brace and upper case. The red area indicates the slave surface and the blue one the master surface

The slave surface is always red and the master surface blue, Figure 29. In the initial model, the mounting block and upper case are bolted together. This leads to a rigid connection between the two components. With the assumption that the C-SMC material of the housing is the weakest part of the connection, and in case of a failure it is going to break first. The Tied contact is definitely not physically correct, but with this assumption, it can be used.

The second connection in Figure 29 is the tied contact between the mounting block and the cross brace. In the original model the mounting block is bolted with two slot nuts onto the brace. The exact modeling of this connection would result in two additional bolts and slot nuts for each block. Since the other connection has already been simplified, it makes no sense to reproduce this connection exactly and thereby increase the calculation time with additional elements.

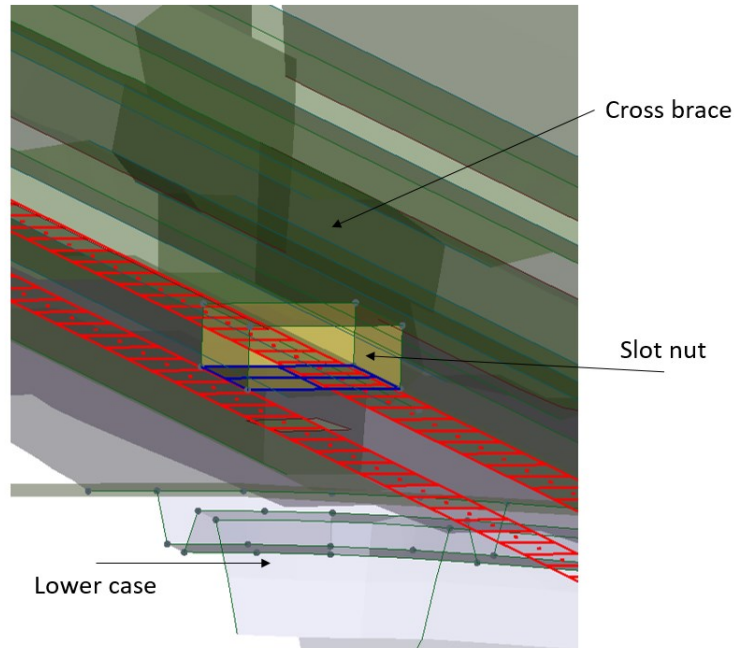


Figure 30 Detailed view of the tied contact between the cross brace and the slot nut

Figure 30 shows the slot nut that is connected, with a tied contact, to the cross brace. In the original model, the slot nut is screwed to the lower half of the housing. The contact pressure of the screw connection then holds the nut in the groove of the cross brace. In this model bolt connections are modeled without the assembly pressure. The model uses a tied contact between the cross brace and the slot nut to ensure a tight fit

3.1.8.2 Contact pair crush plate/Battery case

At the surfaces between the crush plate (blue) and the battery case (red) a friction afflicted contact forms, shown in Figure 31. This contact uses a node to surface contact with a small amount of contact damping to reduce the solution noise.

The friction between the two surfaces depends on many influencing factors and is difficult to model in detail. The two contact partners characterize the behavior of the tribological contact system. In addition to material and surface properties, other factors such as the type of load, speed or temperature play an important role. For modeling of the friction, the simulation uses the simplified approach of Coulomb. It is difficult to determine the coefficient of friction because no test data are available to determine the friction between the two surfaces. For this reason, the coefficient of friction was not dependent on the slip rate or the contact pressure, and was assumed to be 0.1 with the help of the literature. [29]

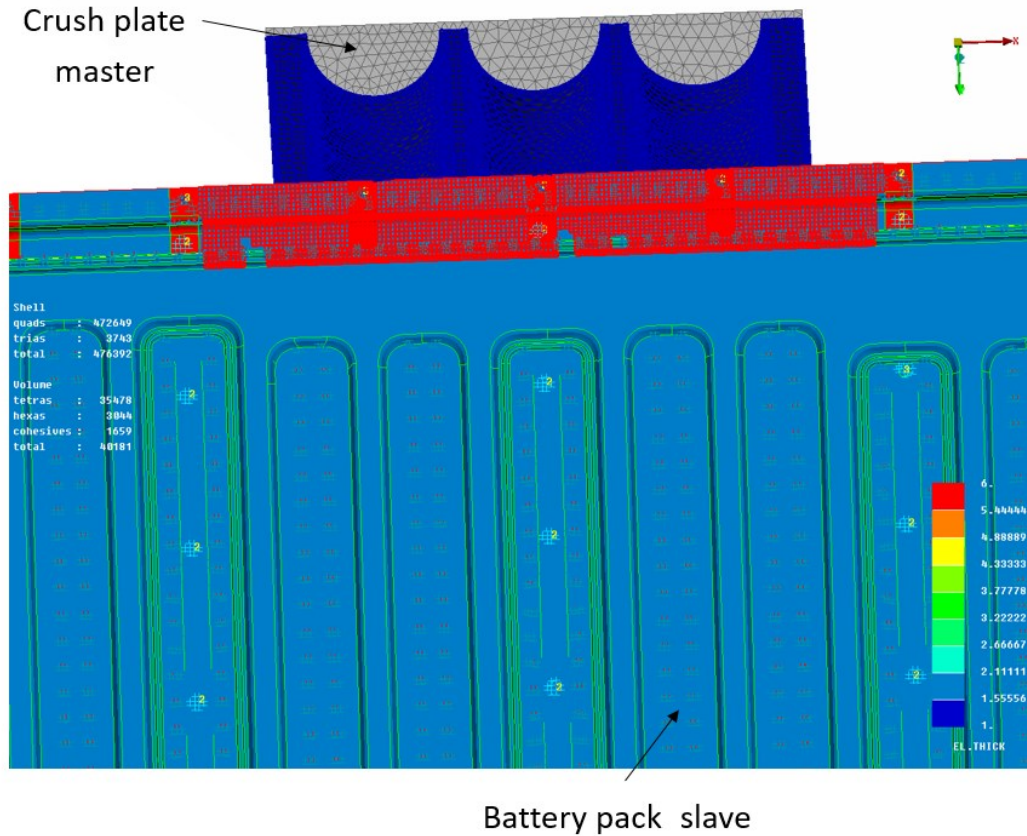


Figure 31 Contact between the battery pack (red area) and the crush plate (blue area)

3.1.8.3 Contact all exterior

The crash simulation leads to very large deformations of the model. This means that it is necessary to define a contact condition for all surfaces. Otherwise, it is possible that the components move into one another without any resistance. It is a very big modeling effort to create a contact condition between each element. As an example, a contact area would have to be defined for all adhesive elements. Therefore, this model uses the contact inclusion function. In Abaqus this function is used to specify self-contact surface pairings that are used by the contact algorithm. [26]

3.1.9 Distributing coupling constraint

A distributing coupling constrains the motion of the coupling nodes to the translation and rotation of the reference node. [30, 26]

3.1.10 Adhesive connection

There are approx. 50 meters of adhesive lines in the model. These lines are modeled with the help of cohesive elements.

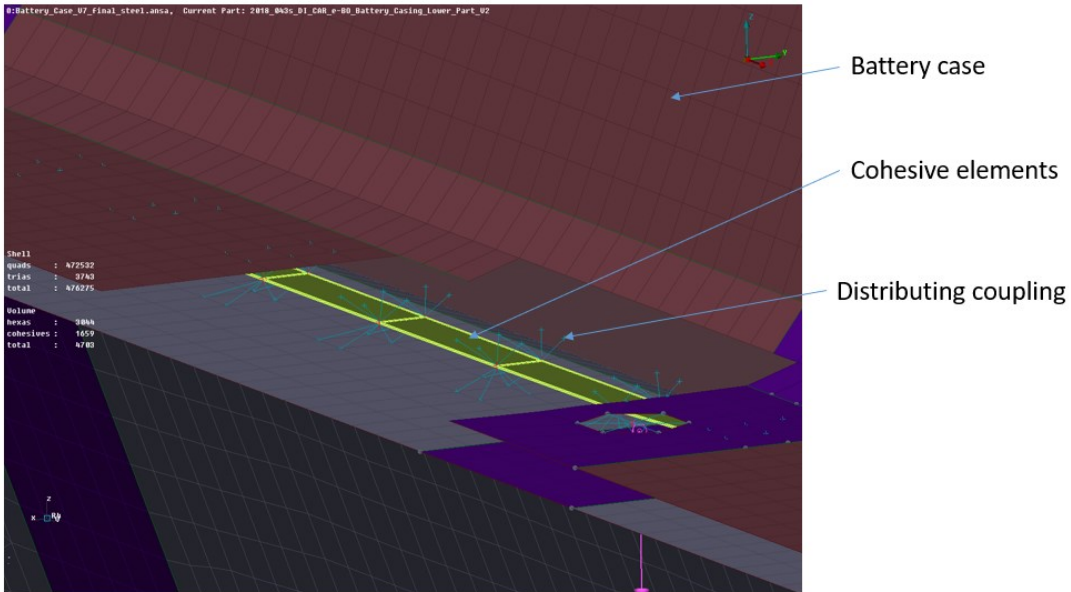


Figure 32 Gasket area of the battery case. The yellow elements represent the cohesive elements, used to model the adhesive connection between the upper and the lower half of the case.

All connections in the model use the same procedure they only differ in the length and width of the individual cohesive elements. Figure 32 shows such a connection schematically, the connection between the element and the parts of the model is achieved through four distributing couplings at each of the four integration points of the element. For the calculation of the damage to the adhesive bond, the simulation uses linear elastic traction-separation behavior, see 3.2.5.1.

3.1.11 Bolt connection

For the bolts in the model B31 Beam, elements are used. In Abaqus B31 is a 2-node linear beam element. A distributing coupling connects the bolt with the part shown in Figure 33. The contact force and assembly pressure of the screws is neglected with this simple design. All the bolts in the simulation model use the same modeling procedure.

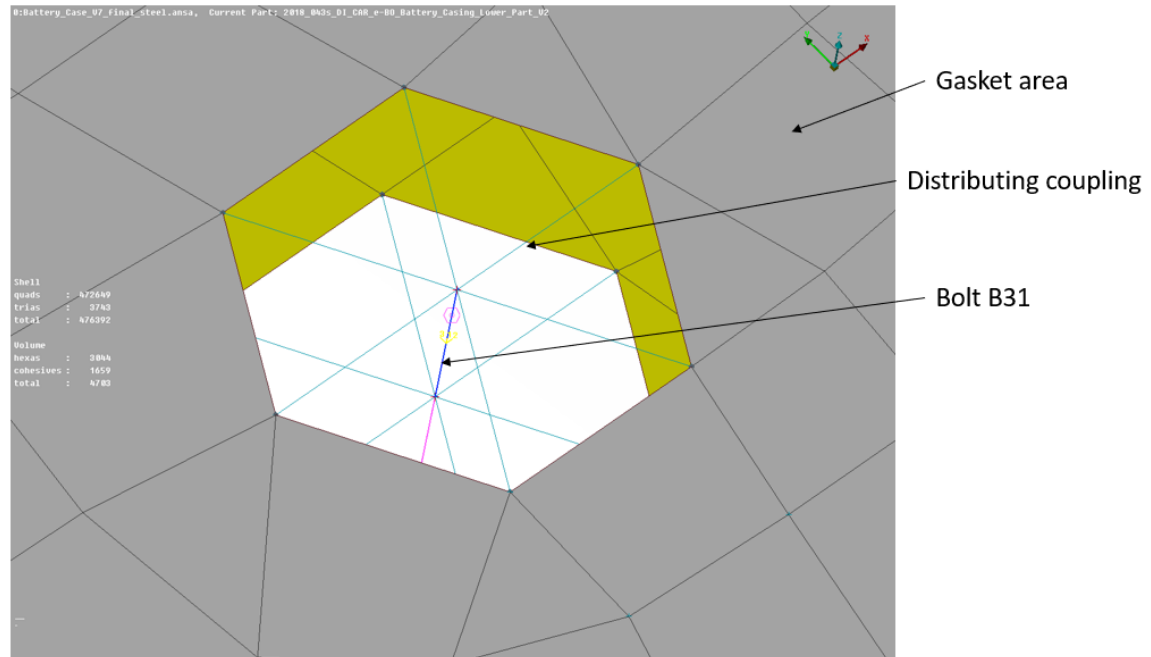


Figure 33 Gasket area of the battery case with the bolt connection

3.1.12 Boundary Conditions and Loads

In order to be able to solve the equations of motion of an FE model, the degrees of freedom of the simulation model must be limited with boundary conditions. With these conditions, you can either block the movement in of nodes in certain directions or specify a displacement, speed or acceleration. The degrees of freedom 1 to 3 correspond to directions x, y and z for the translational movement those from 4 to 6 correspond to the rotation around axis x, y and z. For this reason the model of the battery crash test uses boundary conditions for the battery case and the crush plate, see Figure 34.

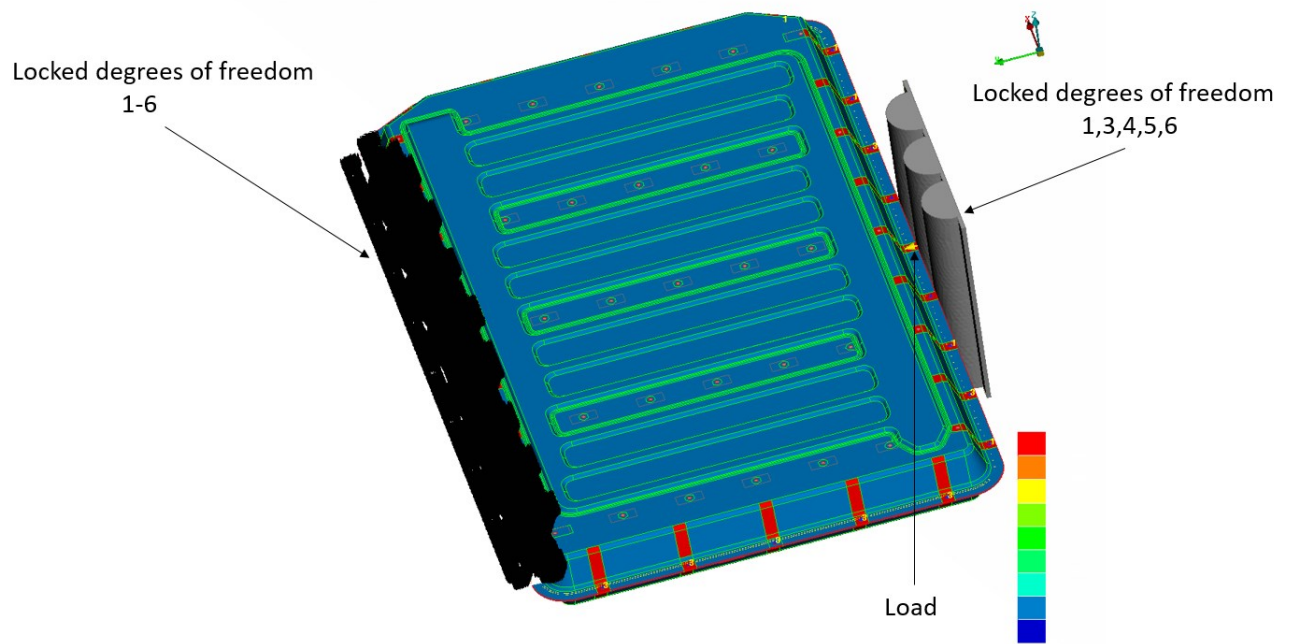


Figure 34 Boundary and loading condition of the Battery Pack

The battery case is fixed at the opposite side of the crush plate (dark grey area marks the nodes that are fixed), that means that all the degrees of freedom 1-6 are locked and this part of the case could not move translational or rotational.

At the crush plate all three rotational degrees of freedom are locked, this should prevent all rotations of the plate. In addition, translational movement in 1 and 3 direction is locked, the plate is only moveable in the y (=2) direction.

The aim of this simulation is to obtain a force-displacement curve for the crush plate and then to compare it with results for the other material definitions of the battery case. For this reason, one of these two variables has to be specified for the simulation model in order to then obtain the second variable as a result from the FE calculation of the model. This calculation uses an increasing force at the reference note of the plate in the y-direction. This corresponds to the in the ISO 12405 defined testing load.

In the test defined by the International Standard the force applied shall be 100 kN with a ramp up time of less than 3 minutes and a holding time of at least 100 ms but not exceeding 10s. [28].

For the explicit simulation, it is not possible to model the whole duration of the real world test, why is described in chapter 0

Simulation. The force at the crush plate increases over the time of the simulation, see Figure 35. The used exponential function is described by:

$$y(t) = \left(\frac{t}{t_1}\right)^3 \times \left(10 - 15 \times \left(\frac{t}{t_1}\right) + 6 \times \left(\frac{t}{t_1}\right)^2\right) \quad 3-1$$

Where t_1 marks, the point where the full load is applied (a multiplication factor of one). The total simulation time for this crash test is 2 seconds and t_1 is 1.8 seconds. That means the ramp up phase is finished at 1.8 seconds and the resulting holding time is 0.2 seconds.

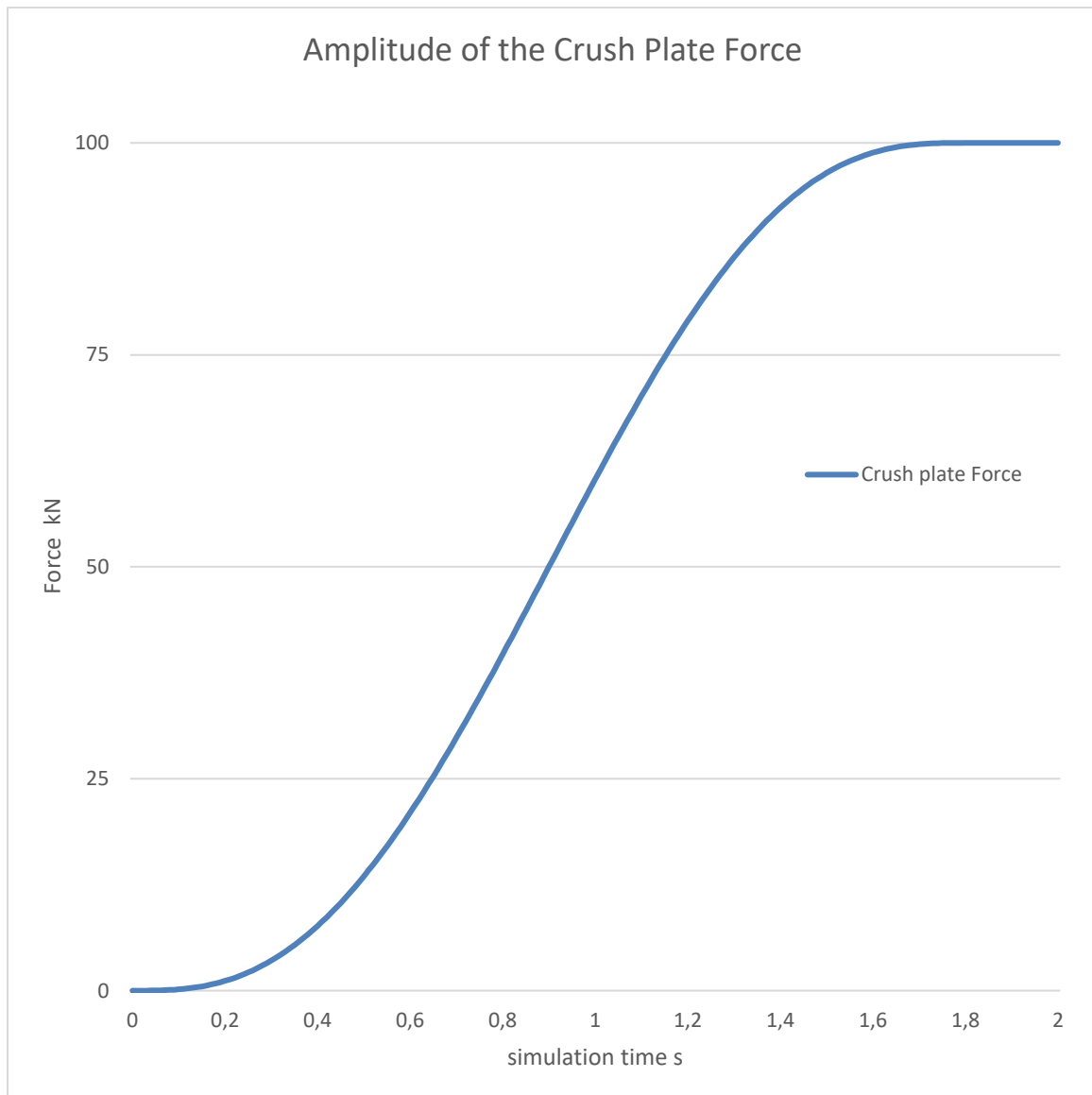


Figure 35 Amplitude for the loading of the crush plate in direction y over the simulation time

3.1.13 Meshing of the FEM-Model

For an explicit simulation, it is necessary to limit the size and number of the elements to keep the computational effort as low as possible. For explicit simulations, the size of the used elements has

a direct impact on the smallest stable increment and thus the computational time. The maximum stable time increment is expressed by the following equation:


$$\Delta t \leq \left(L_e \sqrt{\frac{\rho}{\hat{\lambda} + 2\hat{\mu}}} \right) \quad 3-2$$

Where L_e is the characteristic length of an element and ρ the density of the material and $\hat{\lambda}$ and $\hat{\mu}$ are the effective Lamé's constants for the material. Defined by:

$$\hat{\lambda} = \frac{E\nu}{(1 + \nu)(1 - 2\nu)} \quad 3-3$$

$$\hat{\mu} = \frac{E}{2(1 + \nu)} \quad 3-4$$

For this reason, the target was to keep the element size as big as possible, to get results with reasonable calculation effort. Quality criteria are used to check the elements size and to improve the shape of the elements. Figure 36 shows the used quality criteria; for example the min length of the shell element was set to 4 mm to keep the characteristic length over a certain level. The other criteria should improve the general quality of the mesh in order to avoid stability problems caused by extremely distorted elements.

 Quality Criteria - Presentation Parameters

Name:

Shells Solids Graph Parameters Presentation Parameters








Criteria	Calculation	Color	Failed
<input checked="" type="checkbox"/> aspect ratio	NASTRAN		3.
<input checked="" type="checkbox"/> warping	IDEAS		25.
<input checked="" type="checkbox"/> min length			4.
<input checked="" type="checkbox"/> min angle quads	IDEAS		40.
<input checked="" type="checkbox"/> max angle quads	IDEAS		150.
<input checked="" type="checkbox"/> min angle trias	IDEAS		30.
<input checked="" type="checkbox"/> max angle trias	IDEAS		150.

Figure 36 Quality Criteria used for the discretization of the shell elements for the battery pack

3.2 Material Definition

This chapter gives an overview of the materials used in the FEM simulation and their definition

3.2.1 Orthotropic material behavior

The material data used in this Thesis for the behavior of the material are verified by by static and dynamic experiments. [6]

Table 5 shows the material model used to simulate the crash test. In order to get better simulation results , the strain rate dependence of the SMC material is modeled with the viscous regularization. The values for this were determined by iterating the simulation with different viscosity coefficients.

Table 5 Material Model for Orthotropic material behavior [6]

Failure Energy	[mJ/mm ²]	Failure Stress	[N/mm ²]
G_f^+	180	σ_f^+	600
G_f^-	180	σ_f^+	600
G_m^+	140	σ_m^-	130
G_m^-	140	σ_m^+	130
viscosity coefficient		τ_f	130
η	0.001	τ_m	130

3.2.1.1 Random element orientation

The damage initiation and evolution model used for the simulation differentiate between the longitudinal and transverse fiber direction. Therefore, a fiber direction must be specified for each shell element of the battery case. [6]

The CF-SMC material is composed out of a high number of fiber chips that are held together by resin. Before the curing process, the chips are laid horizontally. While the curing and pressing they move relative to each other and flow into the tool's form. The high number of chips and the complex disposition lead to a great modelling challenge. It might be possible to model the exact orientation of the fibers, thru a process simulation but the calculation effort will be enormous. [7]

Every shell element of the battery case gets an in-plane random orientation with a value between 0°-180° (Figure 37). The FEM input file was modified the with a MATLAB script.

The exact layering of the fibers and the exact size of the fibers is neglected with this approach. But it allows the damage to travel along a complex path. This recreates a stochastic crack propagation which was observed during the tests. [6, 7]

In Figure 37 the fiber orientation is shown across all elements. The fiber orientation is shown averaged over the element boundaries. The lines should represent the fiber orientation of the longitudinal direction of the fibers. In Figure 38 the fiber orientation is visible in an element by means of vectors.

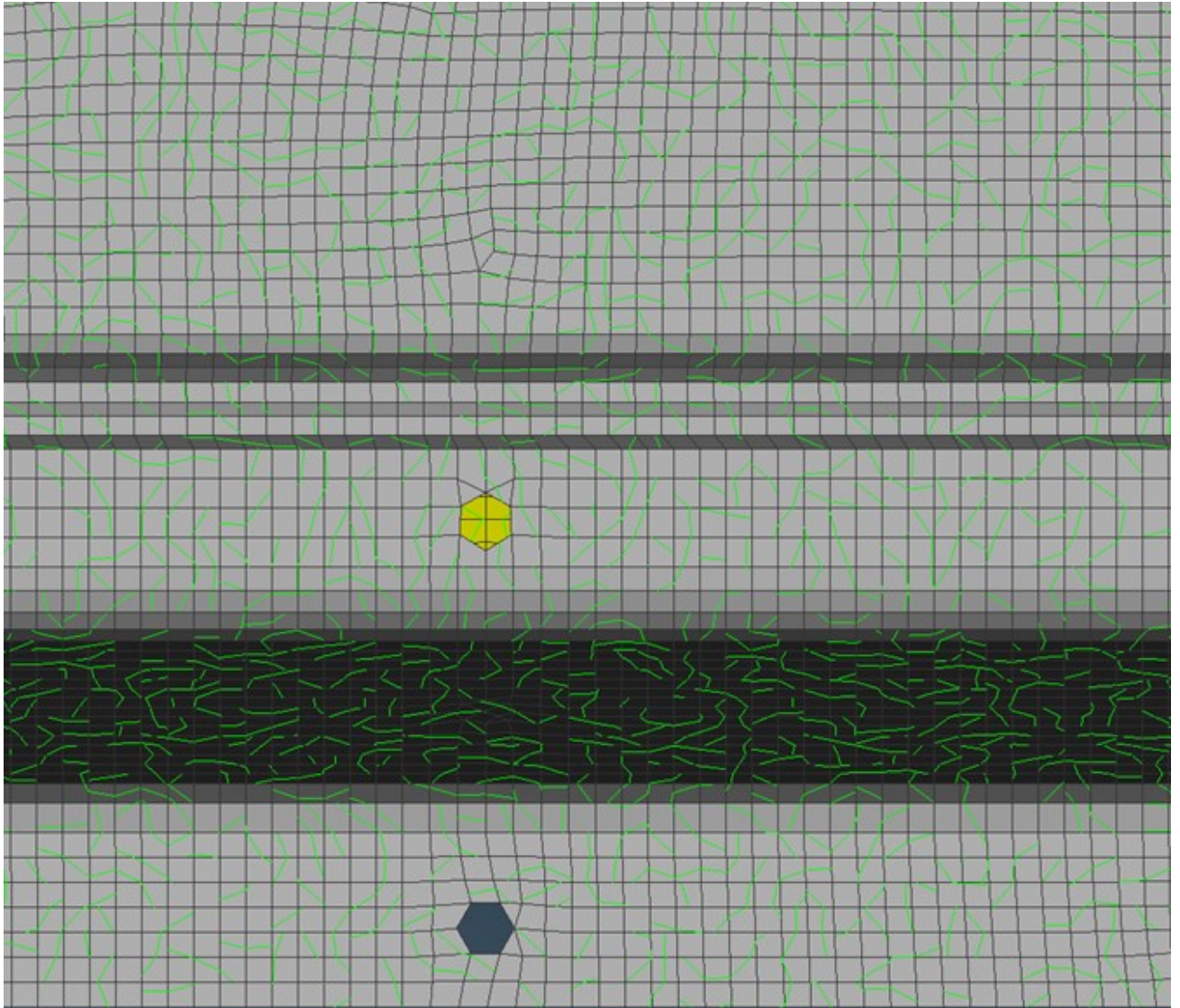


Figure 37 FEM Model close up of the Battery Case shows the random fiber orientation.

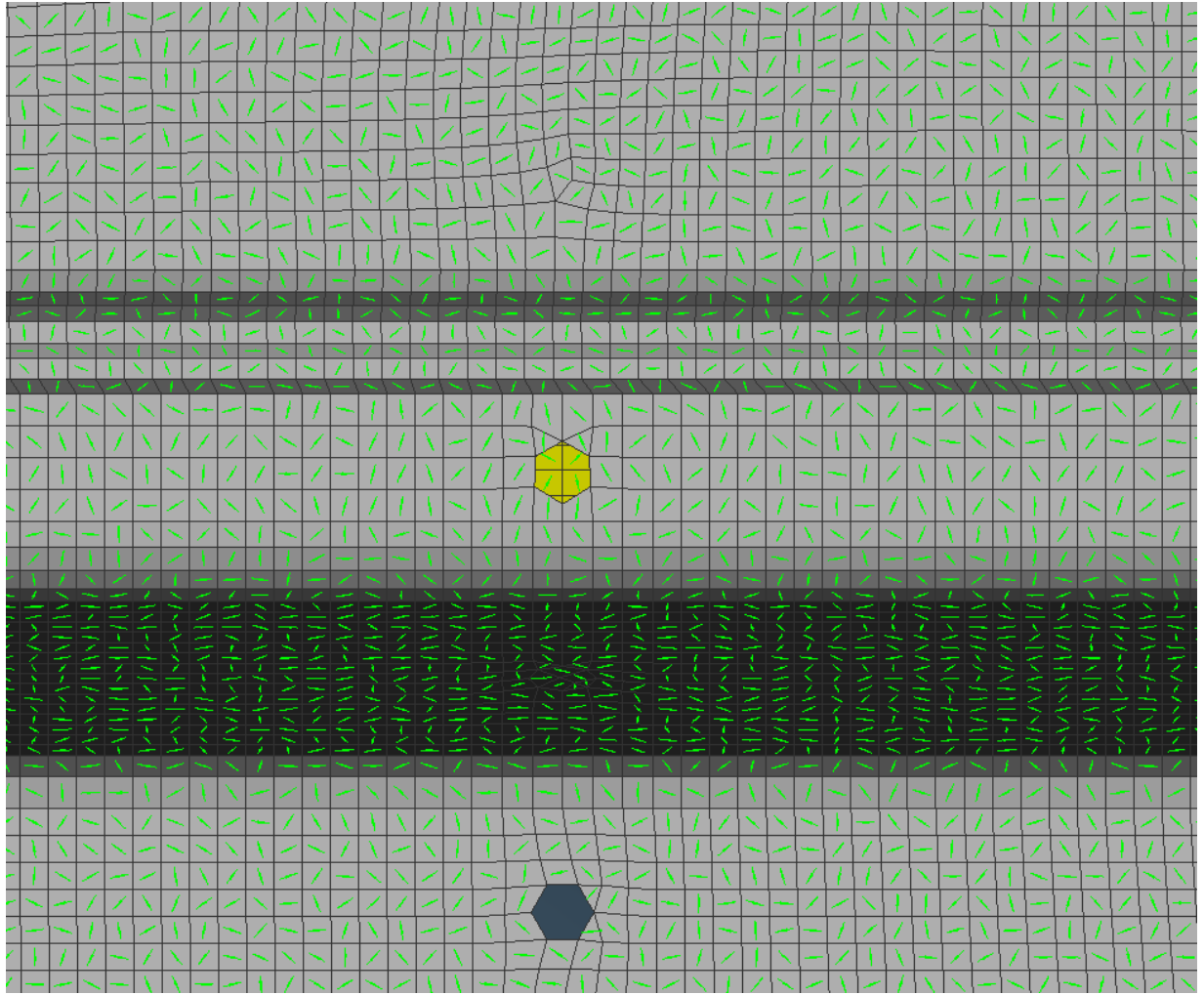


Figure 38 FEM model close up of the Battery Case showing the Fiber orientation by means of a vector (green arrow)

3.2.2 Quasi-isotropic material behavior

In order to understand the possible influences of the modeling technique the SMC material of the case is modeled as a quasi-isotropic material. In the case of isotropic behavior, the material properties in longitudinal and transversal fiber direction are equal. The Johannes Kepler University Linz provided the data [31].

Table 6 quasi-isotropic material behavior with average values Engineering constants for HexMC M77 [32]

E ₁	38000 [MPa]
E ₂	38000 [MPa]
E ₃	9500 [MPa]
ν ₁₂	0.3 [-]
ν ₁₃	0.087 [-]
ν ₂₃	0.087 [-]
G ₁₂	15000 [MPa]
G ₁₃	3900 [MPa]
G ₂₃	3900 [MPa]

The Hashin criterion is used to predict the damage initiation and for the damage evolution the same linear progressive damage evolution model, as for the orthotropic material is applied.

Table 7 Strength and Energy values for quasi-isotropic behavior HexMC M77 [32]

Failure Energy	[mJ/mm ²]	Failure Stress	[N/mm ²]
G _f ⁺	55	σ _f ⁺	300
G _f ⁻	55	σ _f ⁺	300
G _m ⁺	55	σ _m ⁻	290
G _m ⁻	55	σ _m ⁺	290
viscosity coefficient		τ _f	250
η	0.001	τ _m	250

3.2.3 Aluminium

For this thesis no data are available for the aluminum and steel parts. A simple shear failure model is used to model the material fails failure.

3.2.3.1 Shear failure Criterion

The Shear failure model uses the equivalent plastic strain of the element integration points; failure occurs when the damage parameter ω reaches one, ω is defined as:

$$\omega = \frac{\bar{\varepsilon}_0^{pl} + \sum \Delta \bar{\varepsilon}^{pl}}{\bar{\varepsilon}_f^{pl}} \quad 3-5$$

Methodology

Table 8 Damage parameter definition of variables

$\bar{\varepsilon}_0^{pl}$	initial value of the plastic strain
$\Delta\bar{\varepsilon}^{pl}$	is an increment of the equivalent plastic strain of the element
$\bar{\varepsilon}_f^{pl}$	plastic strain at failure (defined with tabular data)

When the criterion is met at an integration point of an element the stress components are set to zero and the point of the element fails. If all of the integration points of one element fail, the element is removed from the model. For example for a S4 shell element, all four integration points must fail before the element is removed. [26]

3.2.3.2 Material Data

Table 9 Equivalent Plastic Strain and Stress Ratio for Shear failure for Al-0.5Mg-0.45Si [33]

Equivalent Plastic Strain	Stress Ratio [MPa]
0	100
0.05	150
0.15	200
0.25	220
0.4	250
0.5	260
0.65	270

Table 9 shows the tabular data used by abaqus to predict the shear failure criterion. Before 100 MPa the aluminum has pure elastic behavior, that means all deformations of the material are elastic and reversible. After reaching 100 MPa Irreversible plastic deformation starts, till the damage parameter reaches 1 and the element is removed from the model.

Table 10 Material Data used in Abaqus for Al-0.5Mg-0.45Si

Density	2.7 [kg/dm ³]
E-Modulus	70000 [MPa]
Poisson-Ratio	0.334 [-]
Equivalent plastic strain at failure	0.5 [-]
Element deletion	yes

3.2.4 Steel

The steel uses the same shear failure criterion as described in chapter 3.2.3.1. Therefore, the material data used are:

Table 11 Equivalent Plastic Strain and Stress Ratio for Shear failure for stainless steel grade 1.4301 [34]

Equivalent Plastic Strain	Stress Ratio [MPa]
0	300
0.02	350
0.05	400
0.15	500
0.4	600
0.6	650

Table 12 Material Data used in Abaqus for stainless steel grade 1.4301 [34]

Density	7.9 [kg/dm ³]
E-Modulus	200000 [MPa]
Poisson-Ratio	0.3 [-]
Equivalent plastiv strain at failure	0.6 [-]
Element deletion	yes

3.2.5 Cohesive Material

There are various adhesive lines in the simulation model of the battery case, see 3.1.9; also for them, a material modell with failure prediction and element deletion must be introduced. The in Abaqus available traction separation model is used for this reason

3.2.5.1 Linear elastic traction-separation behavior [26]

The model assumes linear elastic behavior followed by the damage initiation and a damage evolution model. This is similar to the model that is used for the csmc material of the battery case described in 2.6.2.1. The elastic behavior is modeled by an elastic constitutive matrix that can be written as:

$$\vec{t} = \begin{pmatrix} t_n \\ t_s \\ t_t \end{pmatrix} = \begin{bmatrix} E_{nn} & E_{ns} & E_{nt} \\ E_{ns} & E_{ss} & E_{st} \\ E_{nt} & E_{st} & E_{tt} \end{bmatrix} \begin{pmatrix} \varepsilon_n \\ \varepsilon_s \\ \varepsilon_t \end{pmatrix} = E\varepsilon \quad 3-6$$

The nominal stresses are the force components divided by the original area at each integration point and the nominal strains are the separations divided by the original thickness at each integration point. The traction stress vector \vec{t} has three components: the normal traction t_n , and the two shear tractions t_s , t_t . [26]

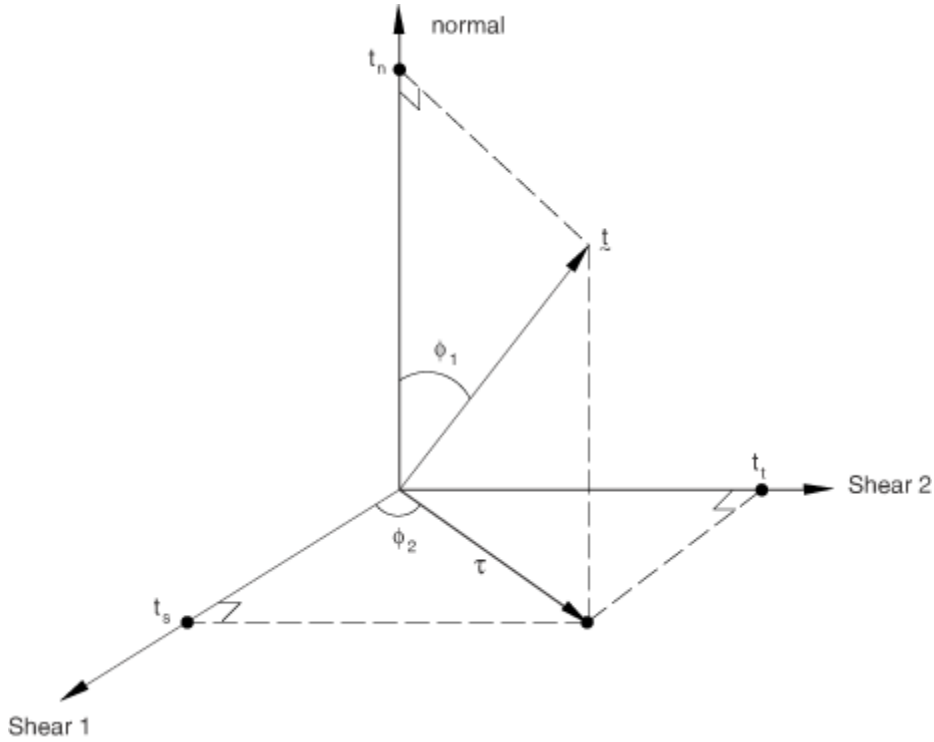


Figure 39 Three directions of the traction stress vector: one normal and two shear directions [26]

The nominal strains are expressed by the following equation:

$$\varepsilon_n = \frac{\delta_n}{T_0}, \varepsilon_s = \frac{\delta_s}{T_0}, \varepsilon_t = \frac{\delta_t}{T_0} \quad 3-7$$

Where δ_n , δ_s and δ_t represent the separations and T_0 is the original thickness of the element. [26]

3.2.5.2 Damage initiation [26]

Damage initiation marks the starting point where the material gets affected first and the degradation starts. To determine the point where the material starts to degrade the maximum stress criterion is used. Damage starts when the nominal stress ratio reaches a value of one which is calculated by:

$$\max \left\{ \frac{\langle t_n \rangle}{t_n^0}, \frac{t_s}{t_s^0}, \frac{t_t}{t_t^0} \right\} = 1, \quad 3-8$$

Where t_n^0 , t_s^0 , t_t^0 represent the stress values in the corresponding direction where the initiation criterion is met.

3.2.5.3 Damage evolution [26]

For the damage evolution a linear progressive model is used based on the effective displacement.

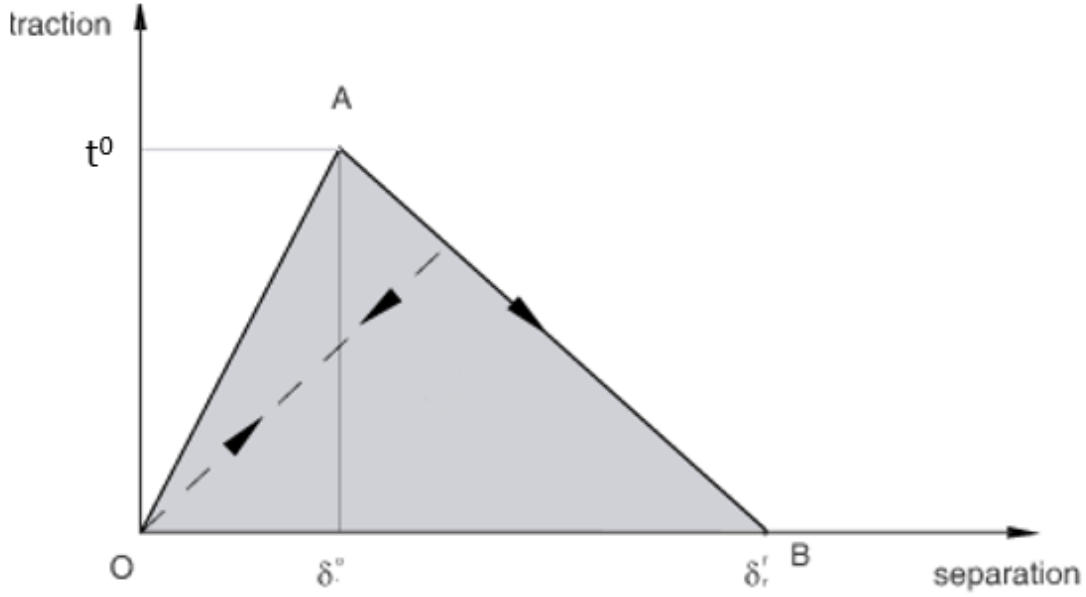


Figure 40 Linear Damage evolution model. O-A shows the pure linear elastic traction behavior before the damage initiation. A-B represents the linear damage evolution model based on separation. At t^0 , the damage criterion is satisfied and the material is degraded. [26]

A scalar damage variable D is introduced to describe the overall damage of the material, the initial value of the variable is zero. After the initiation criterion is satisfied, D starts to evolve until a value of one is reached (=complete damage). The stress components of the traction separation model is affected by the variable D as followed:

$$t_n = \begin{cases} (1 - D)\bar{t}_n & \bar{t}_n \geq 0 \\ \bar{t}_n \text{ no damage to compressive stiffness} & \bar{t}_n < 0 \end{cases}$$

$$t_s = (1 - D)\bar{t}_s \quad 3-9$$

$$t_t = (1 - D)\bar{t}_t$$

where $\bar{t}_n, \bar{t}_s, \bar{t}_t$ are the stress components calculated by the solver without Damage. For the description of the damage under a combination of the normal and shear load across the element an effective displacement after Camanho and Davila, 2002 is introduced which is defined as:

$$\delta_m = \sqrt{(\delta_n)^2 + \delta_s^2 + \delta_t^2} \quad 3-10$$

For evolution of D the model used is based on effective displacement and is described after Camanho and Davila, 2002 by:

$$D = \frac{\delta_m^f (\delta_m^{max} - \delta_m^0)}{\delta_m^{max} (\delta_m^f - \delta_m^0)} \quad 3-11$$

Where δ_m^f refers to the effective displacement at component failure, δ_m^0 to the effective displacement at damage initiation and δ_m^{max} to the maximum value of the effective displacement during the loading history. The maximum value of D can be chosen between zero and one by default the upper value of $D=D_{max}=1$. If the damage variable reaches a value of D_{max} at all integration points the cohesive element gets removed from the model.

3.2.5.4 Material Data for the adhesive

Table 13 Data for the adhesive used in Abaqus [35]

Density	1.6 [kg/dm ³]
E-Modulus	65 [MPa]
Tensile strength	10 [MPa]
effective displacement at failure	0.2 [mm]
Element deletion	Yes

3.3 Simulation Technique

For every FE simulation, it is necessary to define how to analyze the system, before the simulation model is built. There are various techniques to analyze a model and they all lead to different results even if the boundary and loading conditions are the same. [24]

3.3.1 Static vs. Dynamic

The difference between a static and a dynamic analysis is how the forces are balanced within the system. In static analyses the applied loads do not change over time and inertia effects are neglected. If there is any time dependence in the model, a dynamic analysis is needed. In this thesis the load of the crush plate ramps up over the time (see Figure 35), therefore it is mandatory to use a dynamic analysis. In a dynamic analysis, the user determines the total simulation time and then the solver divides it into small increment. The simulation runs until the defined total simulation time is elapsed, even if parts are still moving or the load has not fully been applied. [24]

3.3.2 Implicit vs. Explicit

Since the general equation of motion is a function of time, it must be discretized for the application of numerical methods. This includes explicit and implicit time integration methods. In the case of implicit methods, the stiffness matrix of the new time step depends on the unknown displacement. For this reason for structural mechanical evaluations, an equilibrium iteration between the unknown stiffness matrix and the unknown displacement must be used. The stable time integration of this method makes large time intervals possible, which leads to less computational effort. Non-linearities lead to a high number of iterations or small time increments and thus to a high computational effort. These nonlinearities in the model can lead to divergence and thus lead to the abortion of the simulation. [36, 37, 6]

The explicit time integration does not need an iteration for the unknown stiffness matrix, because it uses the stiffness matrix from the time step before. This is possible since this method assumes a linear behavior of the changes of the stiffness matrix between the increments. This leads to a lower computational effort per increment, but due to the assumption of linear change in state of the element from one increment to the next small-time steps are necessary for this method to be stable. The time steps are orders of magnitude smaller than the time steps in an implicit method. [24]

The size of the time step depends on the density of the material and the size of the used elements. The largest stable time step is defined by the highest eigenvalue of the system ω_{max} . [6]

$$\Delta t_{max} = \frac{2}{\omega_{max}}$$

3-12

Using the highest Eigenvalue to calculate the range of the stable time step has a physical interpretation. By doing so, the maximum time step is set approximately equal to the time for an elastic wave to cross the smallest element dimension in the model. [24]

Explicit methods are best suited for impact dynamic analyses. Furthermore, the explicit method has advantages, if the nonlinear element behavior would bring the implicit calculation to its limits by a large number of equilibrium iterations. [24]

For these reasons, an explicit simulation method was chosen for the simulation of the crash test in this thesis.

3.3.2.1 Quasi static analysis

The real world crash test of the battery pack has very slow loading rate, but large deformations. Therefore a quasi-static simulation model must be used.

Modeling an explicit dynamic simulation as a quasi-static event requires special consideration. It would take a very long time to compute the whole process in its real time, millions of increments would be required. Therefore, the simulation must use a technique to increase the speed of the simulation time. The goal of this is to model the process in the shortest time period possible, in which the inertia forces are still insignificant. To make sure that these forces are insignificant two conditions have to be met: The loading rate and Energy balance.

3.3.2.1.1 Loading Rate

A general recommendation for quasi-static analyses is to limit the impact velocity to less than 1% of the wave speed in the material. As an approximation for the wave speed in the material, the following equation was used: [26]

$$c_{material} = \sqrt{\frac{E}{\rho}} \tag{3-13}$$

The results are:

Table 14 Wave speed in the materials used for the battery case

Material	Young's Modulus E [MPa]	Density ρ [kg/dm ³]	c _{material} [m/s]	1% of c _{material} [m/s]
C-SMC	38000	1.55	4951	49.5
Steel	210000	7.8	5188	51.2
Aluminium	70000	2.7	5091	50.9

It should be mentioned that for the CF-SMC material the wave speed is rough estimate. The data from crash test experiments with the CF-SMC hat profile showed that a value of 5000 m/s a good approximation and accurate enough for this use case. [6, 7]

The simulation time and the loading speed of the crush plate were chosen to not exceed a crush plate speed of 50 m/s. A series of simulations was needed, with variations of the total time and the amplitude of the force acting on the crush plate, to meet this criterion

3.3.2.1.2 Mass Scaling

In this simulation, the speed of the crush plate depends on the duration of the force application. In order to reduce the speed of the crush plate, the simulation time must be increased. Since the maximum time step remains the same, the number of increments required increases. This leads to a higher computational effort.

Mass scaling is used in this simulation to perform the simulation more economically. The following equation shows how the time increment is calculated:

$$\Delta t \leq \left(L_e \sqrt{\frac{\rho}{\hat{\lambda} + 2\hat{\mu}}} \right) \quad 3-2$$

According to this equation artificially increasing the material density ρ by a factor f^2 increases the stable time increment by a factor f . This means the global stability limit for the explicit analysis is increased which leads to fewer increments to perform the same analysis. Scaling the mass of the model excessive can lead to wrong results. It is necessary to monitor the energy balance of the simulation to assure that the results are not influenced by the larger mass. [26]

After several iterations, the whole model was scaled with a factor of 150. It gave a good balance between stability and calculation time.

3.3.2.1.3 Energy Balance in Quasi-Static Analyses

The Energies in the model are monitored in the Energy History Output of the simulation. It is used to help to evaluate if there are kinematic influences on the simulation. In general, the kinetic energy (ALLKE) of the deforming material should not exceed a small fraction (1-5% of ALLIE) of the internal energy (ALLIE) throughout the majority of the analysis. It is not possible to achieve this in the early phase of the simulation because parts start to move before they develop any significant deformation. To keep the kinematic energy in the early phase of the simulation low, the crush plate uses a smooth amplitude for the loading of the force, see Figure 35.

4. Results

4.1 Loading Rate

Figure 41 is showing the velocity data of the reference node of the crush plate in y direction over the simulation time for each material. It was not possible to keep the loading rate under a velocity of 50 m/s for the whole simulation. There is one major peak in the velocity curve of the materials. At this point, the material at the flange of the battery pack fails, due to the resulting low resistance the crush plate gets accelerated, this result in a high velocity in y-direction.

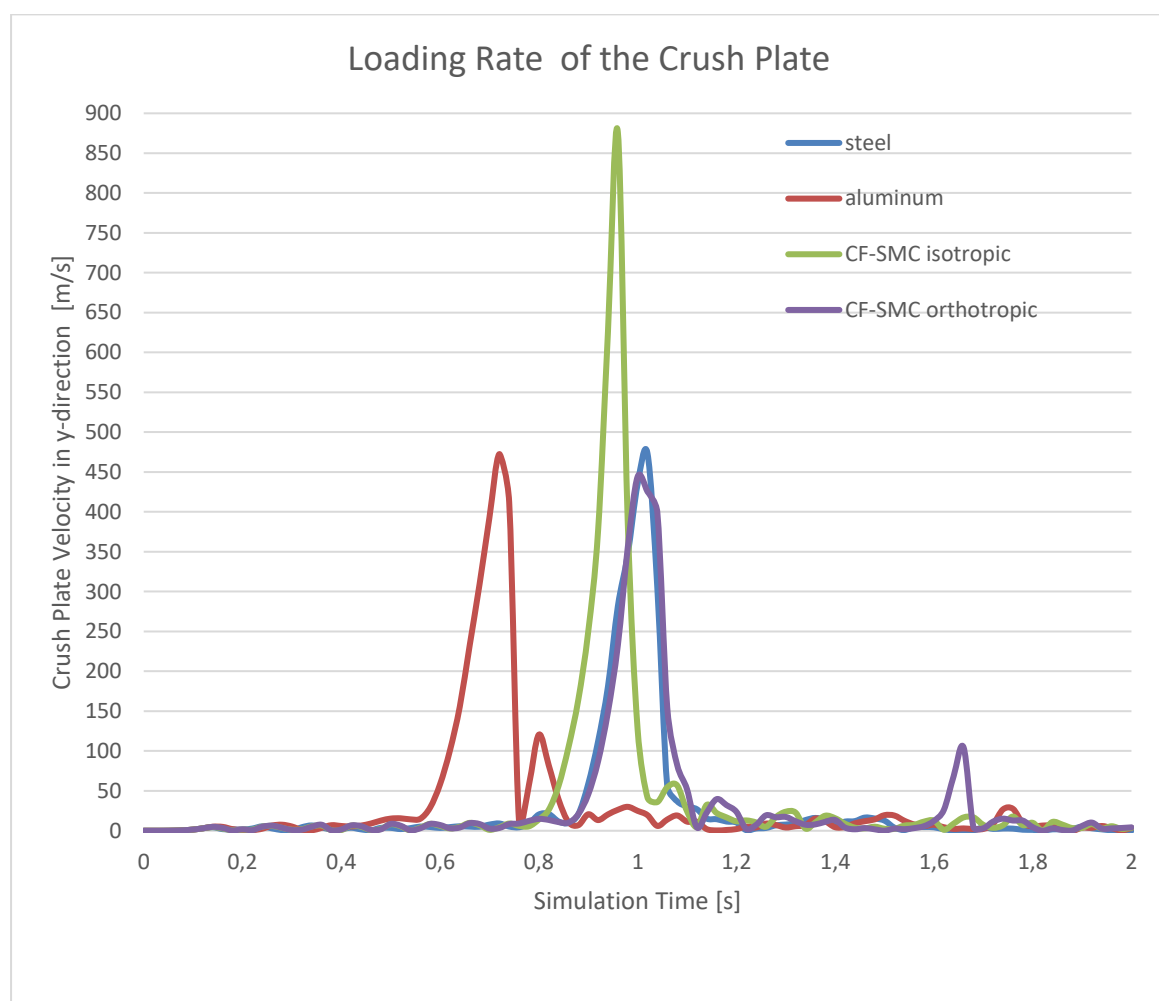


Figure 41 The velocity of the crush plate in y direction for each material

The influence of the loading rate was tested for the 3-point bending test for the CF-SMC material model. The Test showed that the influence of the duration of the simulation and thus the speed of load application has only a minor influence on the results. [6]

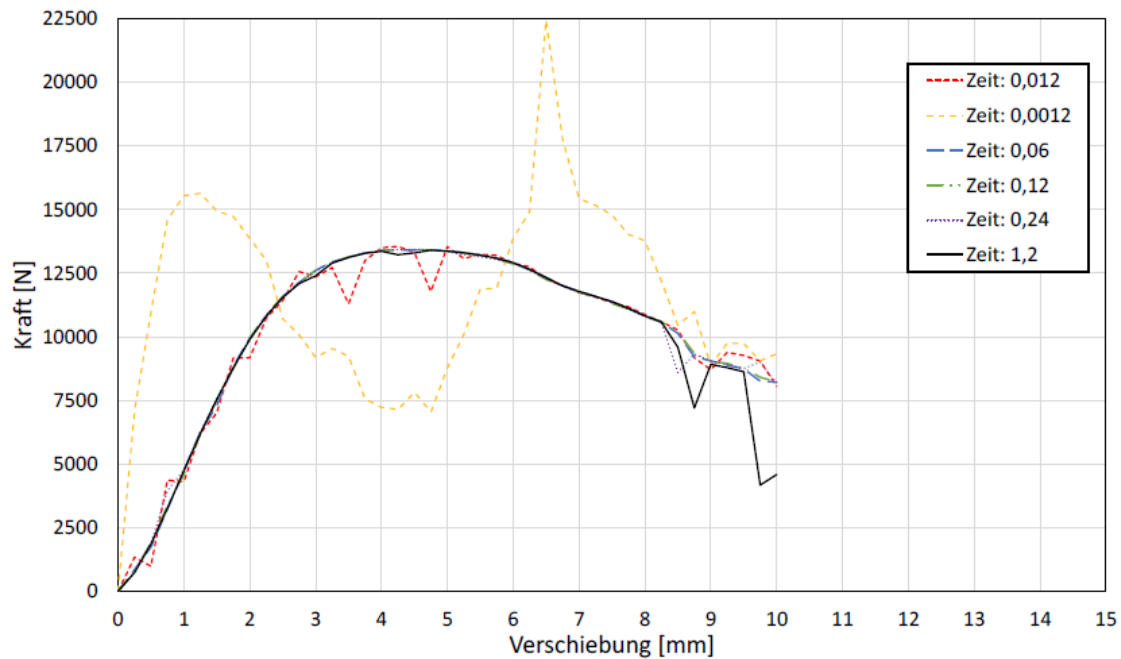


Figure 42 Variation of the load speed application for the 3-point bending test for the C-SMC material. Under 0.06s there is an influence on the results. [6]

Figure 42 shows the influence of the simulation time on the results, the only occur for less than 0.06s.

Since the greatest deformation occurs in an interval of approx. 0.2s (Figure 41) and the results from the 3-point bending test showed that there were no significant influences for this loading speed. The total simulation time for the crash test was chosen to be two seconds after repeated iteration

4.2 Energy Balance

To check if the simulation of the battery is quasi static the Energy History Data are used. In Figure 43 the Energy Ratio [ALLKE/ALLIE] in % for the simulation of: Aluminum, Steel, CF-SMC Isotropic and, CF-SMC Orthotropic is shown. In the early state of the simulation the ratio is higher than 5%, because there is only displacement of the components and no significant deformation. Over the majority of the simulation the energy ratio is about one percent. This fulfills the requirement for a quasi-static simulation.

The diagram also shows that in comparison to the other materials, aluminum is the first that starts to deform because it's energy ratio is the first that drops below 5 percent.

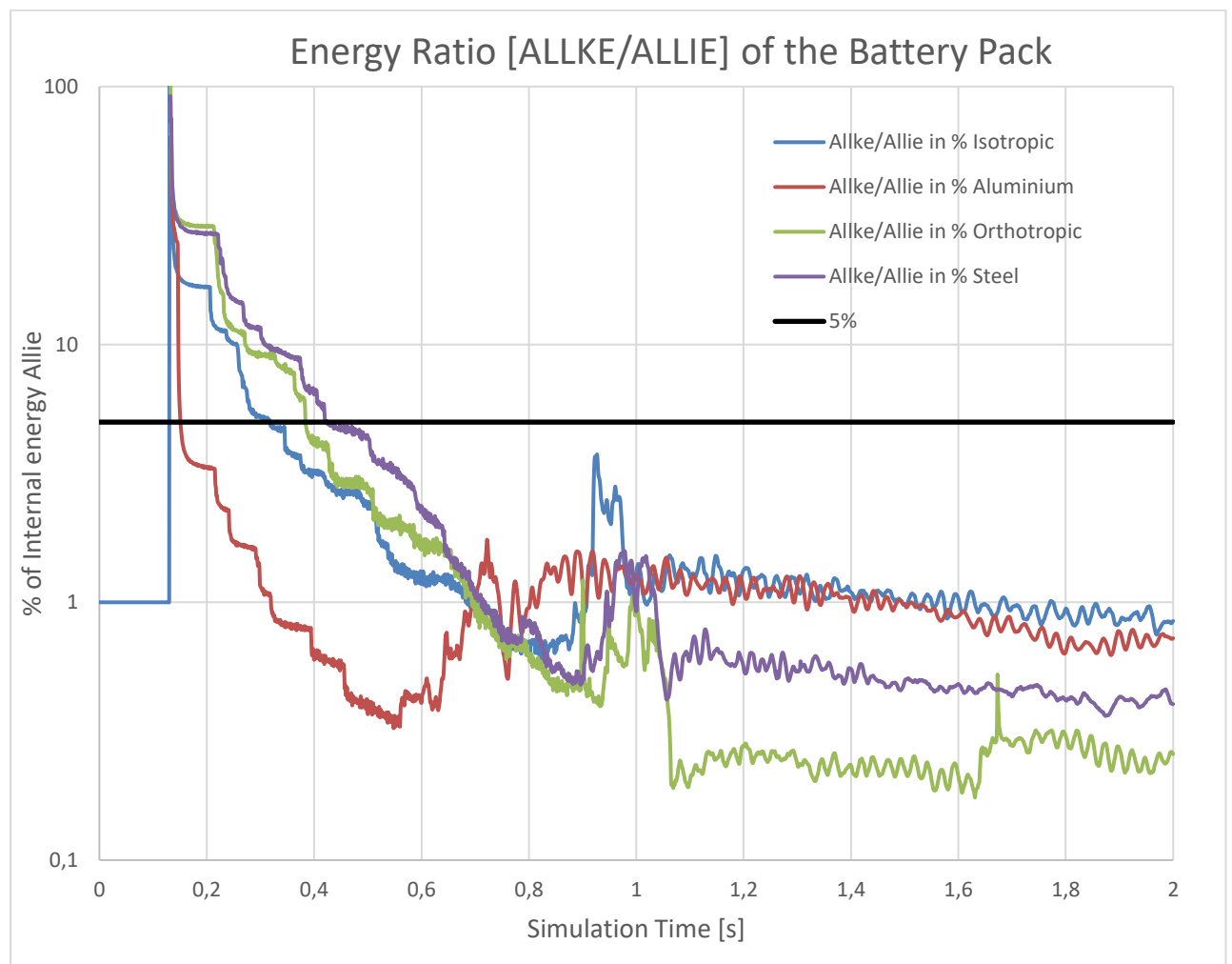


Figure 43 The ratio of the Energies of the battery pack simulation. Over most of the simulation, the Ratio is under 5 %

4.3 Analysis of the influence of the fiber orientations

This chapter shows the influences of different fiber orientations. Each of these four fiber orientations are random.

4.3.1 Total displacement of the Crush plate

The results in Figure 44 and Figure 45 show that there is a noticeable difference with larger displacements in the results. Fiber orientation 1 and 3 are showing nearly the same result, whereas Fiber orientations 2 and 3 are showing less absolute displacement.

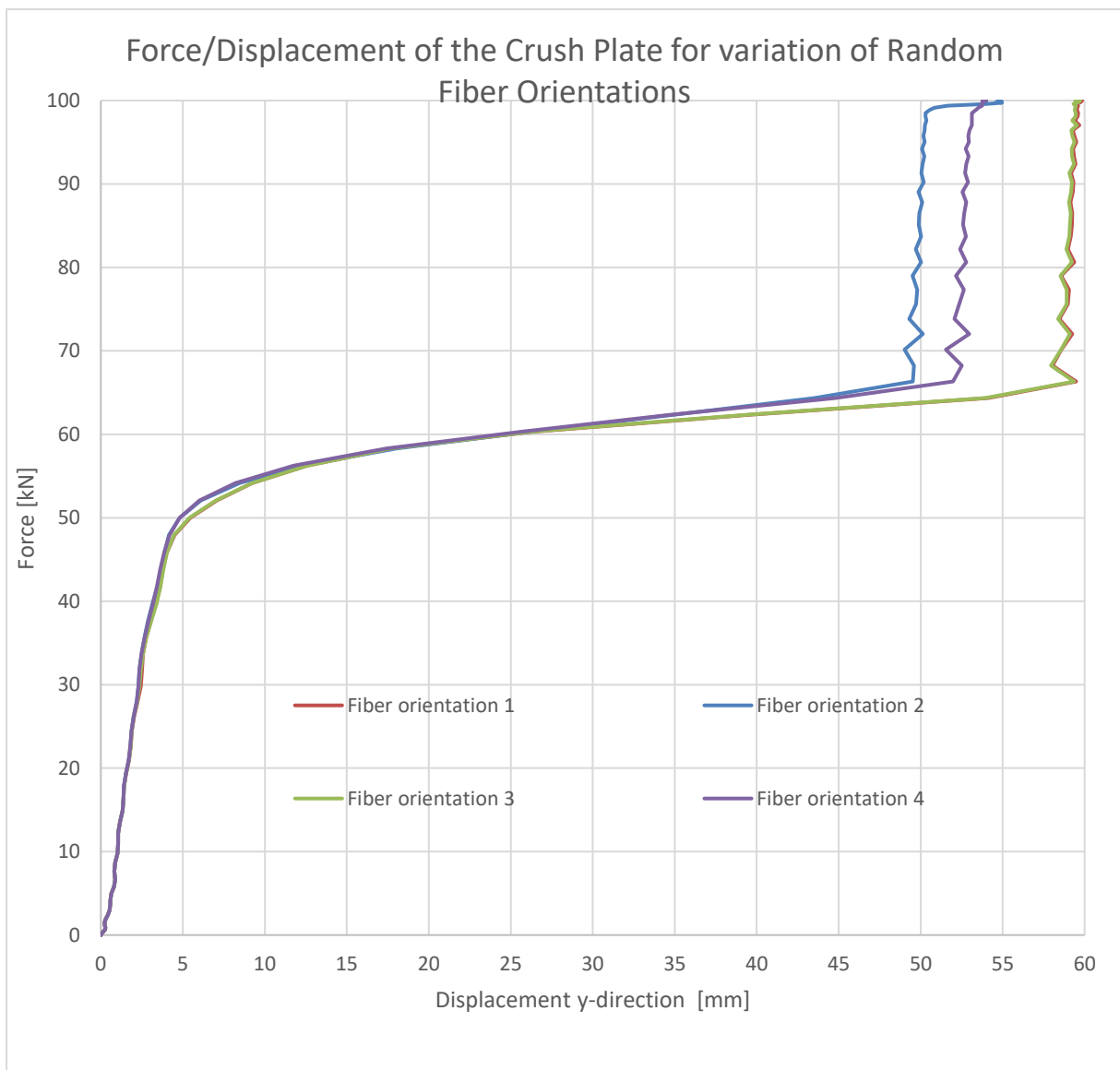


Figure 44 The influence on the results of the different random Fiber orientation Displacement of the Crush Plate in y-direction.

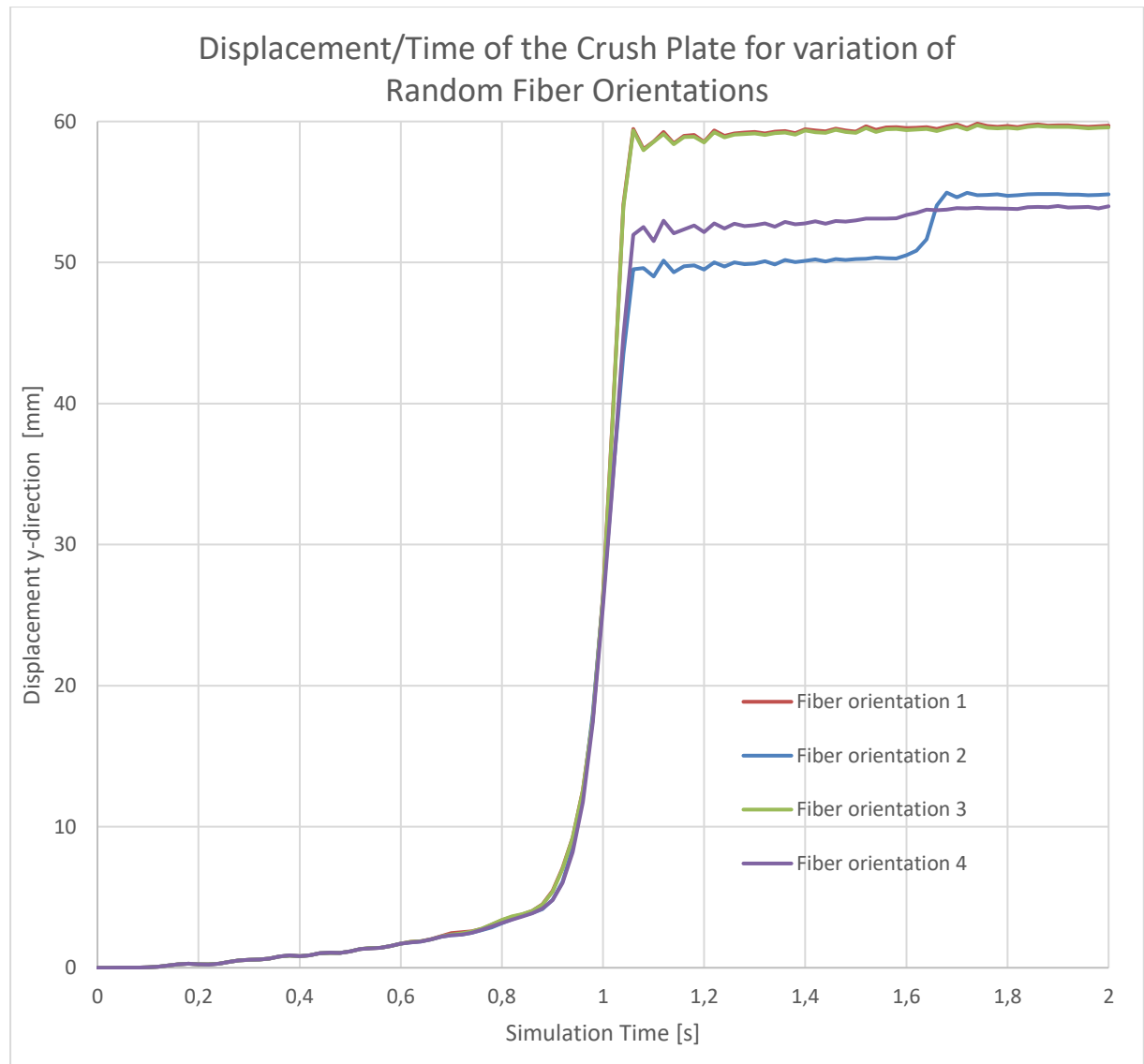


Figure 45 Influence of the different random fiber orientation. Displacement in y-direction of the Crush plate over the simulation time.

Table 15 is showing the max. displacement values for the different fiber orientations. The absolute difference between the results is 5.7 mm. Which is a deviation from the mean value of 10%. In the reality influences from the fiber orientation are expected. Therefore, this deviation is acceptable for the simulation of the Crash test.

Table 15 Comparison of the max displacement for the different fiber orientations

Random Orientation	Max. Displacement [mm]	Deviation from the mean value [%]
Fiber orientation 1	59,7	4,48
Fiber orientation 2	54,8	-4
Fiber orientation 3	59,6	4,29
Fiber orientation 4	54	-5,62
	57,03 Mean Value	

4.3.2 3-point bending test

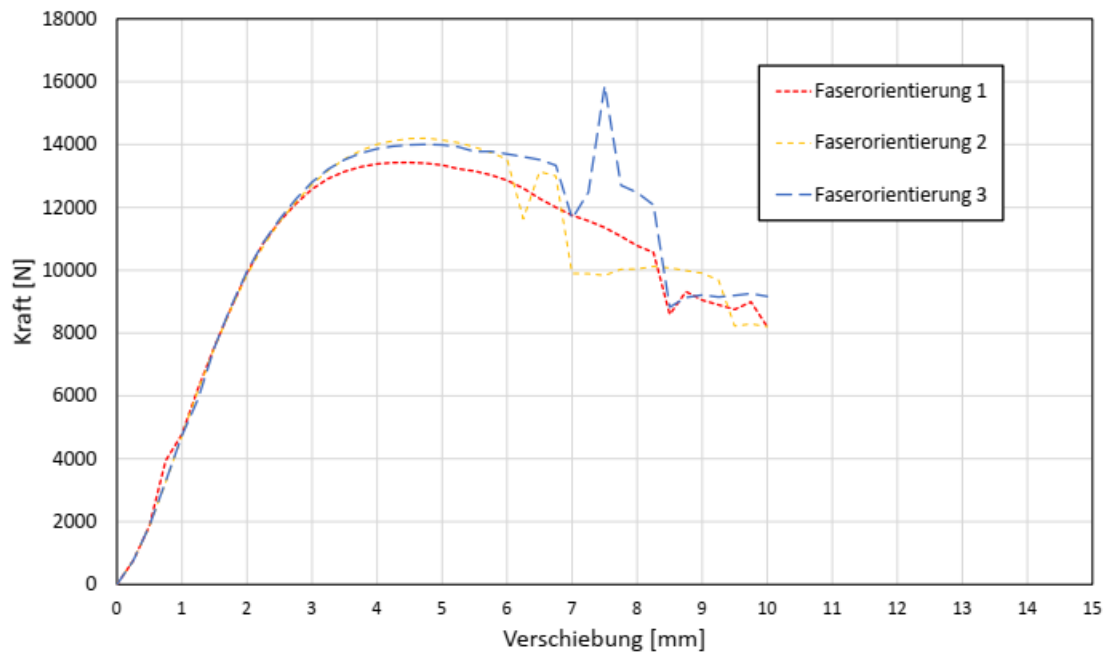


Figure 46 Influence of the Fiber Orientation for dynamic 3-point Bending test [6]

The explicit 3-point bending (Figure 46) test is showing similar behavior. there are also noticeable deviations in the curves for large displacements. [6]

4.3.3 Deformation of the simulation model for the fiber orientations

4.3.3.1 Deformation of the Battery Case

Figure 47, Figure 48, Figure 49 and Figure 50 are showing the simulation results for the four random fiber orientations. The total deformations are similar only the area of the flange is differently deformed.

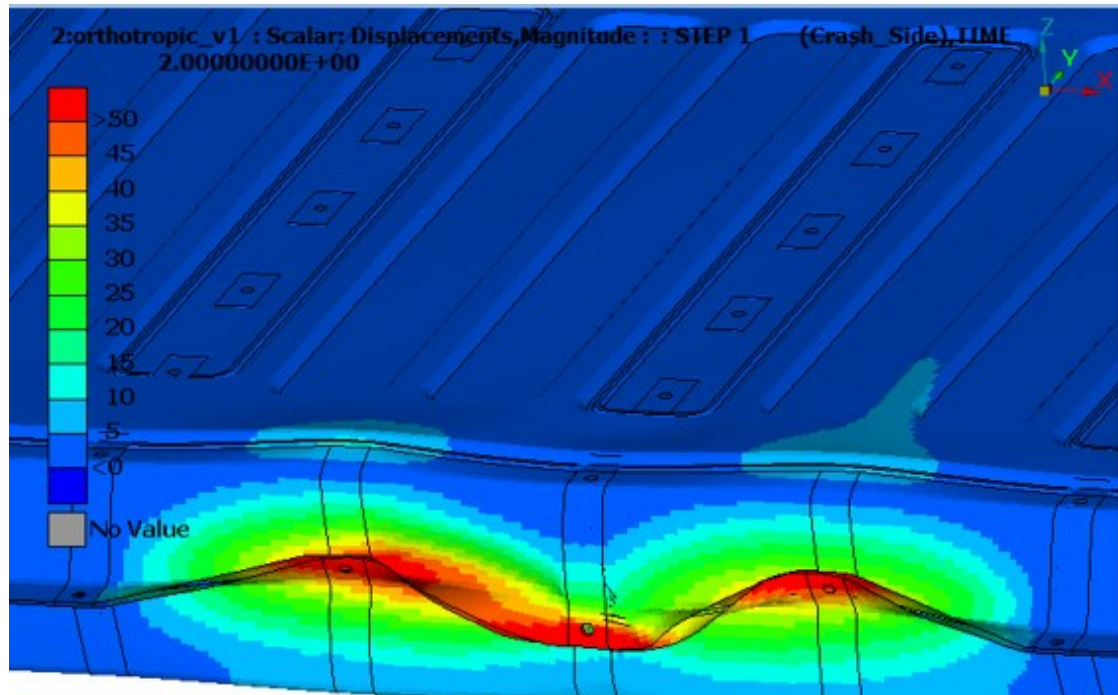


Figure 47 Deformation of the battery case for the first random fiber orientation at the end of the simulation. The scale indicates the scalar magnitude of the deformation of the elements. Red elements with the highest deformation and dark blue ones with no deformation.

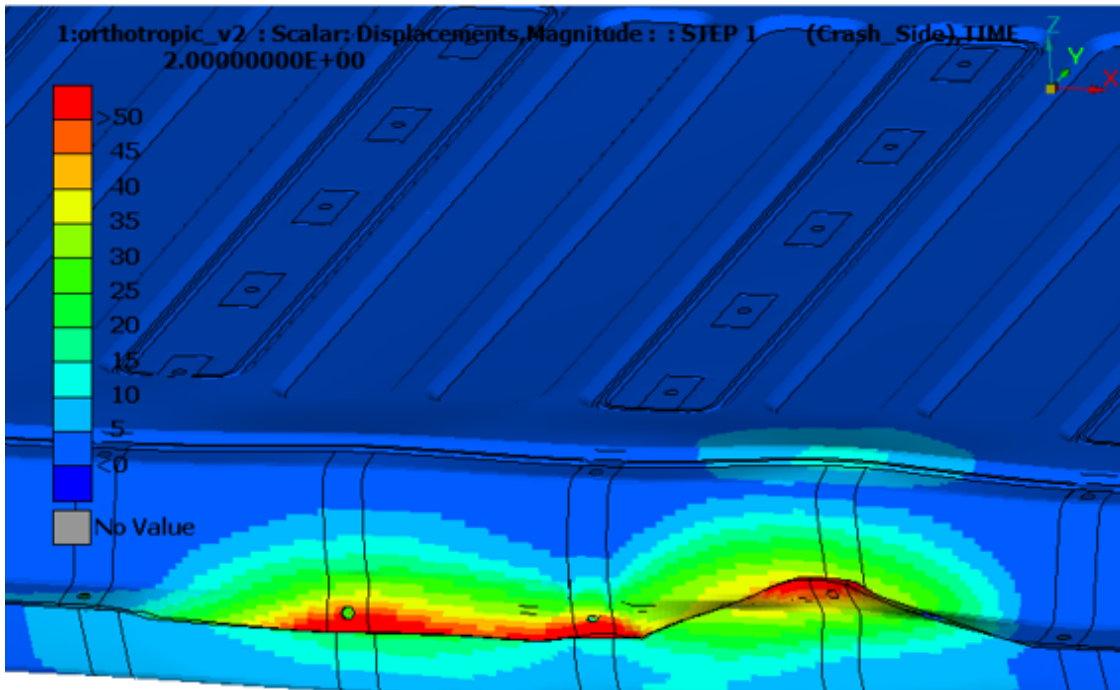


Figure 48 Deformation of the battery case for the second random fiber orientation at the end of the simulation. The scale indicates the scalar magnitude of the deformation of the elements. Red elements with the highest deformation and dark blue ones with no deformation.

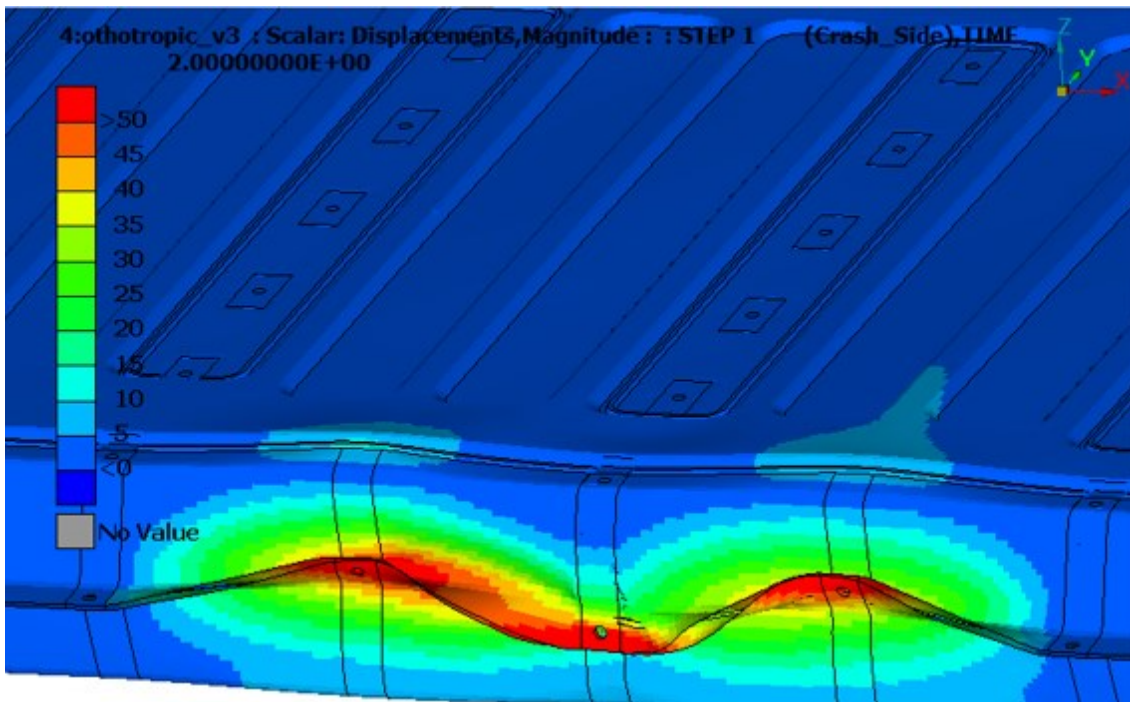


Figure 49 Deformation of the battery case for the third random fiber orientation at the end of the simulation. The scale indicates the scalar magnitude of the deformation of the elements. Red elements with the highest deformation and dark blue ones with no deformation.

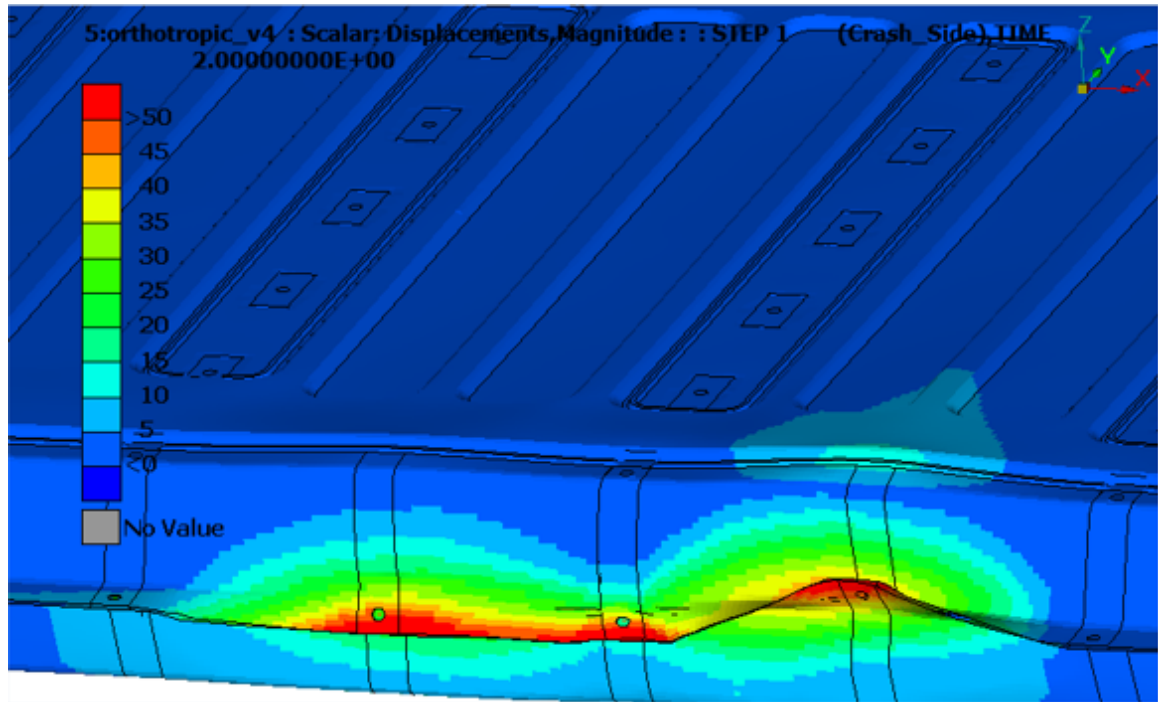


Figure 50 Deformation of the battery case for the fourth random fiber orientation at the end of the simulation. The scale indicates the scalar magnitude of the deformation of the elements. Red elements with the highest deformation and dark blue ones with no deformation.

4.3.3.2 Protection of the Battery modules

Figure 51, Figure 52, Figure 53 and Figure 54 show that for all four random fiber orientations the Battery modules are showing no deformation.

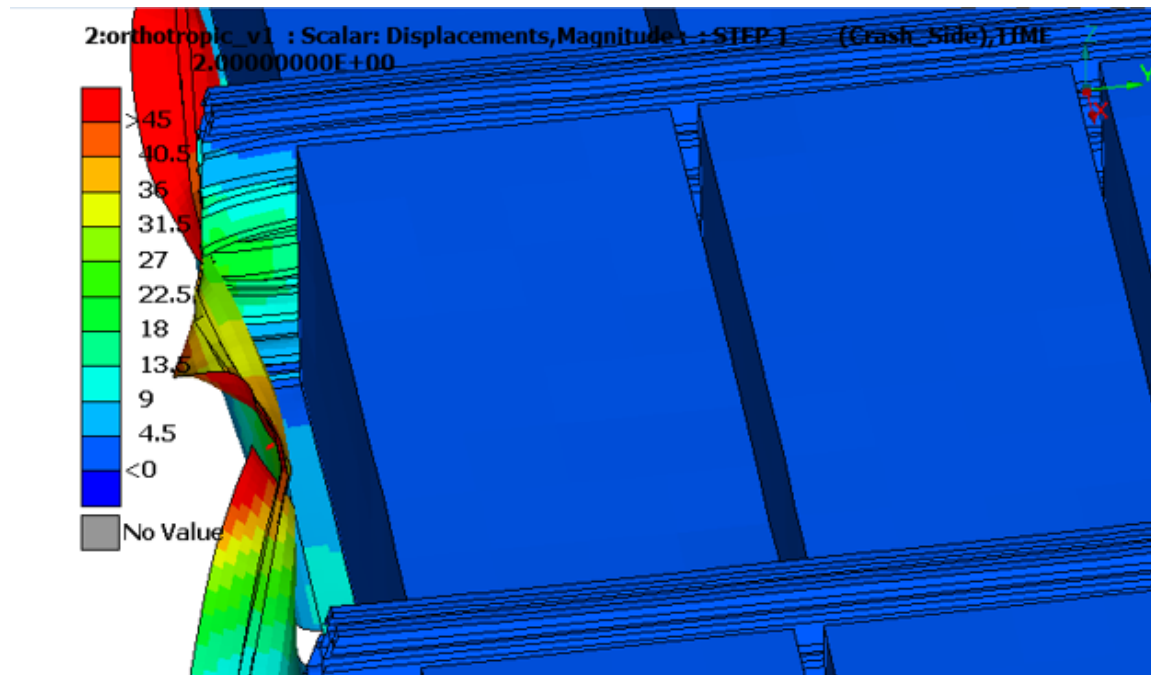


Figure 51 Look inside the Battery case for the first fiber orientation. Deformation at the end of the simulation showing the Battery modules. The scale indicates the scalar magnitude of the deformation of the elements. Red elements with the highest deformation and dark blue ones with no deformation

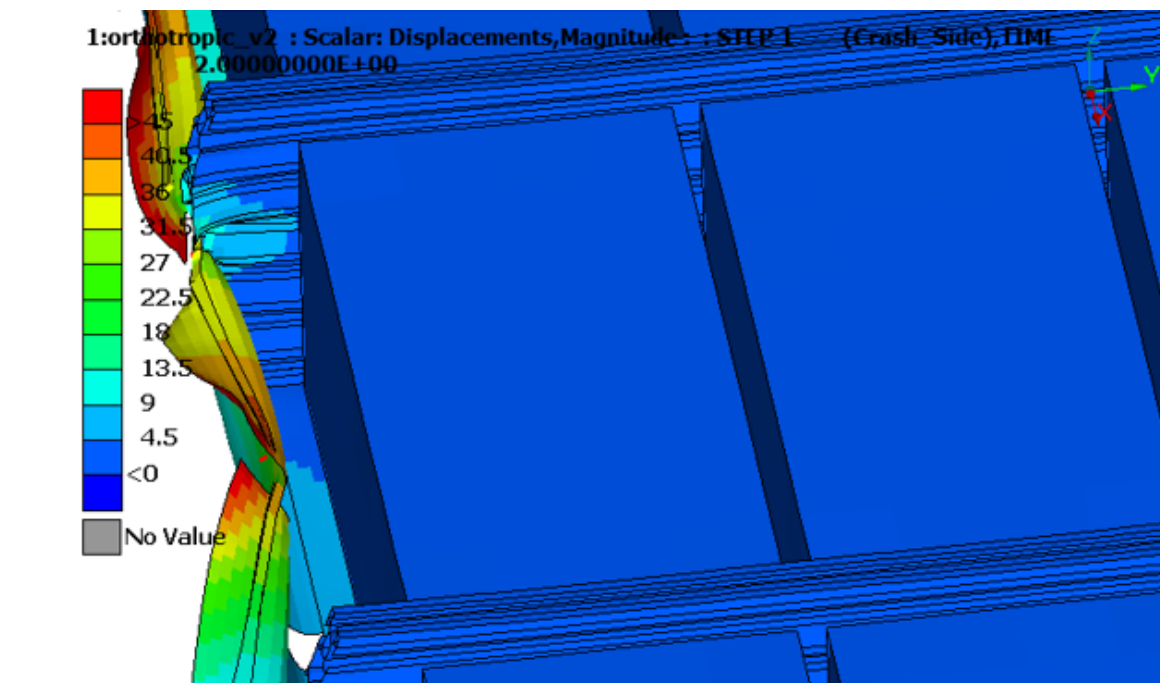


Figure 52 Look inside the Battery case for the second fiber orientation. Deformation at the end of the simulation showing the Battery modules. The scale indicates the scalar magnitude of the deformation of the elements. Red elements with the highest deformation and dark blue ones with no deformation

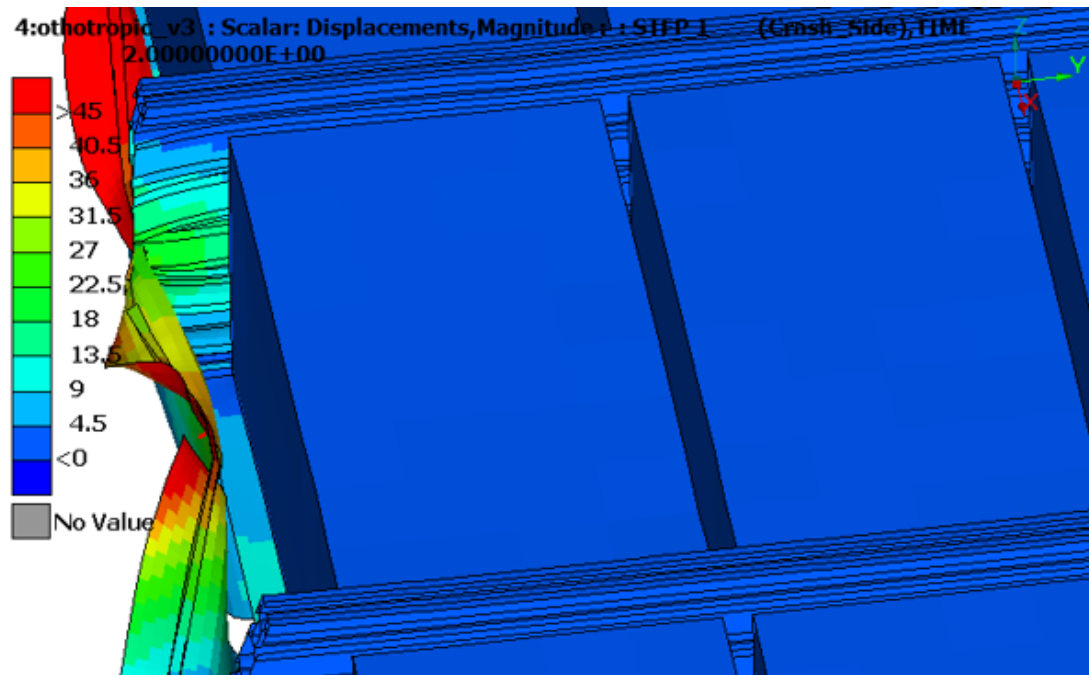


Figure 53 Look inside the Battery case for the third fiber orientation. Deformation at the end of the simulation showing the Battery modules. The scale indicates the scalar magnitude of the deformation of the elements. Red elements with the highest deformation and dark blue ones with no deformation

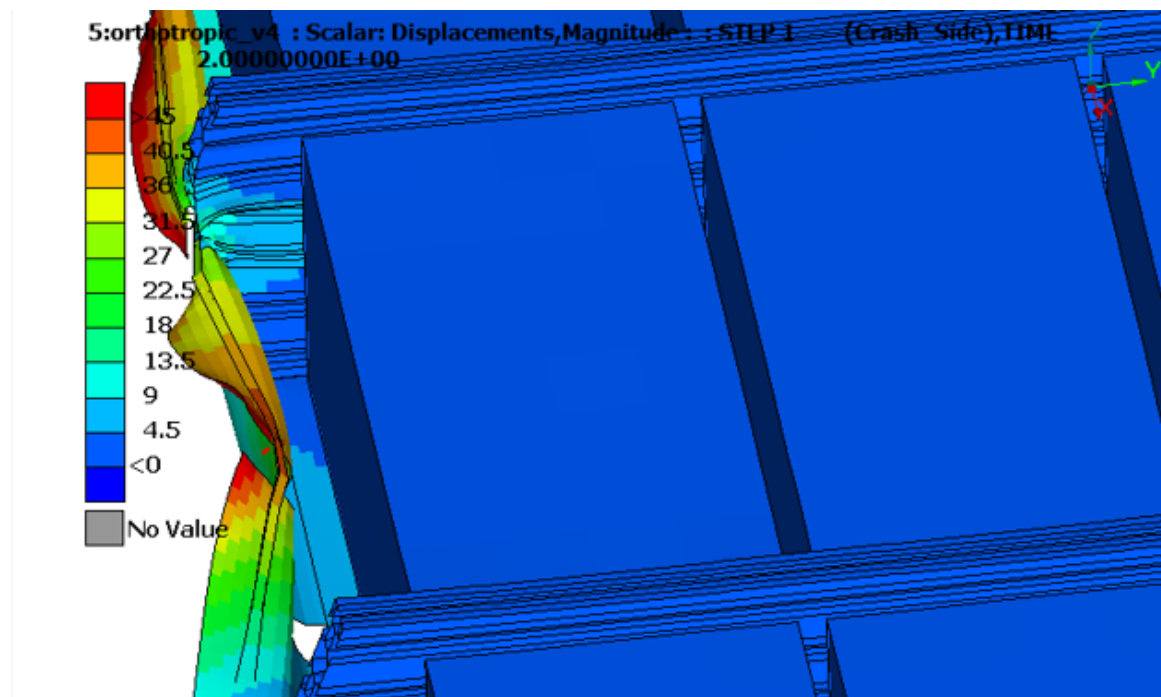


Figure 54 Look inside the Battery case for the fourth fiber orientation. Deformation at the end of the simulation showing the Battery modules. The scale indicates the scalar magnitude of the deformation of the elements. Red elements with the highest deformation and dark blue ones with no deformation

4.4 Comparison of the results of the different materials

4.4.1 Total displacement of the Crush Plate

4.4.1.1 Steel vs. Orthotropic material model

Until 45 mm penetration the CF SMC Orthotropic material is showing nearly same the displacement compared with steel. That means that the orthotropic CF-SMC material model is showing a similar stiffness compared to the steel model. The steel model is showing the smallest total scalar displacement of all four material models.

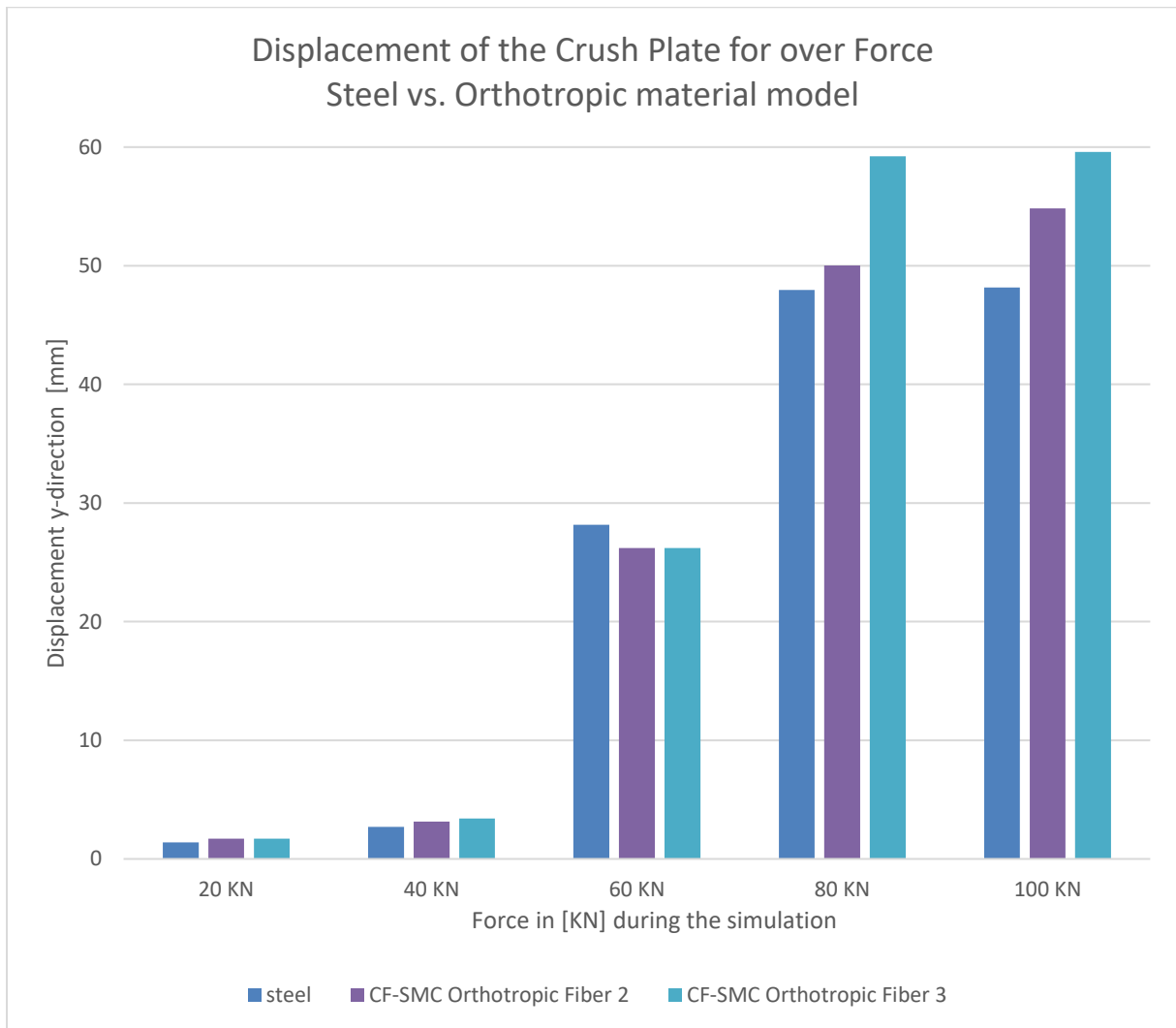


Figure 55 Displacement of the Crush plate in y-direction. The displacements in mm are shown for a certain loading level of the Crush Plate level during the simulation.

4.4.1.2 Isotropic vs. Orthotropic material model

For small displacements of about 4mm the CF-SMC Isotropic model is showing similar stiffness compared to steel and orthotropic material. The total scalar displacement is showing the same result as the CF-SMC Material with the random fiber orientation 3. The CF-SMC Orthotropic model is behaving stiffer than the isotropic one. The total displacement of the two CF-SMC models is very similar.

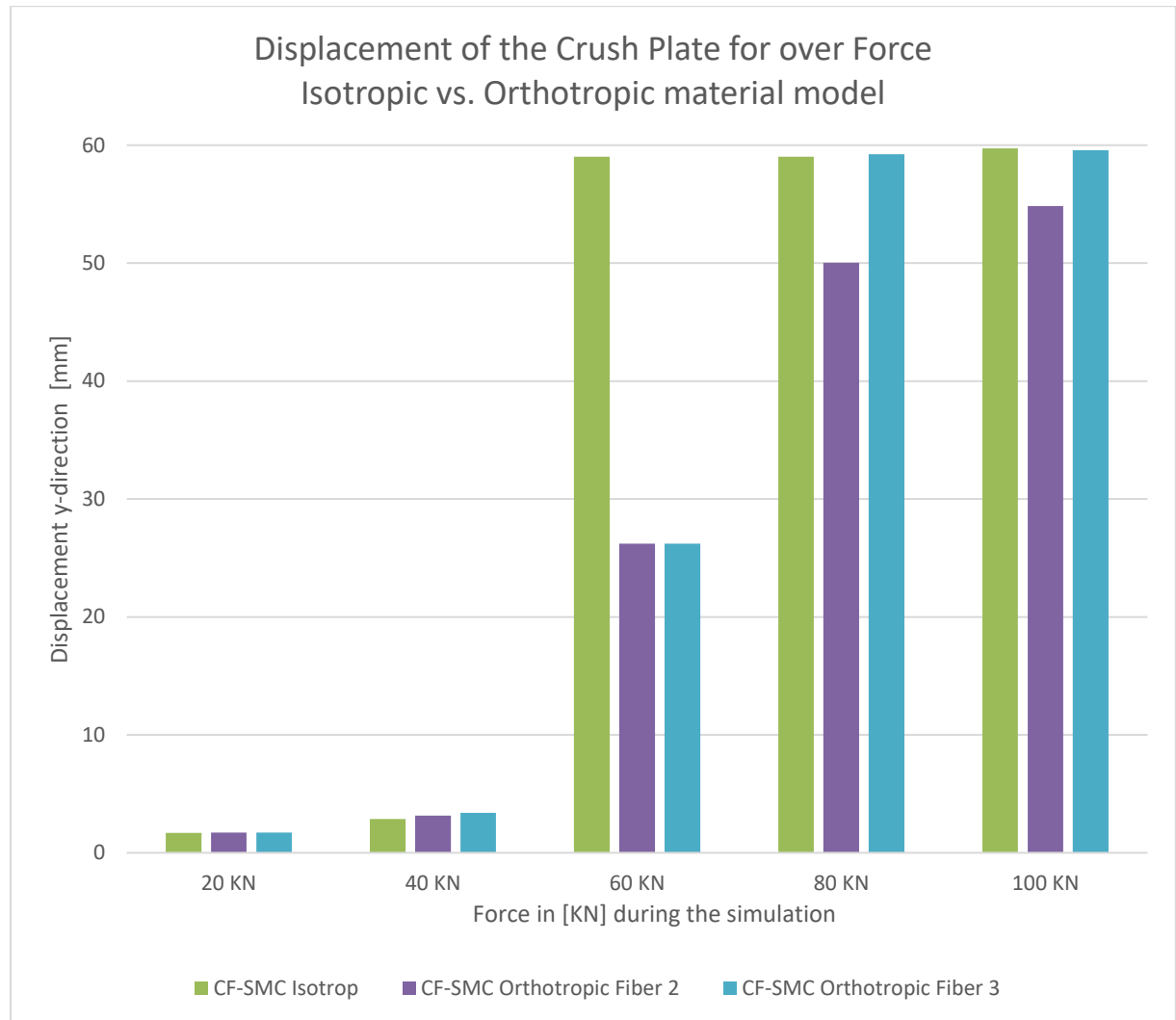


Figure 56 Displacement of the Crush plate in y-direction. The displacements in mm are shown for a certain loading level of the Crush Plate level during the simulation.

4.4.1.3 Aluminum vs. Orthotropic material model

Aluminum is showing the lowest stiffness of all material models. With 51mm the total scalar displacement of the aluminum model is lower than the total displacement of the orthotropic material. This can be attributed to the tougher fracture behavior of aluminum compared to the CF-SMC material

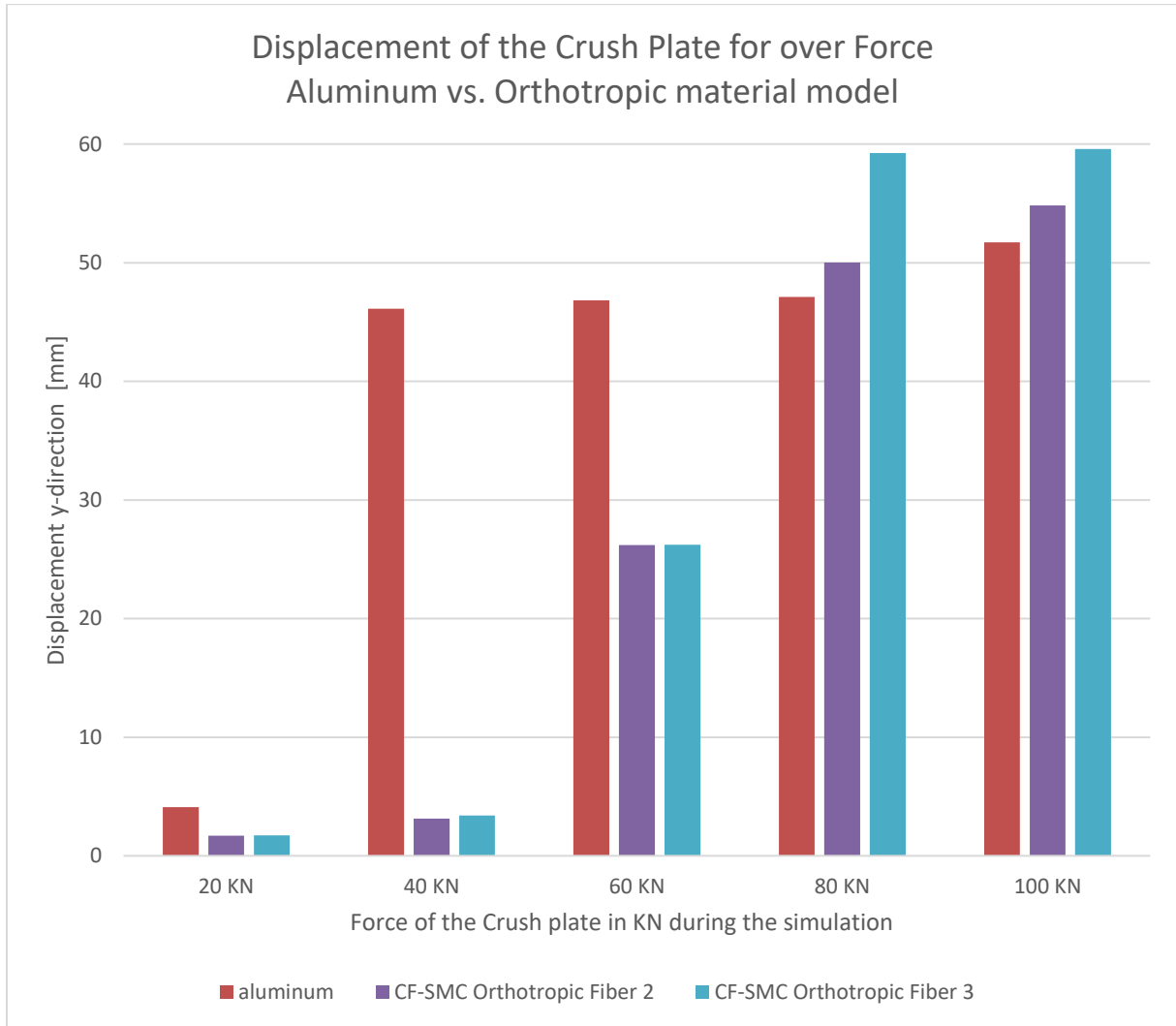


Figure 57 Displacement of the Crush plate in y-direction. The displacements in mm are shown for a certain loading level of the Crush Plate level during the simulation.

Results

4.4.1.4 Force/Displacement curves the Crush plate material comparison

Table 16 Comparison of the maximum scalar Displacement in y-direction of the Crush Plate

Material	Max. Displacement [mm]
Steel	48,2
Aluminum	51,7
CF-SMC Isotropic	59,74
CF-SMC Orthotropic Fiber 2	54,8
CF-SMC Orthotropic Fiber 3	59,6

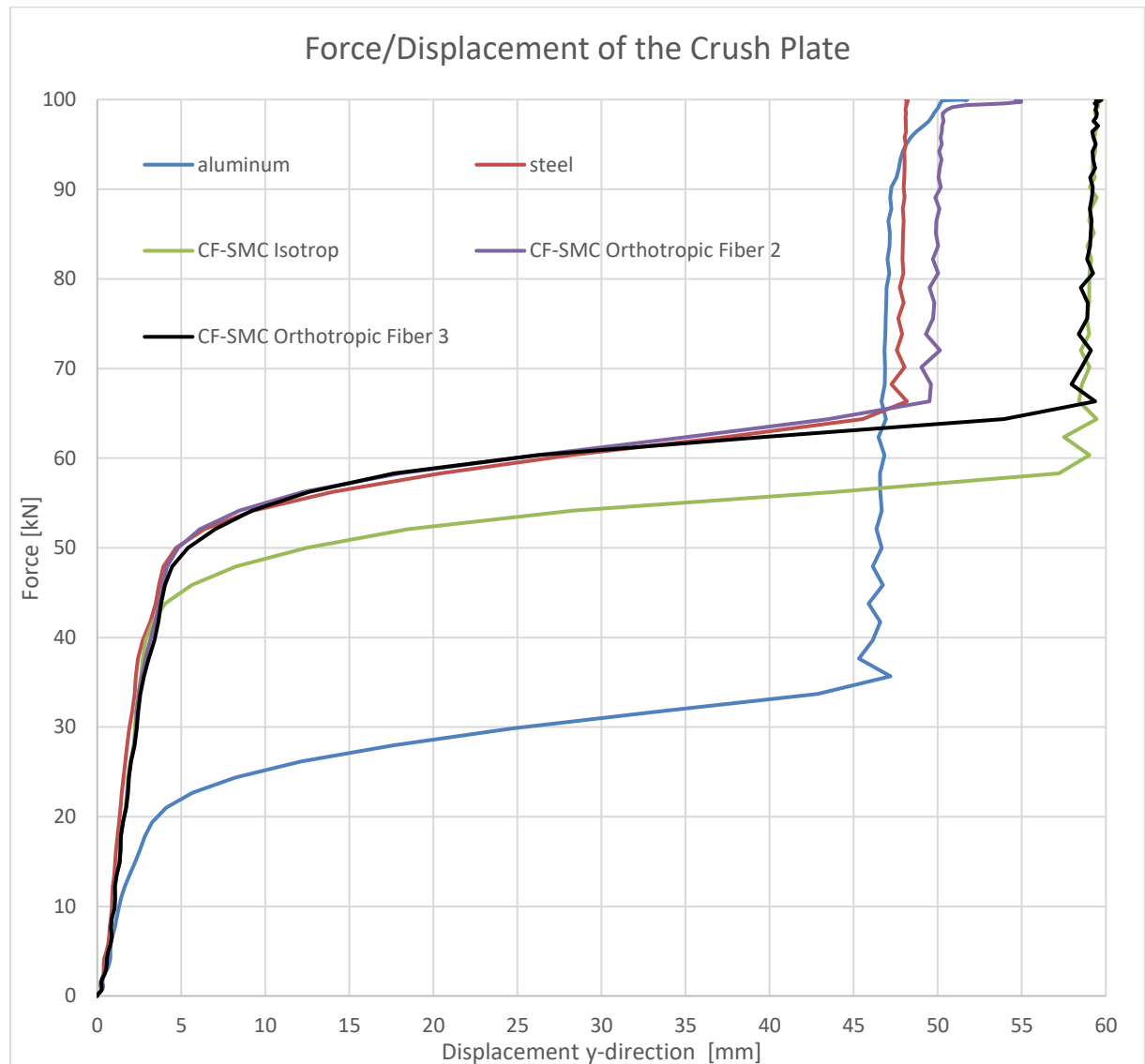


Figure 58 Displacement of the Crush Plate y-direction for aluminum, steel, CF-SMC Isotropic and CF-SMC Orthotropic with two random fiber orientations.

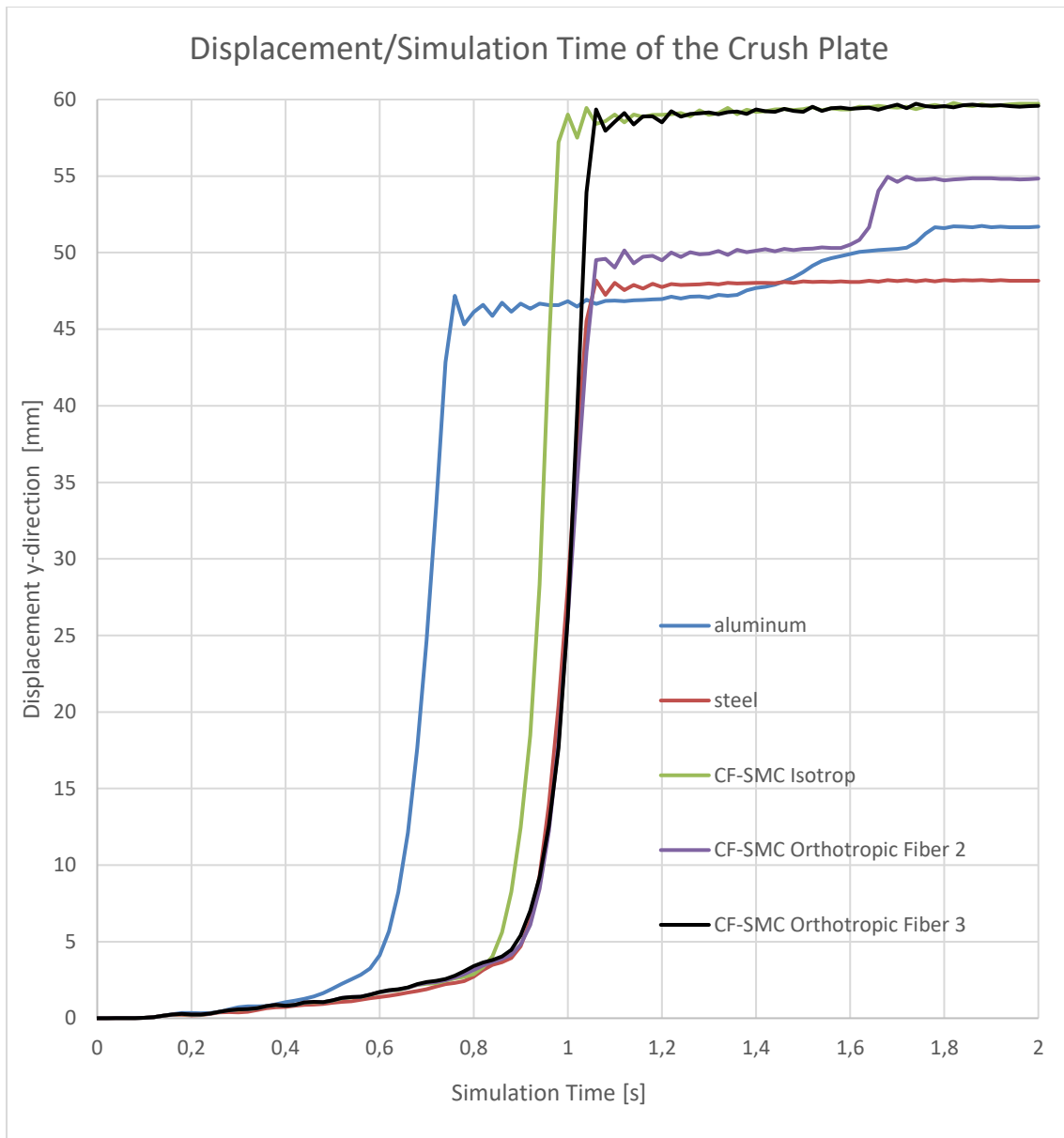


Figure 59 Displacement of the Crush Plate in y-direction for aluminum, steel, CF-SMC Isotropic and CF-SMC Orthotropic with two random fiber orientations over the simulation time

4.4.2 Comparison of the total deformation of the simulation model

This chapter shows the deformation of the battery case of the different case materials.

Figure 60, Figure 62, Figure 64 and Figure 66 show the deformation of the case for the four different materials. By comparing the deformation of the CF-SMC orthotropic material model with the deformation of the other material models there are no implausible deformations or breaks in the material. There are differences in the flange area, these are caused by the fiber orientation of the orthotropic material, see 61.

The deformation values of the aluminum cross brace show how far the crush plate has penetrated the battery pack for the different case materials see, Figure 61, Figure 63, Figure 65 and Figure 67

4.4.2.1 Aluminum Case

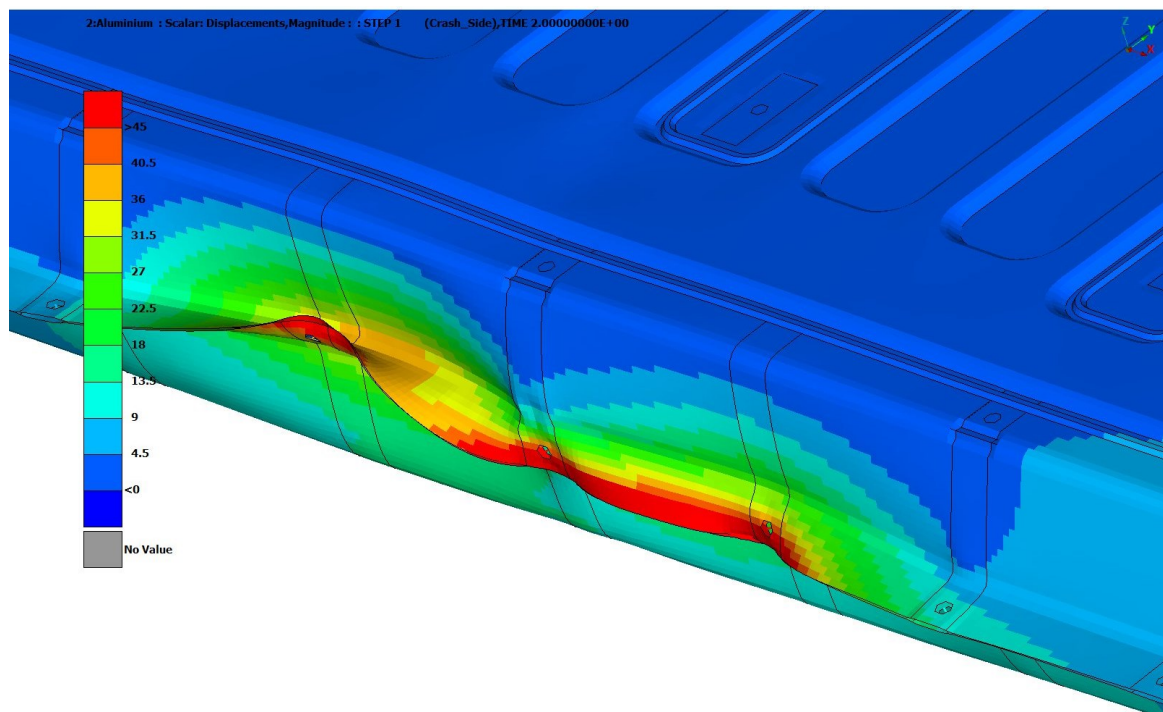


Figure 60 Deformation of the Aluminum Battery Case at the end of the simulation. The scale indicates the scalar magnitude of the deformation of the elements. Red elements with the highest deformation and dark blue ones with no deformation.

2:Aluminium : Scalar: Displacements,Magnitude : : STEP 1 (Crash_Side),TIME 2.00000000E+00

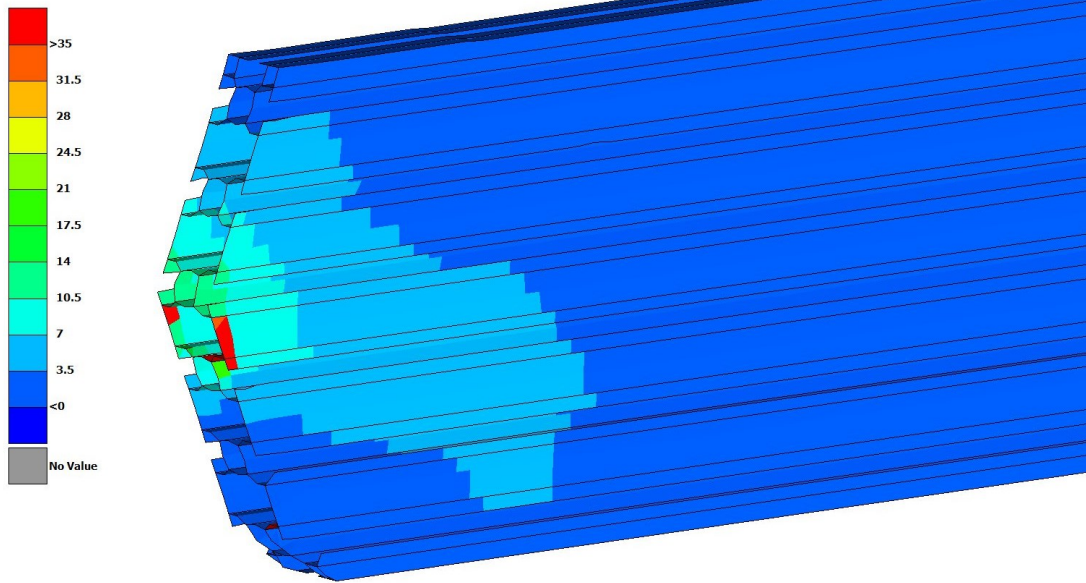


Figure 61 Undeformed cross brace with the max scalar deformation for the Aluminum Battery Case Red elements with the highest deformation and dark blue ones with no deformation.

4.4.2.2 Steel Case

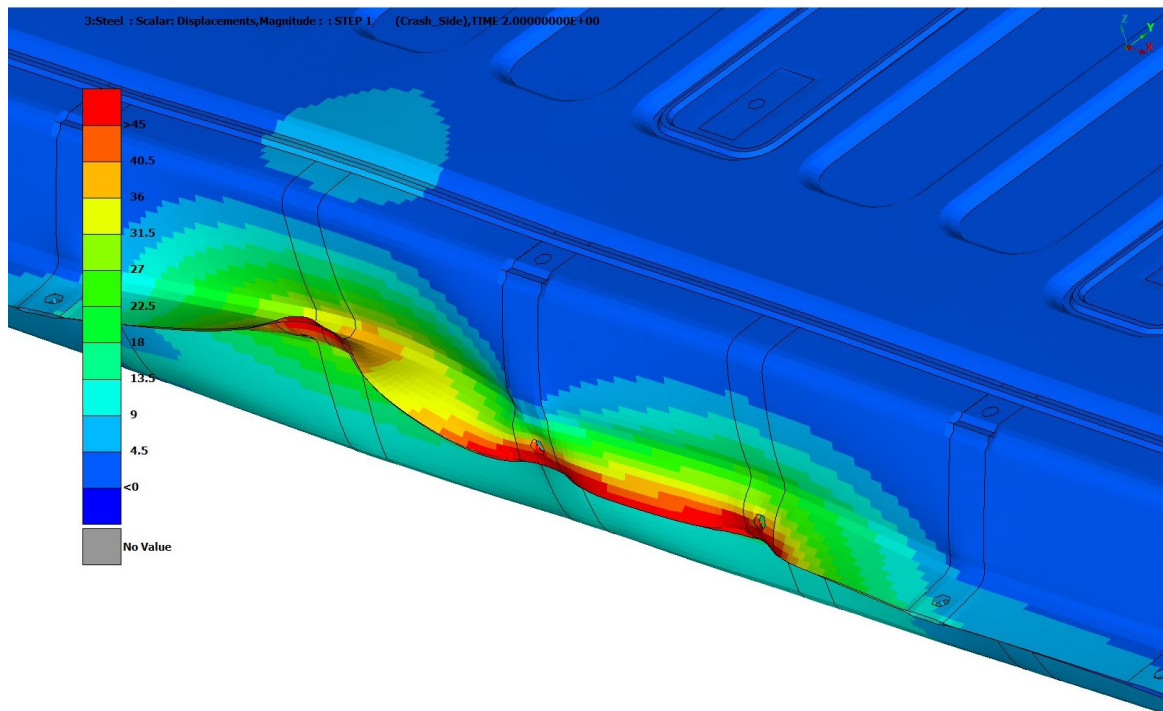


Figure 62 Deformation of the Steel Battery Case at the end of the simulation. The scale indicates the scalar magnitude of the deformation of the elements. Red elements with the highest deformation and dark blue ones with no deformation.

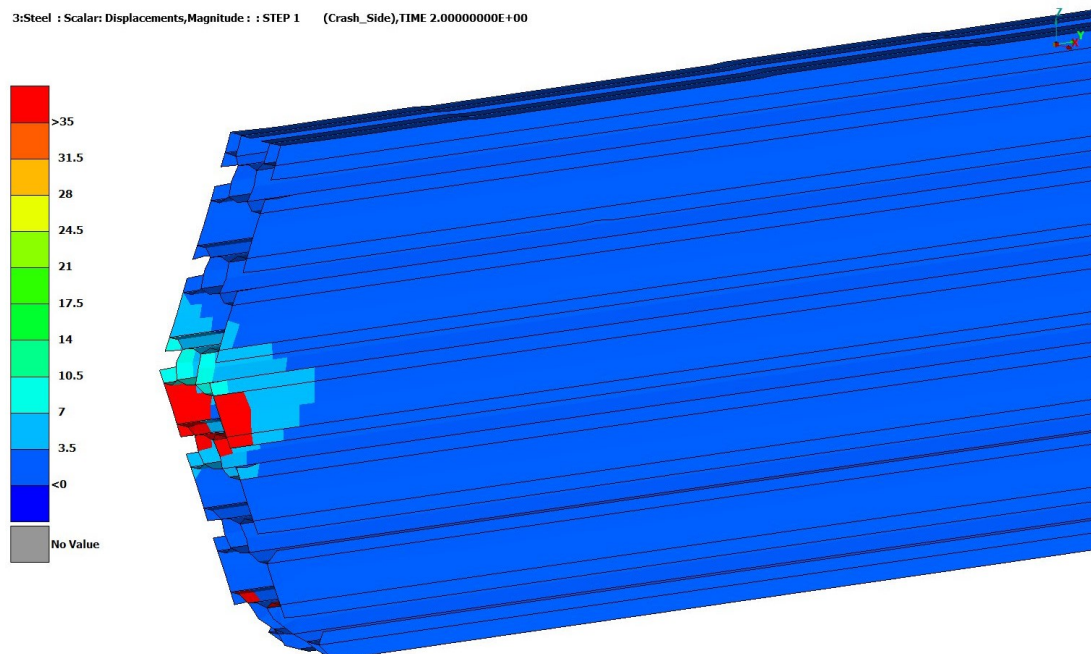


Figure 63 Undeformed cross brace with the max scalar deformation for the Steel Battery Case. Red elements with the highest deformation and dark blue ones with no deformation. Red elements with the highest deformation and dark blue ones with no deformation.

4.4.2.3 CF-SMC Isotropic Case

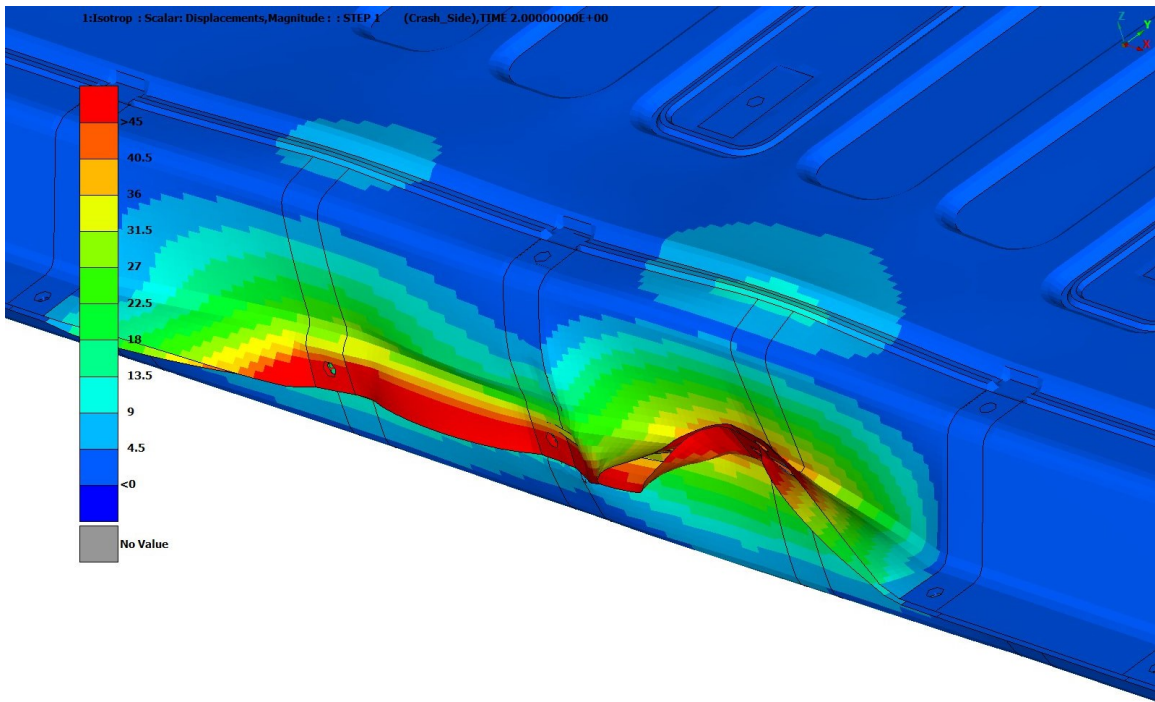


Figure 64 Deformation of the CF-SMC Isotropic Battery Case at the end of the simulation. The scale indicates the scalar magnitude of the deformation of the elements. Red elements with the highest deformation and dark blue ones with no deformation.

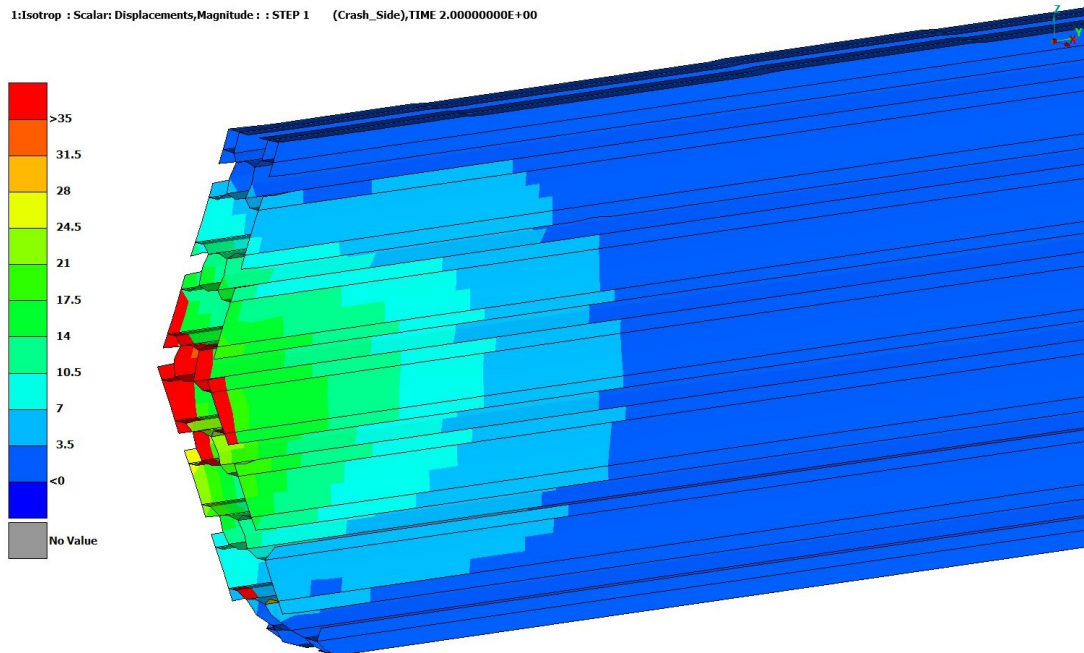


Figure 65 Undeformed cross brace with the max scalar deformation for the CF-SMC Isotropic Battery Case. Red elements with the highest deformation and dark blue ones with no deformation.

4.4.2.4 CF-SMC Orthotropic Case

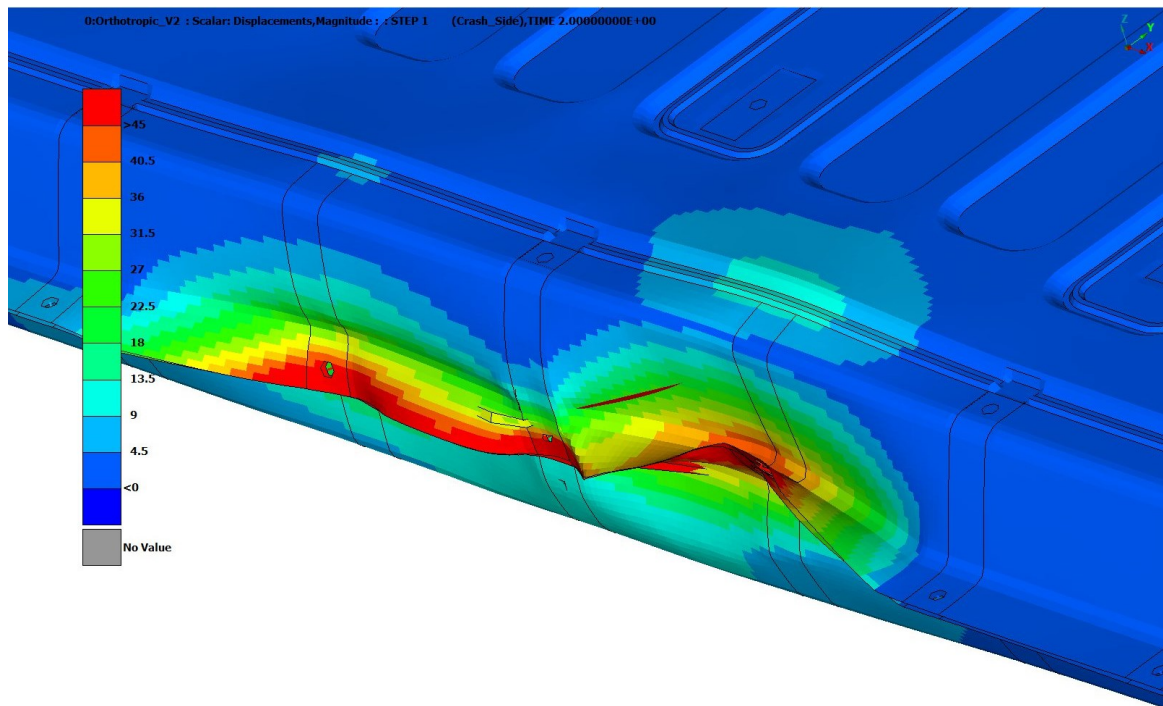


Figure 66 Deformation of the CF-SMC Orthotropic Battery Case at the end of the simulation. The scale indicates the scalar magnitude of the deformation of the elements. Red elements with the highest deformation and dark blue ones with no deformation.

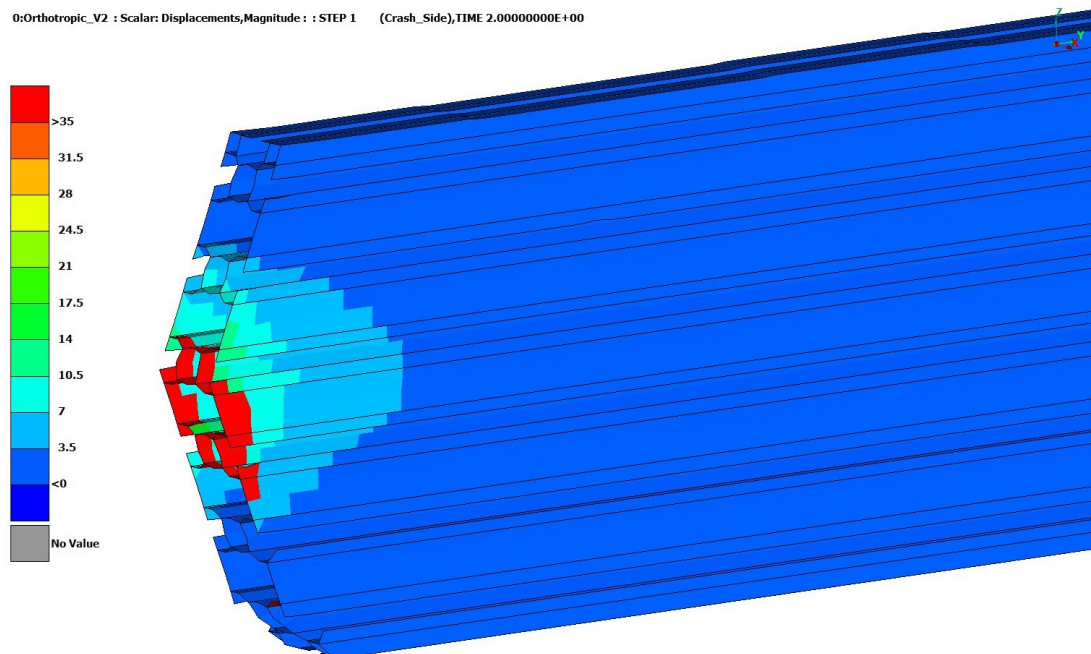


Figure 67 Undeformed cross brace with the max scalar deformation for the CF-SMC Orthotropic Battery Case. Red elements with the highest deformation and dark blue ones with no deformation.

4.5 Damage Distribution in the CF-SMC Orthotropic FEM model

Hashin damage

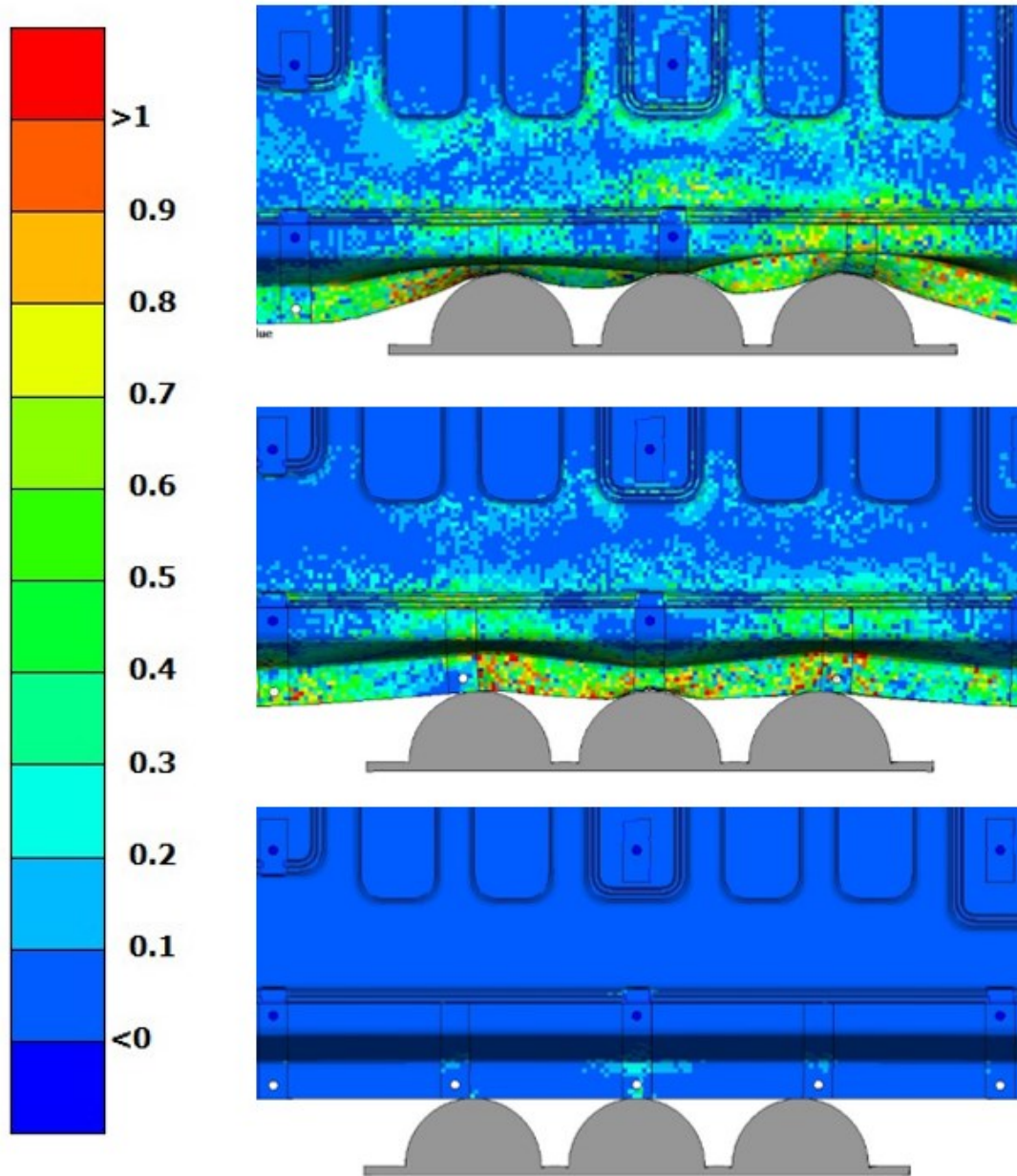


Figure 68 Hashin fiber damage Top view of the simulated crash test of the CF-SMC orthotropic battery Case. Bottom figure shows the early interaction phase. Second figure at half of the simulation time. The third figure represents the maximum deformation of the battery case. In red the elements that have failed under Hashin criteria.

4.5.1 Weight of the Battery case

One of the advantages of using CF-SMC material instead of steel or aluminum is the weight reduction. For the developed battery case the weight reduction would be 14 kg compared to an aluminum case, by maintaining the mechanical properties.

Table 17 Weight of the Battery Case and the whole Battery Pack

Material	Density [kg/dm ³]	Weight of the case half's [kg]	Total Weight of the battery pack [kg]
CF-SMC	1,55	20	516
Aluminum	2,7	34	530
Steel	7,9	127	597

Table 18 Weight reduction of the Battery Pack

CF-SMC compared to	Weight reduction of the case [%]	Weight reduction of the battery pack [kg]
Steel	84,5	81
Aluminum	42,7	14

5. Discussion

5.1 Modelling of the Battery Case

For the simulation of the CF-SMC components it is important to consider the fiber orientation. The variation of the fiber orientation showed that for this simulation the simplified approach without considering the size and orientation of the fibers delivers good results.

The model of the battery pack is using various adhesive lines. This can lead to tensile forces normal to the 1-2 plane. Under certain circumstances the forces can lead to failure through delamination. Neglecting the individual layers can probably lead to inaccuracies in the model, because with single layer shell elements the prediction of the delamination is not possible.

Whether a more precise modeling of the fiber size and orientation is necessary depends on many factors. This thesis shows that the simulation of the Crash Test delivers good results without consideration of the precise fiber orientation and size. That means that there is an acceptable variation of about 10 % in maximum deformation of the model. However, it may be that the comparison with a real test shows that this neglect leads to very large deviations in the results.

It must also be mentioned that this material model approach can only be used for thin-walled components. Using shell elements for thicker components can lead to large deviations.

5.2 Computational effort

To maintain a quasi-static simulation, it is necessary to keep the kinematic effects as low as possible. Through Mass Scaling it is possible to maintain longer simulation times and keep the computational effort low. A simulation time of two seconds was chosen to give a good ratio of accuracy to computational effort.

It should be mentioned that for all simulations the loading rate is over 50 m / s for a short time. When comparing the results to a real test it could be necessary to increase the simulation time to keep the loading rate under 50 m/s. It should be mentioned that increasing the simulation time relates to a larger computational effort.

For this Crash test the whole battery case was discretized by using S4 shell elements. To reduce the computational effort of the model one idea would be to use S4R ("R" for reduced) shell elements in areas with no deformation. S4R have only one integration point and therefore need less computational effort compared to the S4 elements. It should be mentioned that using this type of elements can lead to several stability issues that have to be considered.

5.3 Stability of the Simulation

Modeling the initial contact response between the crush plate and the battery case was very challenging. It needed lots of attempts to maintain a stable contact definition.

The simulation also showed that the progressive damage model had problems with the deletion of element with large deformations. This was especially the case when the smallest increment was increased with mass scaling. This is possible because the solver is checking for the failure criteria before each increment. If the time steps are too large, it could be that the stress increase so much during the calculation step that unphysical deformations occur in an element. The simulation is then aborted due to excessive distortion of the element.

5.4 Simulation Modell

The simulation model that was used for the crash test simulation is the same for every material. The only difference between the steel / aluminum model compared to the CF-SMC model is that there are stiffening ribs for the CF-SMC model. It was assumed that the aluminum and steel model are having a homogeneous thickness of 2mm for the battery case.

It can be assumed that the inaccuracies that were made through the simplification of the model of the battery pack are systematic. This means that the influence of the simplifications on the results is the same for each material model.

5.5 CF-SMC Material model

The comparison with aluminum and steel shows that the CF-SMC material model provides good results for the Crash test simulation of the Battery Case. The prediction of the maximal force, force displacement curves for the CF-SMC model are found to be sufficiently accurate for this simulation.

It should be mentioned that the CF-SMC material model was evaluated by using static and dynamic (crash) tests experiments. [6, 7] The comparison of simulation results of the crash test of the battery pack with other material models showed that this model is delivering good results for the battery case. If the simulation of the crash test is also delivering good results for a real crash test must be determined by validation of the model with experimental crash test data.

6. Conclusion

This work focused on the development of a modelling strategy for large CF-SMC components. In particular, the crushing of a lightweight battery concept was simulated.

The material used for the case of the battery pack is a Carbon Fiber Sheet Molding compound material. Light, stiff and formable, it possesses many properties that make it competitive against more traditional metals. The very nature of the material, a mix of short carbon fibers and epoxy resin, make the simulation of crushing events challenging. The used material model that has already been previously validated using both static and dynamic tests on a small hat profile.

In order to validate the modelling methodology of CF-SMC material model applied to large components, a series of simulations by using well known materials were performed. Specifically, three other material models were used: An Isotropic CF-SMC, aluminum and steel. This choice was based on the availability of literature data on the dynamic behavior of metals.

The comparison showed that the CF-SMC material model delivers sufficiently accurate results for predicting the force displacement curves and maximum deformation.

Based on the simulation of the battery case, this work shows that this material model can be applied to large components made of CF-SMC material. The simulation clearly shows an improvement of the component when adopting CF-SMC as structural material. The weight reduction is estimated to be of 42 % compared to aluminum, while by maintaining similar mechanical properties.

The possibility of accurately predicting the mechanical behavior of large CF-SMC components, while using a computationally efficient shell based method, represent an important step towards the further adoption of such a material class in the Automotive industry

Figures

Figure 1 Battery Case Concept developed at the FTG/TU Graz: Showing the outer shell made of CF-SMC and the inner components such as the battery cells and auxiliaries [7]	2
Figure 2 Inner components of a Battery Module for s BEV [11]	3
Figure 3 Semi-finished CF-SMC material before the SMC-Process	4
Figure 4 Transmission cross member of a car out of a SMC material [9]	5
Figure 5 SMC Manufacturing Process [15]	6
Figure 6 Stresses on an incremental volume element dV [1]	8
Figure 7 Stresses at the UD-Element [1]	11
Figure 8 Fiber Failure under tension [1]	12
Figure 9 Fiber Failure under pressure [1]	13
Figure 10 Possible Matrix failure Modes for a UD-Element [17]	14
Figure 11 Matrix failure under transverse tensile stress σ_1^+ [1]	14
Figure 12 Linear vs. Non-linear martial response [24]	16
Figure 13 Generic element x_1, x_2 are the reference system. x'_1, x'_2 are the material reference system. [7]	18
Figure 14 Equivalent Stress vs. equivalent Displacement $\delta eq0$ corresponds to the damage initiation, $F=1$. At $\delta eq failure$ the element has failed and there is no mechanical resistance for that failure mode. [7, 26]	21
Figure 15 Damage variable as a function of equivalent displacement [26]	22
Figure 16 Linear Damage Evolution: Loading-unloading path [26]	24
Figure 17 CAD-Concept developed by the TuGraz/FTG. Only lower halve of the case is shown without wiring and battery management system.....	25
Figure 18 Simplified model of the Battery case that is used for the Crash Simulation in Abaqus. 26	
Figure 19 Top view and side view of the FEM Simulation model undeformed state. With the modeled crush Plate, see 3.1.7, that's used for the Crash Test simulation.	27
Figure 20 S4and S3 element with their integration points [26]	28
Figure 21 Upper and lower case with adhesive line and bolt connection	29
Figure 22 Connection of the cross brace with the other components of the case.....	30
Figure 23 Detail view connection of the cross brace with the lower case.....	30
Figure 24 Model of the Heat conduction plate with the adhesive connection to the lower case. 31	
Figure 25 Mounting blocks with their connections to the other components of the battery.....	32
Figure 26 Battery module with the adhesive connection to the Heat conduction Plate.....	33
Figure 27 Detailed view distributing coupling between the mounting block and the battery module	33
Figure 28 Crush Plate used for the crash simulation of the battery case. Dimensions after ISO 12405-3:2014(E)	34
Figure 29 Tied contact between the mounting block, the cross brace and upper case. The red area indicates the slave surface and the blue one the master surface.....	35

Figure 30 Detailed view of the tied contact between the cross brace and the slot nut	36
Figure 31 Contact between the battery pack (red area) and the crush plate (blue area).....	37
Figure 32 Gasket area of the battery case. The yellow elements represent the cohesive elements, used to model the adhesive connection between the upper and the lower half of the case.....	38
Figure 33 Gasket area of the battery case with the bolt connection	39
Figure 34 Boundary and loading condition of the Battery Pack	40
Figure 35 Amplitude for the loading of the crush plate in direction y over the simulation time..	41
Figure 36 Quality Criteria used for the discretization of the shell elements for the battery pack	42
Figure 37 FEM Model close up of the Battery Case shows the random fiber orientation.	44
Figure 38 FEM model close up of the Battery Case showing the Fiber orientation by means of a vector (green arrow)	45
Figure 39 Three directions of the traction stress vector: one normal and two shear directions [26]	49
Figure 40 Linear Damage evolution model. 0-A shows the pure linear elastic traction behavior before the damage imitation. A-B represents the linear damage evolution model based on separation. At t^0 , the damage criterion is satisfied and the material is degraded. [26].....	50
Figure 41 The velocity of the crush plate in y direction for each material	55
Figure 42 Variation of the load speed application for the 3-point bending test for the C-SMC material. Under 0.06s there is an influence on the results. [6]	56
Figure 43 The ratio of the Energies of the battery pack simulation. Over most of the simulation, the Ratio is under 5 %	57
Figure 44 The influence on the results of the different random Fiber orientation Displacement of the Crush Plate in y-direction.	58
Figure 45 Influence of the different random fiber orientation. Displacement in y-direction of the Crush plate over the simulation time.	59
Figure 46 Influence of the Fiber Orientation for dynamic 3-point Bending test [6].....	60
Figure 47 Deformation of the battery case for the first random fiber orientation at the end of the simulation. The scale indicates the scalar magnitude of the deformation of the elements. Red elements with the highest deformation and dark blue ones with no deformation.	61
Figure 48 Deformation of the battery case for the second random fiber orientation at the end of the simulation. The scale indicates the scalar magnitude of the deformation of the elements. Red elements with the highest deformation and dark blue ones with no deformation.	62
Figure 49 Deformation of the battery case for the third random fiber orientation at the end of the simulation. The scale indicates the scalar magnitude of the deformation of the elements. Red elements with the highest deformation and dark blue ones with no deformation.	62
Figure 50 Deformation of the battery case for the fourth random fiber orientation at the end of the simulation. The scale indicates the scalar magnitude of the deformation of the elements. Red elements with the highest deformation and dark blue ones with no deformation.	63
Figure 51 Look inside the Battery case for the first fiber orientation. Deformation at the end of the simulation showing the Battery modules. The scale indicates the scalar magnitude of the deformation of the elements. Red elements with the highest deformation and dark blue ones with no deformation	64

Figure 52 Look inside the Battery case for the second fiber orientation. Deformation at the end of the simulation showing the Battery modules. The scale indicates the scalar magnitude of the deformation of the elements. Red elements with the highest deformation and dark blue ones with no deformation 64

Figure 53 Look inside the Battery case for the third fiber orientation. Deformation at the end of the simulation showing the Battery modules. The scale indicates the scalar magnitude of the deformation of the elements. Red elements with the highest deformation and dark blue ones with no deformation 65

Figure 54 Look inside the Battery case for the fourth fiber orientation. Deformation at the end of the simulation showing the Battery modules. The scale indicates the scalar magnitude of the deformation of the elements. Red elements with the highest deformation and dark blue ones with no deformation 65

Figure 55 Displacement of the Crush plate in y-direction. The displacements in mm are shown for a certain loading level of the Crush Plate level during the simulation..... 66

Figure 56 Displacement of the Crush plate in y-direction. The displacements in mm are shown for a certain loading level of the Crush Plate level during the simulation..... 67

Figure 57 Displacement of the Crush plate in y-direction. The displacements in mm are shown for a certain loading level of the Crush Plate level during the simulation..... 68

Figure 58 Displacement of the Crush Plate y-direction for aluminum, steel, CF-SMC Isotropic and CF-SMC Orthotropic with two random fiber orientations. 69

Figure 59 Displacement of the Crush Plate in y-direction for aluminum, steel, CF-SMC Isotropic and CF-SMC Orthotropic with two random fiber orientations over the simulation time..... 70

Figure 60 Deformation of the Aluminum Battery Case at the end of the simulation. The scale indicates the scalar magnitude of the deformation of the elements. Red elements with the highest deformation and dark blue ones with no deformation. 71

Figure 61 Undeformed cross brace with the max scalar deformation for the Aluminum Battery Case Red elements with the highest deformation and dark blue ones with no deformation..... 72

Figure 62 Deformation of the Steel Battery Case at the end of the simulation. The scale indicates the scalar magnitude of the deformation of the elements. Red elements with the highest deformation and dark blue ones with no deformation. 73

Figure 63 Undeformed cross brace with the max scalar deformation for the Steel Battery Case. Red elements with the highest deformation and dark blue ones with no deformation. Red elements with the highest deformation and dark blue ones with no deformation. 73

Figure 64 Deformation of the CF-SMC Isotropic Battery Case at the end of the simulation. The scale indicates the scalar magnitude of the deformation of the elements. Red elements with the highest deformation and dark blue ones with no deformation. 74

Figure 65 Undeformed cross brace with the max scalar deformation for the CF-SMC Isotropic Battery Case. Red elements with the highest deformation and dark blue ones with no deformation. 74

Figure 66 Deformation of the CF-SMC Orthotropic Battery Case at the end of the simulation. The scale indicates the scalar magnitude of the deformation of the elements. Red elements with the highest deformation and dark blue ones with no deformation..... 75

Figure 67 Undeformed cross brace with the max scalar deformation for the CF-SMC Orthotropic Battery Case. Red elements with the highest deformation and dark blue ones with no deformation.

..... 75

Figure 68 Hashin fiber damage Top view of the simulated crash test of the CF-SMC orthotropic battery Case. Bottom figure shows the early interaction phase. Second figure at half of the simulation time. The third figure represents the maximum deformation of the battery case. In red the elements that have failed under Hashin criteria.

..... 76

Tables

Table 1 Specification of HexMC® [16]	7
Table 2 mechanical properties HexMC® material. These are typical values obtained with samples cut from 4mm thick moulded plate, cured 3 min at 150°C [16]	7
Table 3 Loading vs Strength	12
Table 4 General overview over the elements used for the Battery Case Model	28
Table 5 Material Model for Orthotropic material behavior [6]	43
Table 6 quasi-isotropic material behavior with average values Engineering constants for HexMC M77 [32]	46
Table 7 Strength and Energy values for quasi-isotropic behavior HexMC M77 [32]	46
Table 8 Damage parameter definition of variables.....	47
Table 9 Equivalent Plastic Strain and Stress Ratio for Shear failure for Al-0.5Mg-0.45Si [33]	47
Table 10 Material Data used in Abaqus for Al-0.5Mg-0.45Si	47
Table 11 Equivalent Plastic Strain and Stress Ratio for Shear failure for stainless steel grade 1.4301 [34]	48
Table 12 Material Data used in Abaqus for stainless steel grade 1.4301 [34]	48
Table 13 Data for the adhesive used in Abaqus [35].....	51
Table 14 Wave speed in the materials used for the battery case.....	53
Table 15 Comparison of the max displacement for the different fiber orientations.....	59
Table 16 Comparison of the maximum scalar Displacement in y-direction of the Crush Plate.....	69
Table 17 Weight of the Battery Case and the whole Battery Pack	77
Table 18 Weight reduction of the Battery Pack	77

A Appendix

8. Literatur

- [1] *Schürmann, H.*: Konstruieren mit Faser-Kunststoff-Verbunden, VDI-Buch,, 2007.
- [2] © 2018 European Federation for Transport and Environment AISBL: Transport & Environment.
- [3] Die aktuelle Treibhausgasemissionsbilanz von Elektrofahrzeugen in Deutschland.
- [4] Prof. Dr.-Ing. Joachim Böcker: Fahrzeugantriebe 2019-08-09 (2019).
- [5] *Friedrich, H.E.*: Leichtbau in der Fahrzeugtechnik, ATZ/MTZ-Fachbuch,, 2013.
- [6] Daniel Reinbacher: Parametrierung und Validierung von Materialmodellen zur FE-Simulation faserverstärkter SMC-Kunststoffe für E-Fahrzeuge. Graz, Technische Universität Graz, Masterarbeit, 2019.
- [7] Federico Coren, Philipp S. Stelzer, Daniel Reinbacher, Christin Ellersdorfer, Peter Fischer, Zoltan Major: Dynamic failure and crash simulation of carbon fiber sheet moulding compound (CF-SMC) Ausgabe 2020.
- [8] *Scott, A.E.; Mavrogordato, M.; Wright, P. et al.*: In situ fibre fracture measurement in carbon–epoxy laminates using high resolution computed tomography. *In: Composites Science and Technology* 71 (2011), Heft 12, S. 1471-1477.
- [9] Hexcel molding compound enables high-volume, zero-waste process, 2020, <https://www.compositesworld.com/news/hexcel-molding-compound-enables-high-volume-zero-waste-process> [Zugriff am: 02.11.2020].
- [10] C. Linse; R. Kuhn: Design of high-voltage battery packs for electric vehicles. *In: : Advances in Battery Technologies for Electric Vehicles*, Woodhead Publishing Series in Energy Heft 80. Elsevier Science & Technology, Cambridge, 2015, S. 245-263.
- [11] Stefan Kreiling, 2019, <https://www.linkedin.com/pulse/functional-materials-battery-integration-structural-joining-kreiling> [Zugriff am: 29.09.2020].
- [12] ISO: ISO 6469-1:2019, 2020, <https://www.iso.org/standard/68665.html> [Zugriff am: 12.11.2020].
- [13] ISO: ISO 26262-1:2018, 2020, <https://www.iso.org/standard/68383.html> [Zugriff am: 12.11.2020].
- [14] *Witten, E. (Hrsg.)*: Handbuch Faserverbundkunststoffe/Composites – Grundlagen, Verarbeitung, Anwendungen. AVK, Industrievereinigung Verstärkte Kunststoffe. Springer Vieweg, Wiesbaden, 2014.
- [15] 201904171333441784917.jpg (JPEG-Grafik, 350 × 179 Pixel), 2019 [Zugriff am: 03.11.2020].
- [16] Hexcel: HexMC®-i C/2000/M77-RACarbon Epoxy Molding Compound product data sheet, https://www.hexcel.com/user_area/content_media/raw/HexMCi_C_2000_M77_RA_DataSheet.pdf [Zugriff am: 22.09.2020].
- [17] Gerald Kress: Mechanik der Faserverbundwerkstoffe. Zürich, ETH Zürich, Thesis, 2012.
- [18] *Altenbach, H.*: Kontinuumsmechanik – Einführung in die materialunabhängigen und materialabhängigen Gleichungen. Springer-Verlag GmbH. Springer Berlin Heidelberg, Berlin, Heidelberg, 2018.

- [19] Hashin, Z.: Failure Criteria for Unidirectional Fiber Composites. *In: Journal of Applied Mechanics* 47 (1980), Heft 2, S. 329-334.
- [20] Hashin, Z.; Rotem, A.: A Fatigue Failure Criterion for Fiber Reinforced Materials. *In: Journal of Composite Materials* 7 (1973), Heft 4, S. 448-464.
- [21] Lapczyk, I.; Hurtado, J.A.: Progressive damage modeling in fiber-reinforced materials. *In: Composites Part A: Applied Science and Manufacturing* 38 (2007), Heft 11, S. 2333-2341.
- [22] Matzenmiller, A.; Lubliner, J.; Taylor, R.L.: A constitutive model for anisotropic damage in fiber-composites. *In: Mechanics of Materials* 20 (1995), Heft 2, S. 125-152.
- [23] Wang, C.H.; Duong, C.N.: Chapter 2 - Failure criteria. *In: Duong, C.N.(T.F.T.B.C. (Hrsg.): Bonded joints and repairs to composite airframe structures. Elsevier Science Publishing Co, Oxford, 2015, S. 21-45.*
- [24] Matthew Lowell Roberts: DEVELOPMENT OF A FINITE ELEMENT MODEL FOR PREDICTING THE IMPACT ENERGY ABSORBING PERFORMANCE OF A COMPOSITE STRUCTURE, Faculty of California Polytechnic State University, 2014.
- [25] Larbi Chaht, F.; Mokhtari, M.; Benzaama, H.: Using a Hashin Criteria to predict the Damage of composite notched plate under traction and torsion behavior. *In: Frattura ed Integrità Strutturale* 13 (2019), Heft 50, S. 331-341.
- [26] Simulia: Abaqus Documentation, 2017, <https://abaqus-docs.mit.edu/2017/English/SIMA-CAEXX-CrefMap/simaexc-c-docproc.htm> [Zugriff am: 25.09.2020].
- [27] Stack Overflow: Definition of integration point in Abaqus - Stack Overflow, 2020, <https://stackoverflow.com/questions/24956428/definition-of-integration-point-in-abaqus> [Zugriff am: 05.11.2020].
- [28] ISO 12405-3: Electrically propelled road vehicles- Test specification for lithium-ion traction battery packs and systems. ISO,
- [29] Czichos, H.; Habig, K.-H. (Hrsg.): Tribologie-Handbuch – Tribometrie, Tribomaterialien, Tribotechnik. Springer Fachmedien Wiesbaden, Wiesbaden, 2015.
- [30] Mavrodontis, N.: Kinematic vs Distributed coupling constraints in Abaqus, 2020, <https://info.simuleon.com/blog/kinematic-vs-distributed-coupling-constraints-in-abaqus> [Zugriff am: 09.11.2020].
- [31] Johannes Kepler University Linz, Institute of Polymer Product Engineering, Altenberger Straße 69, 4040 Linz, Austria.
- [32] Zoltan Major: HexMC Data. Linz, Johannes Kepler Universität, 2020.
- [33] Vilamosa, V.; Børvik, T.; Hopperstad, O.S. et al.: Behaviour and modelling of aluminium alloy AA6060 subjected to a wide range of strain rates and temperatures. *In: EPJ Web of Conferences* 94 (2015), S. 4018.
- [34] Jelena Dobrić; Zlatko Marković; Dragan Buđevac et al.: Specifičnosti ponašanja tlačnih elemenata od nehrđajućeg čelika. *In: Journal of the Croatian Association of Civil Engineers* 67 (2015), Heft 2.
- [35] ASI: Pliogrip™ 2400/ 2808B EU.
- [36] albs: KEM-_012_2009_0001_P22949.

- [37] Sun, J.S.; Lee, K.H.; Lee, H.P.: Comparison of implicit and explicit finite element methods for dynamic problems. *In: Journal of Materials Processing Technology* 105 (2000), 1-2, S. 110-118.